MOLECULAR MODELING OF POLYELECTROLYTES - NUCLEOTIDES / NUCLEIC ACIDS INTERACTION

A Thesis Submitted to
the Graduate School of Engineering and Sciences of
İzmir Institute of Technology
in Partial Fulfillment of the Requirements for the Degree of

DOCTOR OF PHILOSOPHY

in Chemistry

by
Erman KIBRIS

December 2022
İZMİR

ABBREVIATIONS

ACKNOWLEDGEMENTS

ABSTRACT

MOLECULAR MODELING OF POLYELECTROLYTES - NUCLEOTIDES / NUCLEIC ACIDS INTERACTION

In this thesis, poly- N, N, N-trimethyl-3-(4-methylthiophen-3-yl) oxy) propan-1-aminium force field parameters were generated via ffTK and CHARMM program to perform MD simulations. NBFIX parameters for the interactions of adenosine nucleotides and oligomer were also produced to improve simulations. The parameters were verified by comparing MM vs QM calculations, and simulated vs experimental UV/Vis spectra. Our results revealed that force field parameters obtained by CHARMM program can be applied successfully for the MD simulations of CPTs with different types of adenosine nucleotides (AMP, ADP, and ATP).

Poly-(3-(2-((4-methylthiophen-3-yl) oxy) ethyl)-1-ethyl-4H-1λ4-imidazol-3-ium) and poly- N,N,N-trimethyl-6-((4-methylthiophen-3-yl) oxy) hexan-1-aminium are used for optical sensors, therefore parametrization and MD simulations for these compounds were performed to see the effect of nucleotides on the backbone structures of oligomers. Generally, increasing the phosphate group on nucleotides stretched out the backbone of structures, but the largest response was observed in the presence of ATP.

The salt effect and temperature effect were also investigated on oligomer – nucleotide complexes. The increasing temperature shortened the backbone of the compounds, but not significant as experimentally. Addition of the monovalent or divalent cations do not affect linearity of oligomer structure in ATP medium for O3. However, O1 and O2 have a great respond to ATP with Mg^{2+}, K^+ and Ca^{2+} (most sensed) ions, O2 has almost no respond to ATP without these ions. Ca^{2+} is a key ion which regulates ATP production by mitochondria. O2 may take a part of a biosensor design to recognize ATP in the presence of Ca^{+2}.

ÖZET

POLİELEKTROLİTLER – NÜKLEOTİTLER / NÜKLEİK ASİTLER ETKİLEŞİMİNİN MOLEKÜLER MODELLENMESİ

Bu tezde MD simülasyonları gerçekleştirmek için ffTK ve CHARMM programı kullanılarak poli-N, N, N-trimetil-3-(4-metiltiofen-3-il) oksi) propan-1-aminyum kuvvet alanı parametreleri oluşturulmuştur. Adenozin nükleotidleri ve oligomerin etkileşimleri için NBFIX parametreleri de simülasyonları iyileştirmek için üretilmiştir. Elde edilen parametreler, MM ile QM hesaplamaları ve simüle spectrumla deneysel (UV/Vis) karşılaştırılarak doğrulandı. Sonuçlarımız, CHARMM programı ile sağlanan kuvvet alanı parametrelerinin, farklı adenozin nükleotid tipleri (AMP, ADP ve ATP) ile CPT komplekslerinin MD simülasyonlarında başarıyla uygulanabileceğini ortaya koymuştur.

Poli-(2-((4-metiltiofen-3-yl) oksi) etil)-1-etil-4H-1λ4-imidazol-3-ium) ve poli-N,N,N-trimetil-6-((4-metiltiofen-3-yl) oksi) heksan-1-aminyum optik sensörler olarak kullanılmaktadır, bu nedenle nükleotitlerin oligomerlerin omurga yapıları üzerindeki etkisini görmek amacıyla bu bileşikler için de parametrizasyon ve MD simülasyonları yapılmıştır. Genel olarak, nükleotidler üzerindeki fosfat grubunun arttırılması, yapıların omurgasını uzatmaktadır, ancak en büyük yanıt ATP varlığında gözlenmiştir.

Tuz varlığı ve sıcaklık etkisi de oligomer–nükleotid kompleksleşmeleri için araştırılmıştır. Sıcaklığın arttırılması, bileşiklerin omurgalarının kısalmasına sebeb olmuş, ancak deneysel gözlemdeki gibi kayda değer değişim göstermemiştir. Tek veya iki değerlikli katyonların eklenmesi, O3 için ATP ortamında oligomer yapısının doğrusallığını etkilemediği gözlenmiştir. Ancak, ATP ile O1 ve O2, Mg^{2+}, K^+ ve Ca^{2+} (en çok hissedilen) iyonlarının olduğu ortamda O2 ve O3 tepkisinin büyük olduğu elde edilmiştir, O2'nin bu iyonlar olmadan ATP'ye neredeyse reaksyon vermemiştir. Ca^{2+}, mitokondri ile ATP üretimini düzenleyen anahtar bir iyondur. O2, Ca^{2+} varlığında ATP'yi algılamak amacıyla biyosensör tasarımının bir parçası olabilme potansiyeline sahiptir.

TABLE OF CONTENTS

LIST OF FIGURES

LIST OF TABLES

CHAPTER 1

INTRODUCTION

1.1.General Information about Polythiophenes
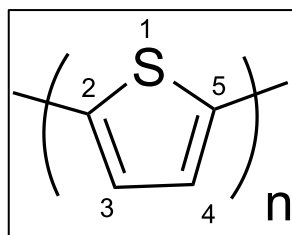
Figure 1.1. Polythiophene fundamental structure (numbers represent the positions)

Polythiophenes (PTs) which are polymerized thiophenes are bonded with covalent bonds at 2, 5 positions and they can be differentiated from 2, 4 positions (Figure 1.1). They have optical properties because of their conjugated backbone. These materials react to environmental stimuli, with a dramatic color shift in response to changes in solvent, temperature, applied potential, and binding to other molecules. When the fundamental structure of polymer is twisted, the conjugation of polymer disrupted. As a result of this property, the polymers are worth researching material to develop chemo- and biosensors.

The polythiophenes having cationic side chain are named CPT (Cationic Polythiophenes). Particular CPTs (like Figure 1.5, Figure 1.6, Figure 1.11) are represented as sensitive probe of biologically active small molecules such as nucleic acids, nucleotides, amino acids, proteins etc. Especially intermolecular interactions between anionic biological molecules and cationic side of CPT act to modify the conformation of conjugated backbone. These interactions are followed by UV-visible absorption spectroscopy, fluorescence spectroscopy, and circular dichroic (CD) spectroscopy. CPT/molecule interaction can lead to form an aggregate structure of complexes. It is demonstrated that these structures directly affect absorption or emission spectra. Other advantage of CPT, its solubility is better than uncharged PT in water

because of its cationic structure. For real time monitoring sensors in living cell, the properties which are solubility in water, low toxicity, red-shift in UV-Vis absorption and intensity in fluorescence spectra especially are very important. The good, functionalized CPT can be potentially involved all these(Zhu et al. 2012).

1.2. Molecular Dynamics Simulations

Molecular dynamics simulation is developed as computer simulation method in order to understand the statistical properties of small molecular system under inter or intramolecular interactions among its constituents by solving Newton's equations of motion for each component. The collective notion is that the statistical ensemble averages are equal to time averages of a system.

After last fifty years, improvement of molecular dynamics simulations made it an acceptable approach for theoretical and experimental investigations. Today, molecular dynamics can be used to verify a theoretical result by performing a numerical experiment (in silica experiment) or to explain an experimental observation by modeling the situation and extracting detailed information to provide a physical insight.

Molecular dynamics provides a detailed perspective at molecular level for experimental findings, like inter and intramolecular interactions. Therefore, it is becoming a preferential tool for both fundamental studies and applied researches. Molecular dynamics simulation is widely applied in physics, chemistry, biochemistry, and materials sciences, studying the behavior of various kinds of solids, liquids, and gases. The most popular simulation packages include AMBER, CHARMM, NAMD, LAMMPS, DL-PLOY and GROMACS, which are available online and some of them are free to download.

1.3. CHARMM (Chemistry at Harvard Macromolecular Mechanics) General Force Fields

CHARMM is presented as computer program which evaluate empirical energy functions for modeling macromolecular systems in 1983 (Brooks et al. 1983). To define empirical energy function (1.1), the terms which include internal and external

interactions are required. The parameters like bond (K_b), angle (K_θ), dihedral angle (K_χ), and improper dihedral angle (K_{imp}) force constants must be described. Force constants are generated by comparing experimental vibrational data and geometric constants that can be derived by crystallographic data (such as X-ray) for isolated molecules. Mackkerell group described how to produce force field parameter in 1998 (MacKerell et al. 1998). A large structure is divided to sub-structural groups;

- The bond potential describes the harmonic vibrational motion between an (i,j) – pair of covalently bonded atoms, where $r_{ij} = \|\vec{r_j} - \vec{r_i}\|$ gives the distance between the atoms, r_0 is the equilibrium distance, and K_b is the spring constant.
- The angular bond potential describes the angular vibrational motion occurring between an (i,j,k) – triple of covalently bonded atoms, where, in the first term, θ is the angle in radians between vectors $\vec{r_{ij}} = \vec{r_j} - \vec{r_i}$ and $\vec{r_{kj}} = \vec{r_j} - \vec{r_k}$, θ_0 is the equilibrium angle, and K_θ is the angle constant.
- The second term is the Urey-Bradley term used to describe a (noncovalent) spring between the outer i and k atoms, it is active when constant $K_{ub} \neq 0$, where, like the spring bond, $r_{ik} = \|\vec{r_k} - \vec{r_i}\|$ gives the distance between the pair of atoms and r_{ub} is the equilibrium distance.
- The dihedral angle potential describes the angular spring between the planes formed by the first three and last three atoms of a consecutively bonded (i,j,k,l) – quadruple of atoms, where χ is the angle in radians between the (i,j,k) – plane and the (j,k,l) – plane. The integer constant n is nonnegative and indicates the periodicity. For $n > 0$, δ is the phase shift angle and k is the multiplicative constant. For $n = 0$, θ acts as an equilibrium angle and the units of k change to potential rad^2. A given (i,j,k,l) –quadruple of atoms might contribute multiple terms to the potential, each with its own parameterization. The use of multiple terms for a torsion angle allows for complex angular variation of the potential, effectively a truncated Fourier series.
- Improper dihedral angles are used to select the correct geometry or chirality of atoms. Consider four atoms (i,j,k,l) among which j is linked covalently to (i,l,k). The improper angle is defined as the angle between the (jl) line and the plane (ijk),

where φ is the angle of (jl), φ_0 is the equilibrium angle and K_{imp} is the angle constant.

- The Lennard-Jones potential involve interactions between all (i, j) −pairs of atoms, where $r_{ij} = \|\vec{r_j} - \vec{r_i}\|$ gives the distance between the pair of atoms, E_{min} and R_{min} are energy and distance at minimum potential respectively.

- The electrostatic potential is repulsive for atomic charges with the same sign and attractive for atomic charges with opposite signs, where $r_{ij} = \|\vec{r_j} - \vec{r_i}\|$ gives the distance between the pair of atoms, and q_i and q_j are the charges on the respective atoms, the dielectric constant $\in_0$ are fixed for all electrostatic interaction, and The parameter $\in$ is a unitless scaling factor whose value is 1 except for a modified 1-4 interaction.

$$
\begin{aligned}
R(\vec{U}) = {} & \sum_{bonds} K_b (r_{ij} - r_0)^2 + \sum_{UB} K_{UB} (r_{ik} - r_{ub})^2 \\
& + \sum_{angle} K_\theta (\theta - \theta_0)^2 \\
& + \sum_{dihedrals} K_\chi (1 + \cos(n\chi - \delta)) + \sum_{impropers} K_{imp} (\varphi - \varphi_0)^2 \\
& + \sum_{nonbond} -E_{min} \left[\left(\frac{R_{min_{ij}}}{r_{ij}} \right)^{12} - 2 \left(\frac{R_{min_{ij}}}{r_{ij}} \right)^6 \right] + \in \frac{q_i q_j}{\in_0 r_{ij}}
\end{aligned}
\qquad (1.1)
$$

In 1998, the protein parameters are reported for all-atom energy function in CHARMM program. The parameter must include a balance between the internal (bonding) and interaction (nonbonding) terms of force field and among the solvent–solvent, solvent–solute and solute–solute interactions. Internal interaction parameters generally optimized with experimental gas-phase geometries, vibrational spectra and torsional energy surfaces supplemented with ab initio results.
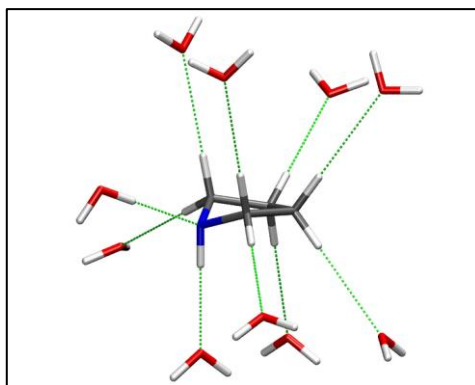
Figure 1.2. Interaction orientations of pyrrolidine with water molecules that were used for charge

The atomic charges are determined by fitting ab initio energies and geometries of complexes between water and model compounds. This model (Figure 1.2) also was represented for pyrrolidine parametrization by same group in 2009 (Vanommeslaeghe et al. 2009a). The PED (Potential Energy Distribution) of QM and MM is used to derive and optimize bond, angle, and dihedral parameters, also the torsional parameters are which converged and verified using PES (Potential Surface Energy).

1.4. NAMD and VMD

Nanoscale Molecular Dynamics (NAMD) developed by the Theoretical and Computational Biophysics Group (TCB) and Parallel Programing Laboratory (PLL) at University of Urbana−Champaign is a MD program for performing high performance MD simulations nearly one million atoms. NAMD have lots of advantage, one of them is that different forcefield and structure file can be used in it (X-PLOR, CHARMM, AMBER, and GROMACS). The simulation parameters can be extended through the Tcl scripting language interactive MD. (Phillips et al. 2005)

VMD (Visual Molecular Dynamics) is graphical interface of MD simulations, and with NAMD it become a complete modeling environment. Same scripting language can be used for analysis MD simulations trajectory files. Day by day, the ready plugins have been added for different type simulations, analysis, structure drawing or

visualizing. One of the useful plugins of VMD is ffTK (forcefield toolkit) that facilitate to creating the CHARMM compatible parameters (Mayne et al. 2013).

1.5.Literature Works

The Wikipedia definition of Adenosine triphosphate (ATP) (Figure ...), "it is an organic compound that provides energy to drive many processes in living cells, such as muscle contraction, nerve impulse propagation, condensate dissolution, and chemical synthesis. Found in all known forms of life, ATP is often referred to as the "molecular unit of currency" of intracellular energy transfer ". Adenosine triphosphate (ATP) is known as to ensure the cell of life activities of energy supply. It is an extracellular signaling mediator in many biological metabolic processes, activating signaling cascades. Therefore, the detection and quantification of ATP is important in biochemistry and clinical diagnosis. (Gourine et al. 2005; Dennis 2001).
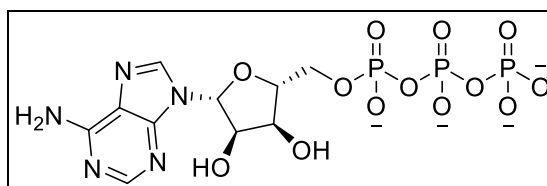
Figure 1.3. Adenosine triphosphate

Conjugated polymers are a type of organic polymers having π-conjugated backbone and versatile side chains. The history of conductive polymers started with polythiazyl (poly-sulfur nitride, (SN)x), followed by polyacetylene, polythiophene, polyaniline, polypyrole (Shirakawa, McDiarmid, and Heeger 2003; Swager 2017). They become very attractive to many scientists because of their unique structures and properties, due their electrical conductance they are used in LEDs, transistors, solar cells etc.

Water-soluble conjugated polyelectrolytes (CPEs) are a kind of water-soluble macromolecules which possess excellent optical and electronic characters. This unique characteristic has been applied to design optical sensors based on both colorimetric (Figure 1.4) and fluorometric modes (Dennis 2001). Using CPEs, in recent years,

chemo- or biosensors have been developed for sensing biologically relevant targets such as proteins(Thomas, Joly, and Swager 2007), DNA(Miranda et al. 2007), polysaccharides (Hoang-Anh Ho, Béra-Abérem, and Leclerc 2005), folic acid (Ma, Li, and Shi 2007) and ATP (Wang et al. 2014). In a very recent work, a comprehensive review has been provided with the various CPEs which bind covalently to biofunctional groups (Sun and Schanze 2022).
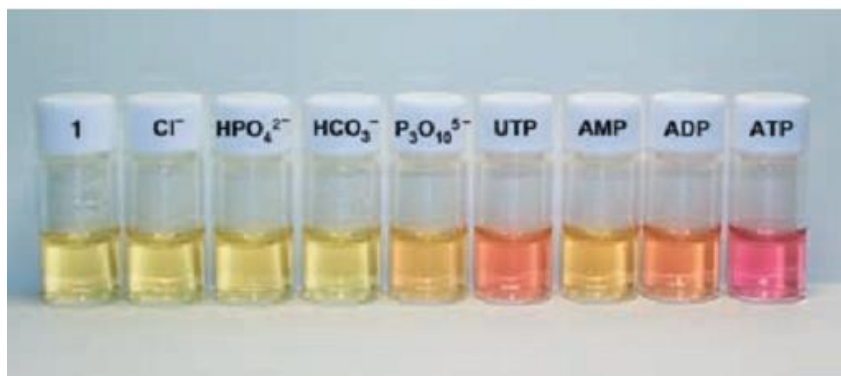
Figure 1.4. Colorimetric Detection of ATP (Source :Li et al. 2005)

In 2003, Hoang and Leclerc developed iodine ion selective colorimetric and fluorometric chemosensor based on CPE derivative (Figure 1.5). The conformational changes in polymer which are induced with different ions included mono- and dihydrogen phosphate ions polymer structure, had been followed by absorbance and fluorescence spectra (H. A. Ho and Leclerc 2003).
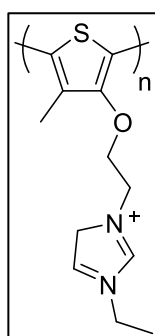
Figure 1.5. Poly-(3-(2-((4-methylthiophen-3-yl) oxy) ethyl)-1-ethyl-4H-1λ4-imidazol-3-ium)

Lİ C. and coworkers studied on the development/building-up of a colorimetric ATP sensor with a cationic polythiophene (CPT in Figure 1.6). Increasing concentrations of ATP in water is tracked by the absorbance spectra in which nearly 138 nm red shift is observed. ATP addition caused a color change in solution from yellow to red. Authors proposed that exposure to ATP were due to formation of an electrostatic complex between the cationic polymer and anionic ATP, which led to increase planarity of the conjugated polymer backbone. At equimolar of ATP concentration, the complex planarity is enough to produce polymer aggregation through hydrophobic effects. The positively charged CPT bind the negatively charged ATP with much stronger attraction than other biologically active nucleotide phosphates like adenosine monophosphate (AMP) and adenosine diphosphate (ADP). According to their results (Figure 1.8), ATP form supramolecular complexes and have influence on PT′s structure and mode of aggregation. Because it has higher negative charge density than other nucleotide phosphates (Li et al. 2005).
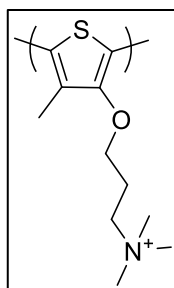
Figure 1.6. Poly- N, N, N-trimethyl-3-(4-methylthiophen-3-yl) oxy) propan-1-aminium

After a year, the mixtures of CPT which is included increasing concentrations of ATP was examined with CD (circular dichroism) spectroscopy. There is no CD pattern at $\pi-\pi*$ translation region. It indicates that CPT formed as an achiral random-coiled conformation in water. When the $\pi-\pi*$ translation being noticed at 1:4 concentration ratio (CPT: ATP) compared with absorption spectrum, the maximum absorbance point refers to the presence of strong exciton coupling between PT backbones in the chirality π-stacked CPT/ATP complex. (Figure 1.7)
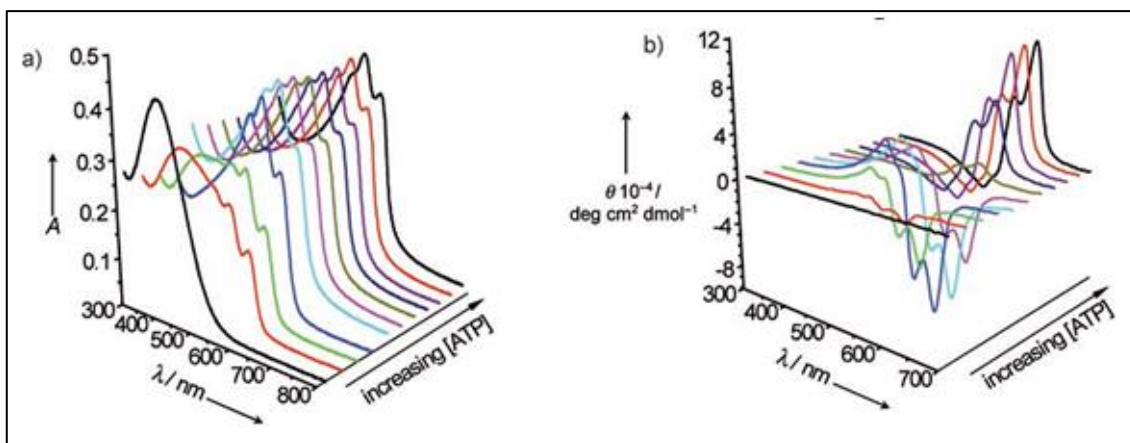
Figure 1.7.a) UV/Vis and b) CD spectra of PT-1(0.10 mm) in the absence and the presence of various amounts of ATP in water at 208C. ATP concentrations (from front to back): 0, 0.001, 0.0125, 0.025, 0.10, 0.15, 0.175, 0.20, 0.25, 0.375, and 0.50 mm (Source: Li et al. 2006b)

Temperature (Figure 1.8 a)) and cation effect on ATP/CPT structure (Figure 1.6) was examined by same group. The cation is not effective on complex structure, on the other hand, while the solution was cooling, absorbance wavelength of the complex in UV-vis spectrum was increasing. Since above 60°C the complex dissociated into non-aggregated polythiophene with the achiral random-coiled conformation(Li et al. 2006b). It is claimed that the optically active supramolecular complex (CPT/ATP) is prepared from a chiral water-soluble CPT host and a chiral ATP guest through electrostatic interactions. The construction of chiral superstructures of CPT is based on intermolecular π-stacking interactions.
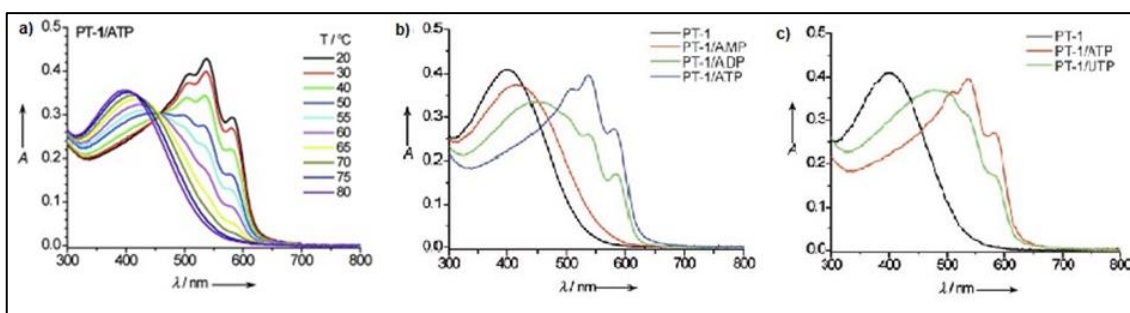
Figure 1.8. UV-vis Spectrum of a) ATP at various Temperature, b) Adenosine mono, di and tri phosphate c) ATP and UTP (Source: Li et al. 2006b)

The presence of adenosine nucleotides which have different phosphate group (AMP, ADP, ATP) in CPT solution affected the absorption maxima (Figure 1.8 b)). While the strength of intermolecular forces was increasing, the red shift on absorption spectrum extended. According to CD, AMP do not demonstrate chiral superstructure of CPT, but ATP makes this structure optically active and planar, so the red shift of complex becomes much longer. When nucleobases were compered (ATP vs UTP), more-ordered aggregates are formed with ATP. It is demonstrated that nucleobases of triphosphates structures play a key role on structure′s π-stacking interactions (Figure 1.8 c)).
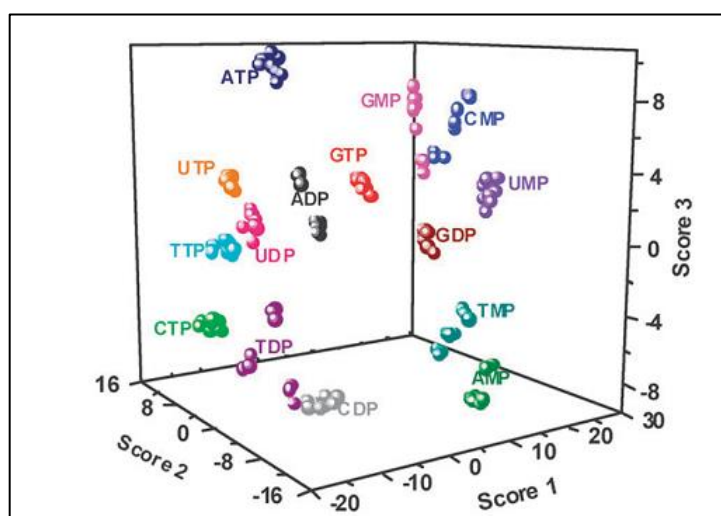
Figure 1.9.Three-dimensional LDA score plot for the analysis of fifteen nucleotides
(Source: Yao et al. 2009)

It is shown that the complex CPT (Figure 1.6) in with various nucleotides reflected specific signal in absorption spectra. This situation is seen an opportunity to improve the probe that can determine the type of nucleotide in solution. To achieve that, the analytical score method which named a linear discriminant analysis (LDA) is used by authors (Yao et al. 2009). LDA is successfully discriminate among 15 nucleotides with 100% confidence limit (Figure 1.9).
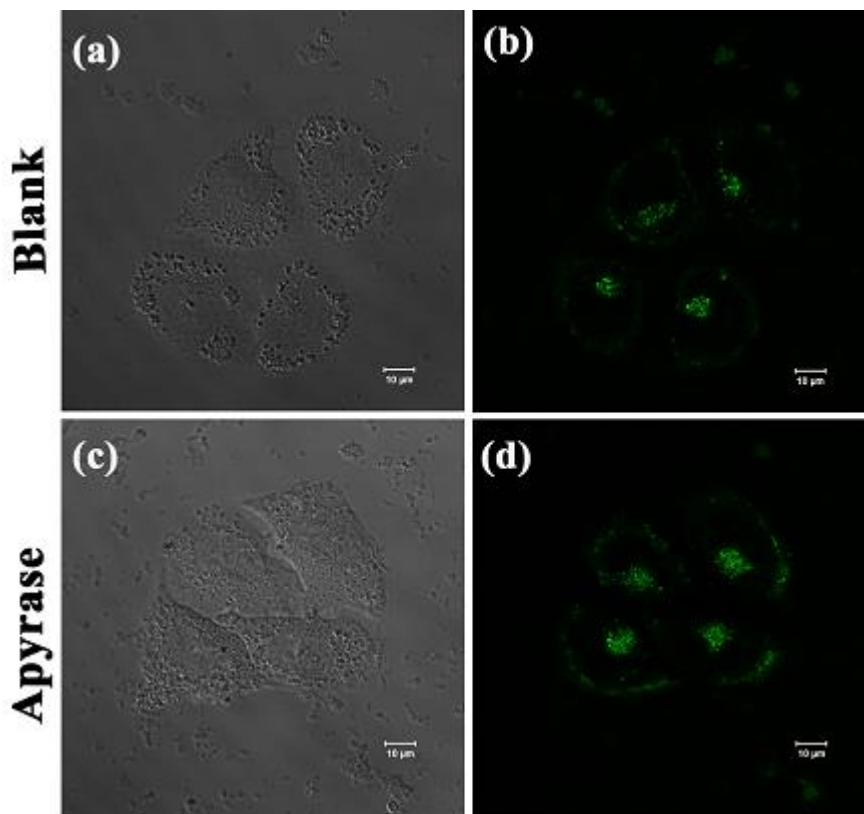
Figure 1.10. Confocal microscopy images of HeLa cells stained with CPT and then incubated with (c, d) or without (a, b) apyrase (0.05 U/mL) in DMEM for 90 min at 37°C. (a, c) Bright-field images. (b, d) CPT (10mM) (λ_{ex}:488 nm, λ_{em}:500−600 nm). Scale bars: 10mm (Source: Huang et al. 2016)

The water soluble cationic thiophene (Figure 1.5) derivative is tried on living cell. This process is successful because CPT possesses low cytotoxicity, good permeability and high photostability in there. Apyrase is an enzyme which hydrolyze ATP to yield AMP and inorganic phosphate. As a fluorescent probe, CPT demonstrate its good sensor ability to detect ATP in cells. It is expected the amount of ATP in Hela cell is decreasing when the enzyme is injected to cell. In Figure 1.10, this variation is assigned using CPT's fluorescence activity to ATP. This is an important feature, since ATP level in cells is followed real-time thanks to CPT using fluorescence microscopy. (Huang et al. 2016)

Like ATP, especially DNA hybridization can be detected by CPT derivatives. In 2008, CPT based DNA probes are reported and Rubio-Magnieto et al. successfully synthesized tri-methyl phosphonium based CPT (Figure 1.11). DNA/CPT complexes

11

investigated by CD spectra. DNA sequence-specific interactions with CPT played important role to produce chiral supramolecular CPT/DNA complex. Also it is claimed that planarization of the polymer backbone is important for the development of biosensors. (Rubio-Magnieto et al. 2013)
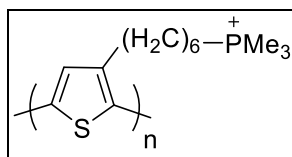
Figure 1.11. Poly [3-(60-(trimethyl phosphonium) hexyl) thiophene-2,5-diyl]

In 2015, the same group were more deeply researched the same cationic polythiophene derivative (Figure 1.11) DNA interactions. According to experimentally results, the homo-nucleotide squence ssDNA (dT and dA) / CPT complex show right handed ICD (Induced Circular Dichroism) but CPT complexation with oligonucleotides of a mixed sequence (in ssDNA or dsDNA topologies) gives rise to left-handed ICD signatures. To explain these evidence, the MD (Molecular Dynamics) simulation was applied for dA/CPT and dT/CPT comlexes. In these simulation, the interactions which are electrostatic, π−cation , π (on thiophene) − π (on nucleotide) and H−bonds were studied for selected ten frames in simulations. The results showed that π-π interactions are dominant for both comlexes (dA/CPT and dT/CPT). Also, It is not only observed on frames of simulations that dT/DNA complex is more compact than dT/CPT, but also its determined easly by radius of gyration analysis of frames. This differences on structures of complexes can be caused that electrostatic , π−cation and H−bond, because these interactions are more affective on dA/CPT than dT/CPT (Figure 1.12). Despide of all anaysis, it isn′t declared by authors that the flourecence change is based on only intermolecular forces, because the chiral superstructre formation is occurred by intramolecular forces of thiophene aggregation. (Rubio-Magnieto et al. 2015a)
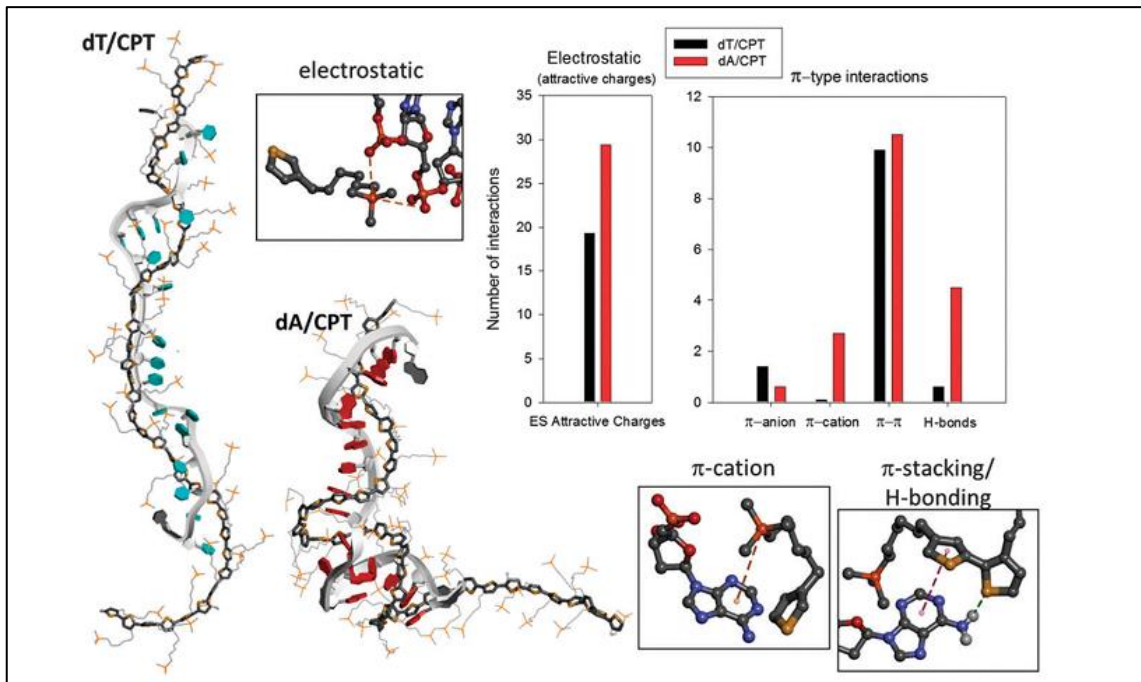
Figure 1.12. Left: Snapshots of dT/CPT and dA/CPT complexes extracted at the end of the MD simulations. The polythiophene backbone is shown as thick sticks, the thymine and adenine nucleobases in blue and red, respectively, and the DNA backbone as a gray ribbon. (Source Rubio-Magnieto et al. 2015a)

$$< R_F > \; = \; N^v \cdot l \qquad\qquad (1.2)$$

In 2019, poly [1,4-dimethyl-1- (3-((2,4,5- trimethylthiophen- 3-yl)oxy) propyl) piperazin-1-ium bromide] was synthesized as single chain cationic polymer dots (Pdots) (Özenler et al. 2019). Using polar aprotic solvent properties, they indicate that the oligomer which have 20 monomer merge from bulk solution as a single polymer chain using ethylene glycol. In Figure 1.13, the oligomer (Pdot) was calculated using Chem3D for simple force field and MM2 energy minimization and molecular dynamics. After that, end to end distance and length of step of the optimum geometry were determined by Gaussian 09 software to use Flory Theory via Equation(1.2(1.2 where R: Flory radius, N : The number of linear steps in a random polymer chain, v: Flory exponent and l: length of a step. For a real single chain containing only the volume exclusion, the proper analogy becomes a self-avoiding walk and a typical excluded volume chain have Flory exponent as v = 3/5. Equation(1.2 was applied to

20-mer and with 2.2 nm end to end distance. The results of end to end distance obtained from MD simulation for 20mer is same with RF calculated. While absorbance spectrum of the bulk polymer in water have two major peak (respectively, 365 and 415 nm), Pdot give absorbance at 415 nm. This situation provide that bulk solution include only coiled form but also longer conjugation length species.
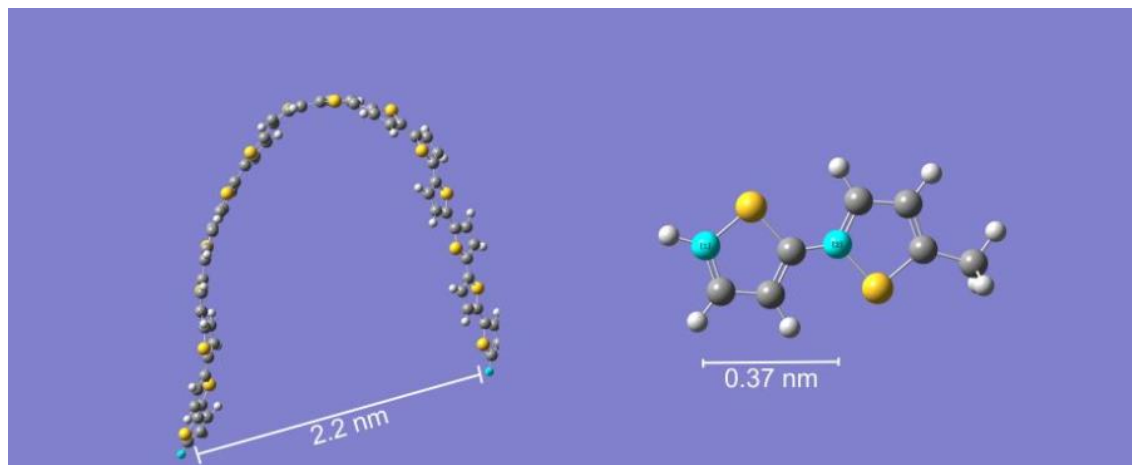
Figure 1.13. Theoretical calculation of end-to-end distance and length of a step
(Source: Özenler et al. 2019)

CHAPTER 2

COMPUTATIONAL METHODS

2.1.CHARMM Force Field

2.1.1.Intermolecular Interactions

The possible chemical interactions between molecules are investigated via a threshold distance since they can be used to explain the spectral change of CPTs. These interactions are specified Cation − Anion Interaction and π − Cation Interaction as shown in Figure 2.1. The summation of interactions in which the distance lower than 6.5 Å (Rubio-Magnieto et al. 2015b) is counted for each snapshot of MD. After calculating all interactions, the value is divided by possible number of interactions present in the duplex and the total number of frames to normalize the interaction value.
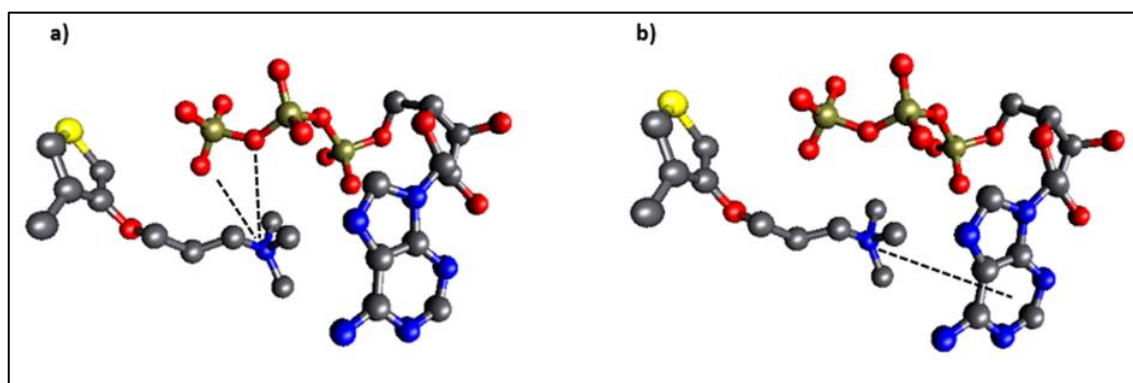
Figure 2.1. Cation − Anion Interaction and π − Cation Interaction

2.1.2.Parametrization Methodology

The CHARMM potential energy function contains intramolecular terms given in (2.1) and intermolecular terms given in (2.2).

$$\sum_{bonds} K_b(b - b_0)^2 + \sum_{UB} K_{UB}(S - S_0)^2$$

$$+ \sum_{angle} K_\theta(\theta - \theta_0)^2 + \sum_{dihedrals} K_\chi(1 + \cos(n\chi - \delta))$$

$$+ \sum_{impropers} K_{imp}(\varphi - \varphi_0)^2$$

(2.1)

In intramolecular part of energy function, there are bond, angle, dihedral angle, and improper dihedral terms where K_b, K_{UB}, K_θ, K_χ, and K_{imp} are force constants, respectively; b, S, θ, χ , and φ are the bond length, Urey-Bradley 1,3-distance, bond angle, dihedral angle, and improper torsion angle, respectively the ones with the subscript zero representing the equilibrium values of the corresponding terms.

$$\sum_{nonbond} \in_{ij} \left[\left(\frac{R_{min_{ij}}}{r_{ij}} \right)^{12} - 2 \left(\frac{R_{min_{ij}}}{r_{ij}} \right)^6 \right] + \frac{q_i q_j}{\in_l r_{ij}}$$

(2.2)

The intermolecular terms include electrostatic and van der Waals (vdW) interactions, where q_i and q_j are the partial atomic charges on atom i and j, respectively, ϵ_{ij} is the well depth, $R_{min,ij}$ is the distance in the Lennard-Jones (LJ) 6−12 term at the minimum energy used to treat the vdW interactions, and r_{ij} is the distance between i and j atoms.

$R_{min} = 2^{1/6}\sigma$; where σ is the distance at zero LJ potential, and two times the van der Waals radius of the atom. When two different atoms interacting, σ and ε values are obtained by the Lorentz-Berthelot combination rule which involve arithmetic and geometric means respectively, $\sigma_{ij} = (\sigma_i + \sigma_j)/2$ and $\varepsilon_{ij} = (\varepsilon_i \varepsilon_j)^{1/2}$.

2.1.3. Parametrization Strategy of Charmm

The CHARMM parameters for CPT in the subject of this thesis were generated as described in the literature for CPT in the subject of this thesis (Vanommeslaeghe et al. 2009a). The terms of energy function can be generated at CHARMM software in which force field have extensible properties. More clearly, after identification of similar

compounds, these parameters being placed in CGenFF (CHARMM General Force Field) such as atom types, charges, force constants can be used as starting point of the new compound.

LJ (Lennard Jones) parameters are necessary to develop CHARMM additive forcefields, bonded parameters can be generated for CGenFF extensions from QM calculations. The parametrization procedure is given in Figure 2.2. Details of target data generation as follow;

1. the various possible conformers of molecule are optimized at the MP2/6-31G(d) [MP2/6-311G(d)in the case of anions]. The minimum energetic conformer is used to calculate Melz-Kollman charges. In CHARMM forcefield the aliphatic hydrogen charge is +0.09. After setting aliphatic hydrogens, the structure charges optimized according calculated Merz-Kollman charges. A complex between optimizing structure and water molecule is built for a possible hydrogen bond interaction (Figure 1.2). The complexes which are created for each possible hydrogen bonds are minimized at HF/6-31(d) level. These interaction energies as a function of distance are compared with MM calculation using optimized charges. Ideally, the model compound-water interaction energies should be within 0.2 kcal/mol from the target interaction energies.

2. After charges are guessed, the initial structure minimized in CHARMM. The bond and angle parameters of MM are examined comparatively with QM minimization structure at MP2/6-31G(d) level of theory. Respectively, 0.03 Å and 3° differences are generally acceptable.

3. The potential energy distribution (PED) analysis is performed by the help of MOLVIB in CHARMM, and these frequencies are compared with MP2/6-31G(d) vibrational spectra. The F-matrix of QM are scaled by a factor 0.89 (Pulay et al. 1979). Using PED analysis, the force constants are optimized.

4. Optimization of dihedral force constants is verified with potential energy surface (PES). Torsion parameters are initially optimized on vibrational spectra in part 3. The dihedrals are scanned with CHARMM and MP2/6-31G(d) calculation, after that the energy of MM and QM are compared. If the results of QM and MM have large difference, these steps are repeated.
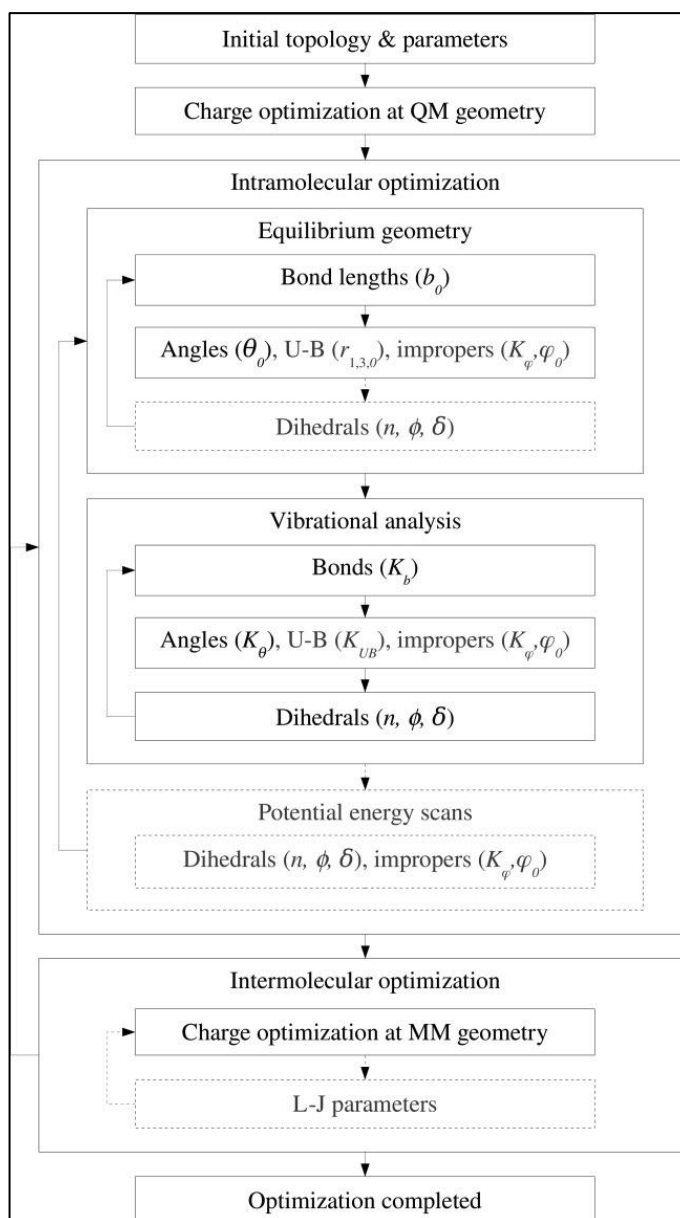
Figure 2.2. Parametrization procedure. Steps that are printed in gray and/or dotted lines are optional, depending on the molecule. Upward arrows that cause part of the procedure to be repeated are only followed if the changes induced by the parameter optimization a larger than a certain convergence criterion

2.1.4. Generating CHARMM Compatible Force Field Using ffTK (Force Field ToolKit)

ffTK is distributed as VMD plugin to produce CHARMM compatible forcefield. The GUI of it is easy to produce QM input and compare QM and MM results. The

parametrization steps depend on the CHARMM parametrization technique described in (Vanommeslaeghe et al. 2009)'s article (Mayne et al. 2013). In Figure 2.3, the workflow of ffTK is shown, these steps are explained below.
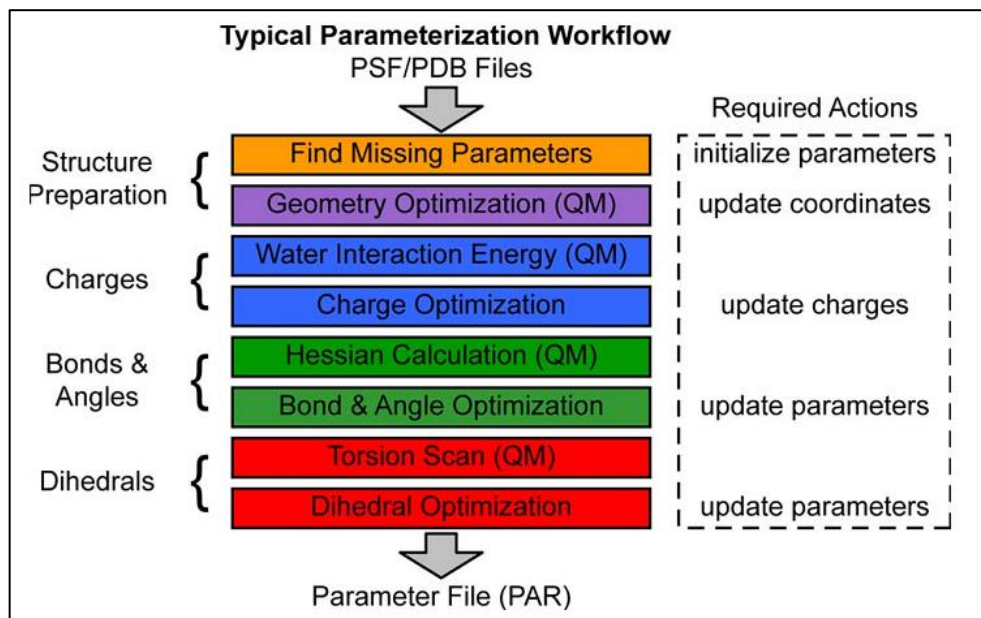
Figure 2.3. A typical parameterization workflow addresses four major stages (left), each of which requires a specific set of calculations (center), and subsequent action to update a variety of file types (right). ffTK is designed as a GUI that facilitates traversal of the workflow without obscuring the underlying processes or data.

Firstly, the PDB file which include the x, y, z coordinates of atoms and the PSF file including type, charge, identity of atoms and molecule name are prepared, and the missing parameters have been searched in CHARMM parameters. After identification of potential hydrogen bond acceptor or donor atoms, the QM input designed at HF/6–31G(d) level of theory via Gaussian09 program is generated by ffTK. In the second part, the results of water interactions of molecule (QM calculation) are uploaded to program and the energies of QM and MM (scaled by 1.16) minimizations have fitted each other. Result of this part, the charges of atoms are determined as that aliphatic hydrogens charge have + 0.09. After this step, the MM and QM calculated hessian matrices which contain the second derivatives of the potential energy with respect to pairs of the input coordinates are compared and the iterative procedure is applied to bond and angle parameter until MM results are nearly matched to QM (at MP2/6–

31G(d) level) calculations. This part is different to CHARMM parametrization because method of CHARMM parametrization use the PED analysis. Finally, the dihedral angles are scanned for PES analysis. Since QM and MM torsional energy is matched on PES, the parametrization is completed like in CHARMM parametrization.

2.2. Nanoscale Molecular Dynamics (NAMD) and Visual Molecular Dynamics (VMD)

Before starting NAMD, four type files must be prepared. NAMD has four file types. These are parameter file (CHARMM), molecular structure file (PSF), the coordinate file of molecular system (PDB) and configuration file of NAMD.

PDB (Protein Data Bank): it has the coordinates of atoms in simulation system, and it identify which atom relates to which molecule. In the Figure 2.4, The fields in order from left to right are the record type, atom ID, atom name, residue name, residue ID, x, y, and z coordinates, occupancy, temperature factor (called beta), segment name.

```
ATOM      1  C1  ERM 1   1    -28.991  25.648 -16.609  1.00  0.00      101 C
ATOM      2  C2  ERM 1   1    -29.928  26.617 -17.094  1.00  0.00      101 C
ATOM      3  C3  ERM 1   1    -29.866  27.784 -16.367  1.00  0.00      101 C
ATOM      4  S1  ERM 1   1    -28.721  27.698 -15.151  1.00  0.00      101 S
ATOM      5  C4  ERM 1   1    -28.270  26.130 -15.541  1.00  0.00      101 C
ATOM      6  C5  ERM 1   1    -30.846  26.364 -18.252  1.00  0.00      101 C
```

Figure 2.4. Protein Data Bank (PDB) file example

PSF (Protein Structure File): it contains at least five different sections which are atoms, bonds, angles, dihedrals, impropers (dihedral force terms used to maintain planarity). In atom section have atom ID, segment name, residue ID, atom name, atom type, charge, and mass.

```
37185 !NATOM
       1 101     1         ERM    C1    CTM    -0.146000      12.0107      0
       2 101     1         ERM    C2    CTM     0.268000      12.0107      0
       3 101     1         ERM    C3    CTM    -0.052000      12.0107      0
       4 101     1         ERM    S1    STM    -0.427000      32.0650      0
       5 101     1         ERM    C4    CTM    -0.019000      12.0107      0
       6 101     1         ERM    C5    CT1    -0.661000      12.0107      0
       7 101     1         ERM    O1    OG1     0.444000      15.9994      0
       8 101     1         ERM    H1    HGA4    0.090000       1.0079      0
```

Figure 2.5. Atom Section of Protein Structure File (PSF) example

On the other sections, bonds, angles, dihedrals, and improper dihedrals are described, this part is key to connect atoms to its force field parameters. As shown in Figure 2.6, the bond, angle and dihedrals are described using atom ID.

```
   25078 !NBOND: bonds
       1        2        1        5        1        7        2        3
       2        6        3        4        3      641        4        5
       5       35        6       23        6       24        6       25
       7       10        8       20        9       20       10       11
      10       12       10       13       13       14       13       15

   13726 !NTHETA: angles
       1        7       10        1        5       35        1        5        4
       1        2        6        1        2        3        2        6       25
       2        6       24        2        6       23        2        3      641
       2        3        4        2        1        7        2        1        5
       3        4        5        3        2        6        4        5       35

    2216 !NPHI: dihedrals
       1        7       10       11        1        7       10       12
       1        7       10       13        1        5        4        3
       1        5       35       34        1        5       35       36
       1        2        3        4        1        2        3      641
```

Figure 2.6. Bond, Angle and Dihedral Section of PSF example

Configuration File (NAMD): In this file, all input and output paths are inserted, and the simulation conditions are described like temperature, pressure, cut-off distance and timestep. The change of simulation is recorded to trajectory file (DCD) and for each frame the simulation information such as energies, frame temperature and pressure is written to output file. The information of output file is described also in configuration file.

Before starting MD simulation for isothermal–isobaric (NPT) ensemble, to equilibrate the simulation environment a few steps which are given in below are applied in NAMD.

- Preparation of Initial Structure: initialize atoms coordinates, add solvent, balance charge with ions, etc.

- Energy Minimization: To adjust the structure to force field, distribution of solvent molecules. To relax possible steric clash created by initial coordinates

- Heating the Simulation System: The temperature of system is linearly increased from 0 K to intended temperature within specified time

- Equilibration of the System: After pumping kinetic energy in the heating step, kinetic energy converted to potential energy and its fluctuations nearly equilibrated

These steps and simulation output files can be easily processed to analyze the simulation, and trajectory file can be visualized in Visual Molecular Dynamics.

2.3. Analysis Methods

2.3.1. RMSD (Root Mean Squared Deviation)

General description of RMSD (root mean square deviation) is measuring of the differences between two values which are predicted and observed. It is a comparative tool for two differ or similar atomic structures. The Root Mean Squared Deviation (RMSD) is defined in eq. (2.3);

$$RMSD = \sqrt{\frac{1}{N_{atoms}} \sum_{i=1}^{N_{atoms}} (\vec{r}_i(t_1) - \vec{r}_i(t_2))^2} \qquad (2.3)$$

where N_{atoms} is the number of atoms whose positions are being compared, and $\vec{r}_i(t)$ is the position of atom i at time t. Especially, to understand the minimization step whether it is enough or not, the RMSD vs timestep graph must be applied.

2.3.2. The Radius of Gyration (R_g)

The radius of gyration (R_g) refers to the center of mass of selected atoms or the mean square distance from a given axis. It is suitable for identifying branched chains and defining the dimensions of a polymer chain can also be used to measure the degree of folding in the chains. In other word, it is used as a measure of compactness of a polymer chain.

$$R_g = \sqrt{\frac{\sum_{i=1}^{n} w_i (r(i) - \bar{r})^2}{\sum_{i=1}^{n} w_i}} \qquad (2.4)$$

The radius of gyration is computed by the equation 2.4 where w_i and $r(i)$ the mass and the position of the i' th atom respectively and is $\bar{r}$ is the weighted center.

CHAPTER 3
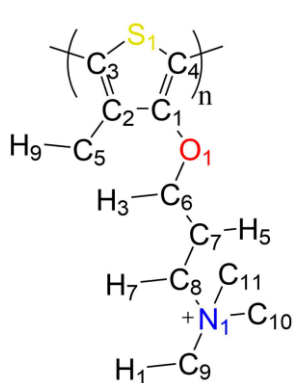
RESULT AND DISCUSSION

3.1. Parameterization of CPT

3.1.1. Force Field ToolKit Parametrization

The force field parameters of the cationic thiophene oligomers do not exist in the literature, so the unknown parameter sets which are necessary to perform MD simulations were generated by using quantum mechanical potential energy surface scans and ffTK plugin for VMD. ffTK plugins in VMD and Gaussian09 are the programs were used to generate CHARMM-compatible force field parameters for the monomer of a cationic polythiophene (see Table 3.1). The dihedral parameters were found by using its dimer. The LJ/vdW parameters were identified in monomer as its constituent atoms which are named as in Table 3.1, then they were compared with existing parameters in the literature, and the matched ones were used.

Table 3.1 The list of names, types, and charges of atoms in CPT

	Atom	Type	Charge	Atom	Type	Charge
	S_1	SG2R50	-0.16	C_5	CG331	-0.24
	C_1	CG2R51	0.03	H_9	HGA3	0.09
	C_2	CG2R51	0.33	C_6	CG321	-0.01
	C_3	CG2R57	-0.14	H_3	HGA2	0.09
	C_4	CG2R57	0.07	C_7	CG321	-0.17
	O_1	OG301	-0.33	H_5	HGA2	0.09
	C_8	CG321	-0.11	N_1	NG3P0	-0.6
	H_7	HGP5	0.25	C_9	CG334	0.25
	H_1	HGP5	0.09			

The most favorable structure of the monomer was obtained at MP2/6-31G* level of theory. The partial charges of non-polar hydrogens are fixed to +0.09 for aliphatic. QM calculations at HF /6-31G* level of theory was used to obtain charges of monomer interacting with a water molecule.

QM calculations of the Hessian matrix whose elements are the second derivatives of potential energy function are used to reproduce the potential energy surface by distortions along the angles and bonds. MP2/6-31G* level of theory is applied to optimize structure for Hessian calculations fitting the targeted bonds and angles data.

Table 3.2 The List of High Penalty Parameters

Types	Penalty
CG2R51 OG301	45
CG2R51 CG2R51 OG301	39
CG2R51 CG2R51 CG2R51 OG301	45
CG331 CG2R51 CG2R51 OG301	46
CG331 CG2R51 CG2R51 SG2R51	115
OG301 CG2R51 CG2R51 SG2R51	111
CG2R51 CG2R51 OG301 CG321	94
*CG324 CG321 CG321 OG301	17

Bonds and angles are expressed using a simple harmonic potential. NAMD performed a short geometry optimization in the background during the ffTK optimization. The first change ensures a good fit of MM-optimized geometry and QM-optimized geometry. The optimization iterations were performed until increasing the current final objective value. The bond, angle and dihedral parameters were determined by comparing QM and MM calculations. Some parameters were obtained from CGenFF for the thiophene derivatives (Paramchem https://cgenff.umaryland.edu (Vanommeslaeghe et al. 2009a)). We calculated the parameters which have penalties higher than 10 (see Table 3.2). According to CHARMM parameters, the difference 0.03 Å for bonds and 3° for angles are acceptable, the calculated parameters in this work

were found in this range. The target QM bond and angle deviations values were obtained as 0.01 Å and 2.67° respectively for our calculations. On the other hand, for all parameters the maximum deviations are 0.07 Å and 9.53° for distances and angles respectively, belong to the parameters taken from CGenFF list (see Figure 3.1).

The relaxed PES scan with dihedrals were performed at the MP2/6- 31G* level of theory and refinement was applied to catch good fitting of QM-MM as shown in Figure 3.1. Dihedral scan parameters were fitted as described in the computational methods part. The root-mean square error (RMSE) value for our calculated dihedral parameters was obtained as 0.6 kcal/mol. After all refinement, the result demonstrates that MM data nearly fit to the target QM data. 0.5 kcal/mol is recommended RMSE value for the compatible-CHARMM force field. Although the RMSE was not the same as the recommended value, it was nearly well-matched.
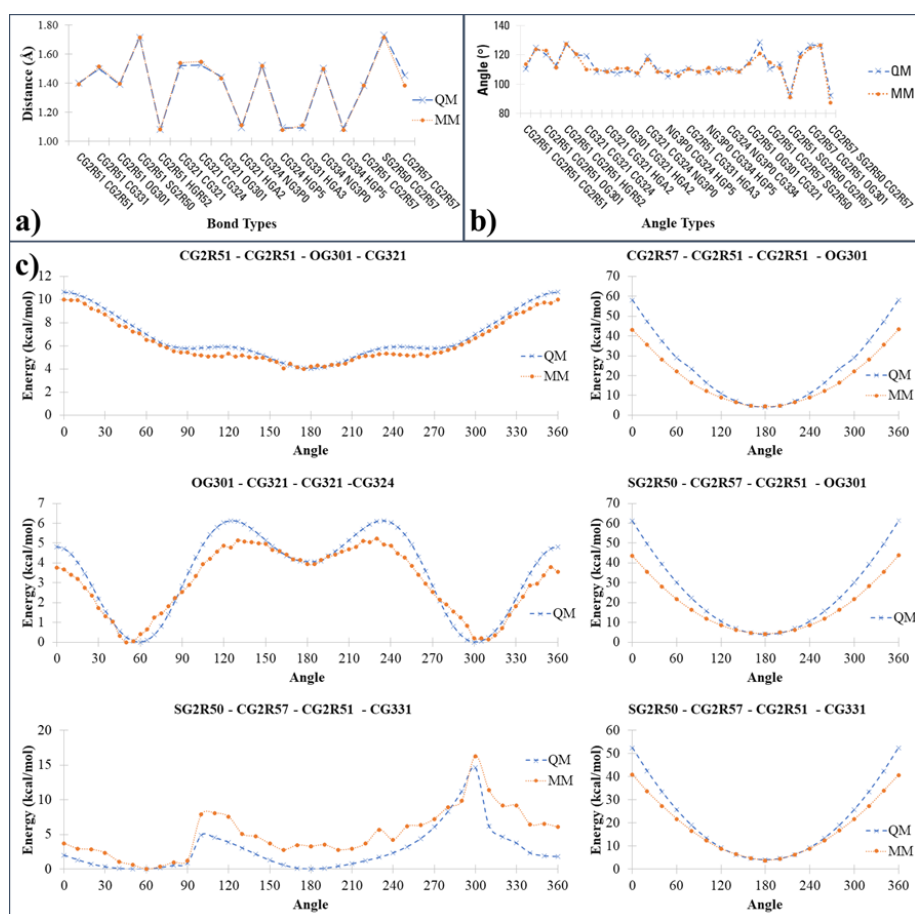
Figure 3.1. The comparison QM and MM data a) for the bond fitting, b) for the angle fitting, c) for the dihedral optimization.

3.1.2. Charmm (Chemistry at HARvard Macromolecular Mechanics) Parametrization

3.1.2.1. Parametrization of Poly-N,N,N-trimethyl -3-(4 methylthiophen -3 -yl) oxy) propan- 1-aminium

The monomer structure was split into two groups one of them is thiophene and the other one is 3-hydroxy-N,N,N-trimethylpropan-1-aminium. The Charmm Forcefield include thiophene (RESI THIP) charge and parameters. For the 3-hydroxy-N,N,N-trimethylpropan-1-aminium, the charges were calculated as mentioned at Parametrization Strategy of Charmm (Table 3.3).
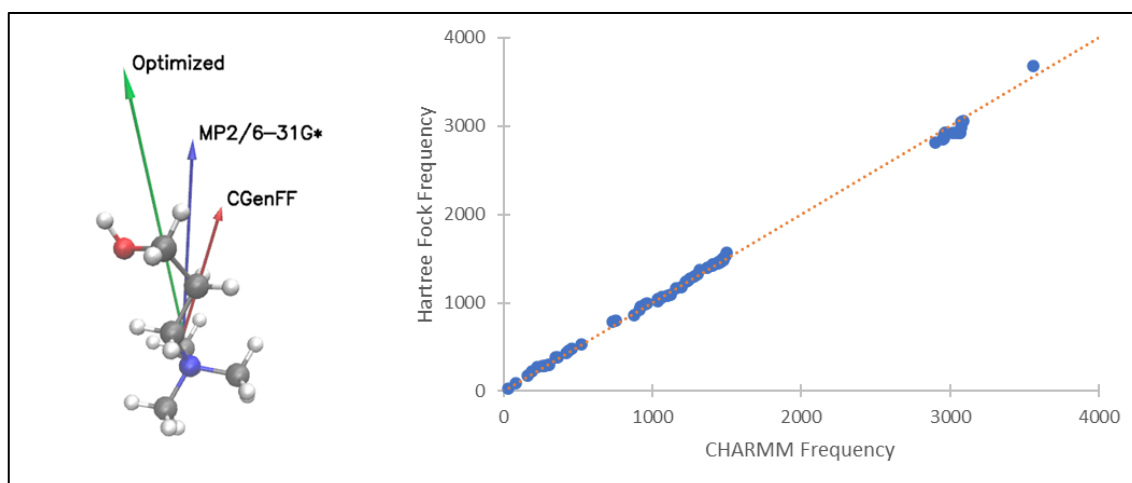
Figure 3.2. Electric dipole moments, originating from the center of mass, as calculated quantum mechanically using MP2/6-31G* (Blue arrow), or from MD simulations using the optimized parameters (Green arrow) or the initial CGenFF guess (Red arrow). Normal mode frequency

To validate the charges which are optimized charges in Table 3.3, the electric dipole moments were calculated. Based on the result of dipole moments, the optimized and initial CGenFF values are away from MP2/6-31G* as 16-18°. On the other hand, while the magnitude of CGenFF is 22% lower than quantum calculation, the optimized one is 1.20 times of QM dipole moment. The comparison of vibrational frequencies was obtained by vibran module of Charmm for MM and Gaussian 09 (HF/6-31G*) for QM

calculations (Figure 3.2). The mean absolute deviation between MM and QM frequencies is 3.02%.

Table 3.3. Atom types and charges of atoms and optimized charges

Name	Type	CHARMM	Name	Type	CHARMM
N	NG3P0	-0.60	C2	CG334	-0.35
C1	CG324	-0.10	H21	HGP5	0.25
H11	HGP5	0.25	H22	HGP5	0.25
H12	HGP5	0.25	H23	HGP5	0.25
C6	CG321	-0.18	C3	CG334	-0.35
H61	HGA2	0.09	H31	HGP5	0.25
H62	HGA2	0.09	H32	HGP5	0.25
C5	CG321	0.05	H33	HGP5	0.25
H51	HGA2	0.09	C4	CG334	-0.35
H52	HGA2	0.09	H41	HGP5	0.25
OH1	OG311	-0.65	H42	HGP5	0.25
HO1	HGP1	0.42	H43	HGP5	0.25

QM and MM water interactions were produced to control charge of atoms. The distances of optimized water − atom interactions of QM and MM are calculated lower than 0.41 Å, and MM interaction distance are found between 1.79 and 2.79 Å (APPENDIX J). Difference of internal bond distances (QM -MM) are diverse from 0.00013 to 0.012 Å and RMSE is nearly 5×10^{-3}. QM – MM calculated angle gaps are individually lower than 3°. RMSE of angle optimization was calculated as 1.5 (Figure 3.3). After charge, bond and angle optimization, potential energy surface graphs of 3-hydroxy-N,N,N-trimethylpropan-1-aminium were obtained as shown in Figure 3.4. Average RMSE of these graphs is 0.45, and the individual values of dihedrals labeled as C2-N-C1-C6, C3-N-C1-C6, C4-N-C1-C6, N-C1-C6-C5, C1-C6-C5-OH1 and C6-C5-

OH1-HO1 are 0.21, 0.21, 0.21, 0.93, 0.33and 0.81, respectively. Finally, to create whole monomer structure, the methyl group and side chain was merged (see Figure 3.5). According to potentials surface scans, only RMSE of dihedral which connect ring and side chain is little higher than confidence level (nearly 0.71).
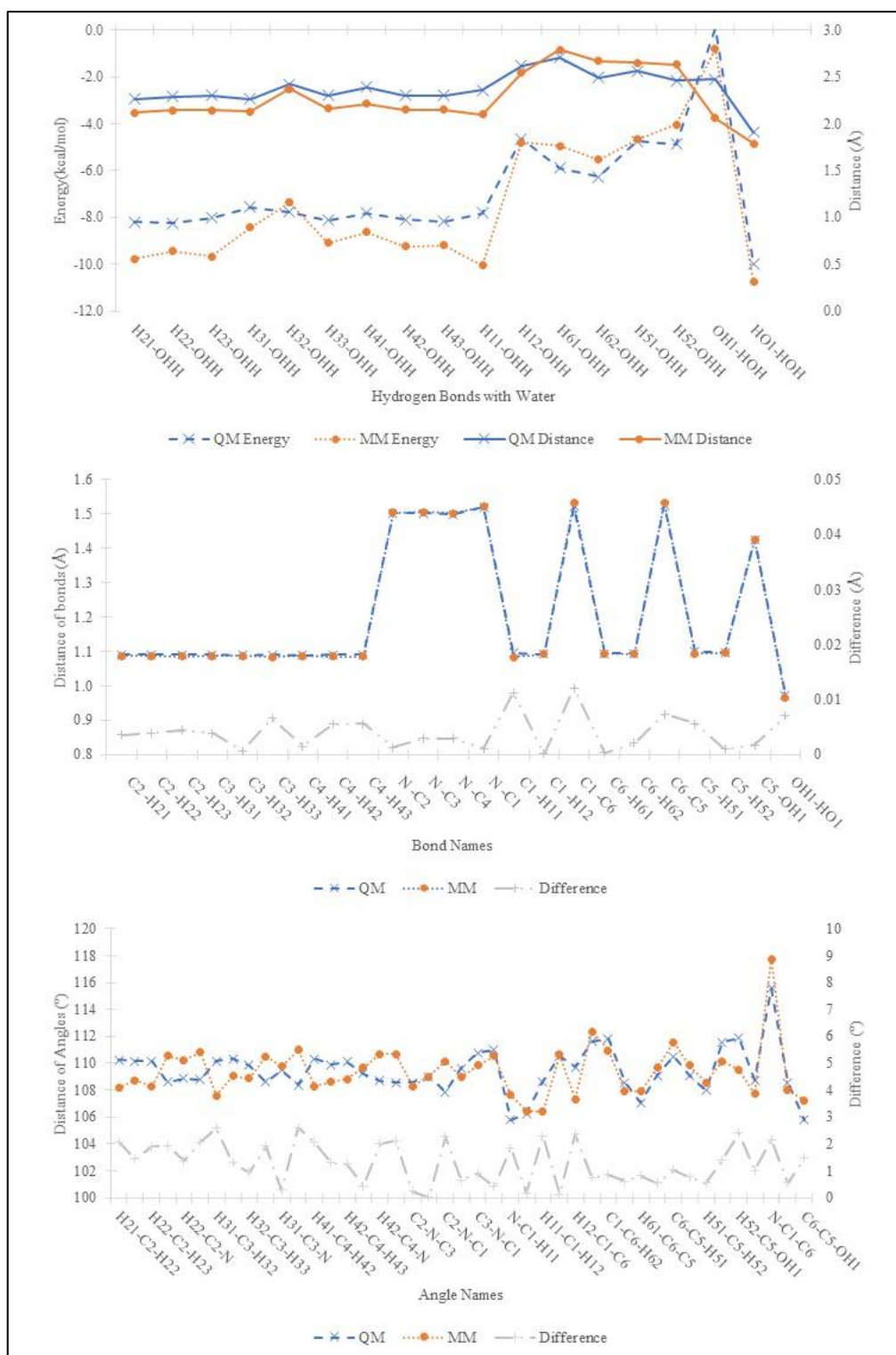
Figure 3.3. Water Interaction Comparison, Bond and Angle Comparison between QM and MM
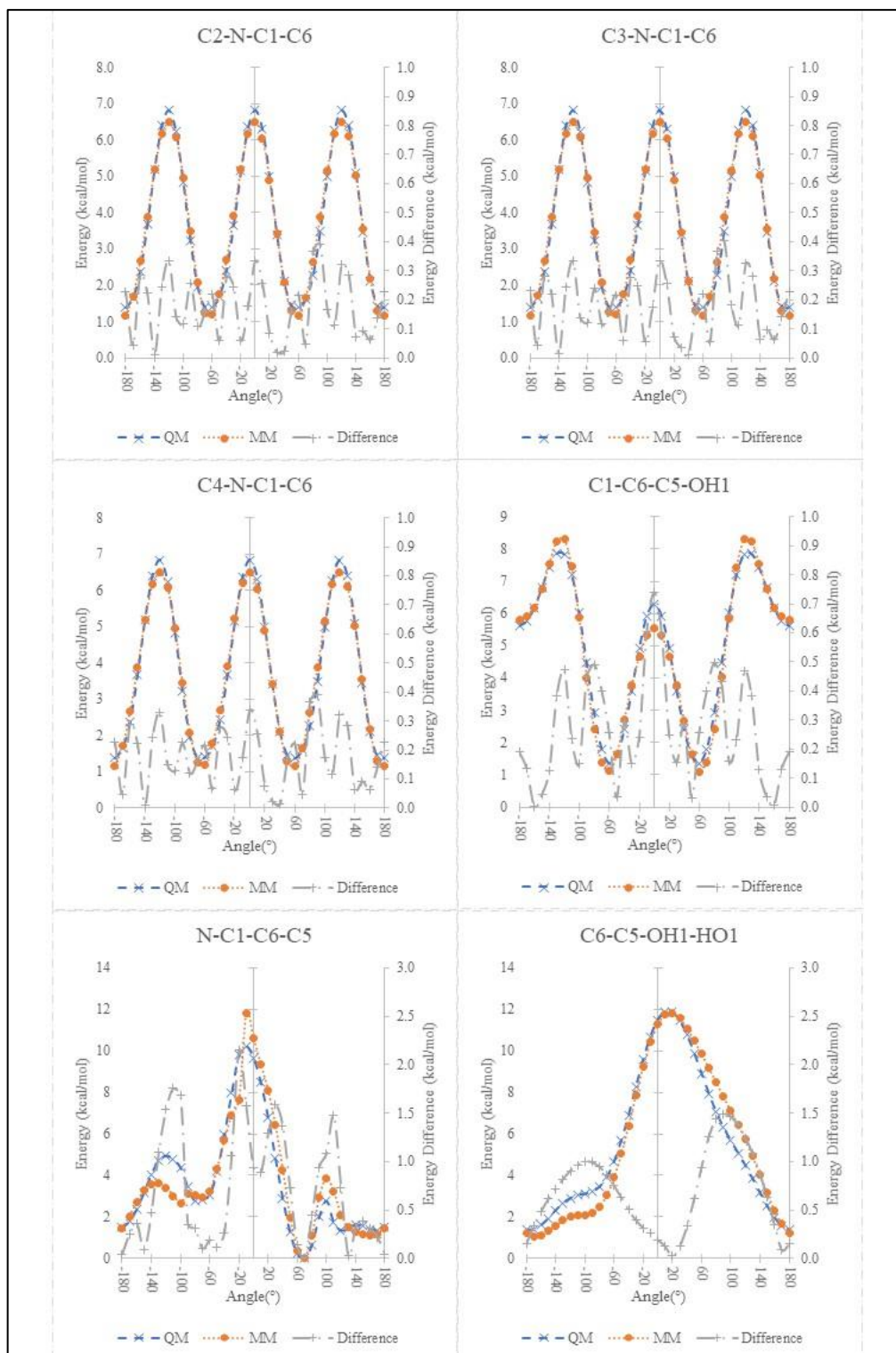
Figure 3.4. PES of dihedrals
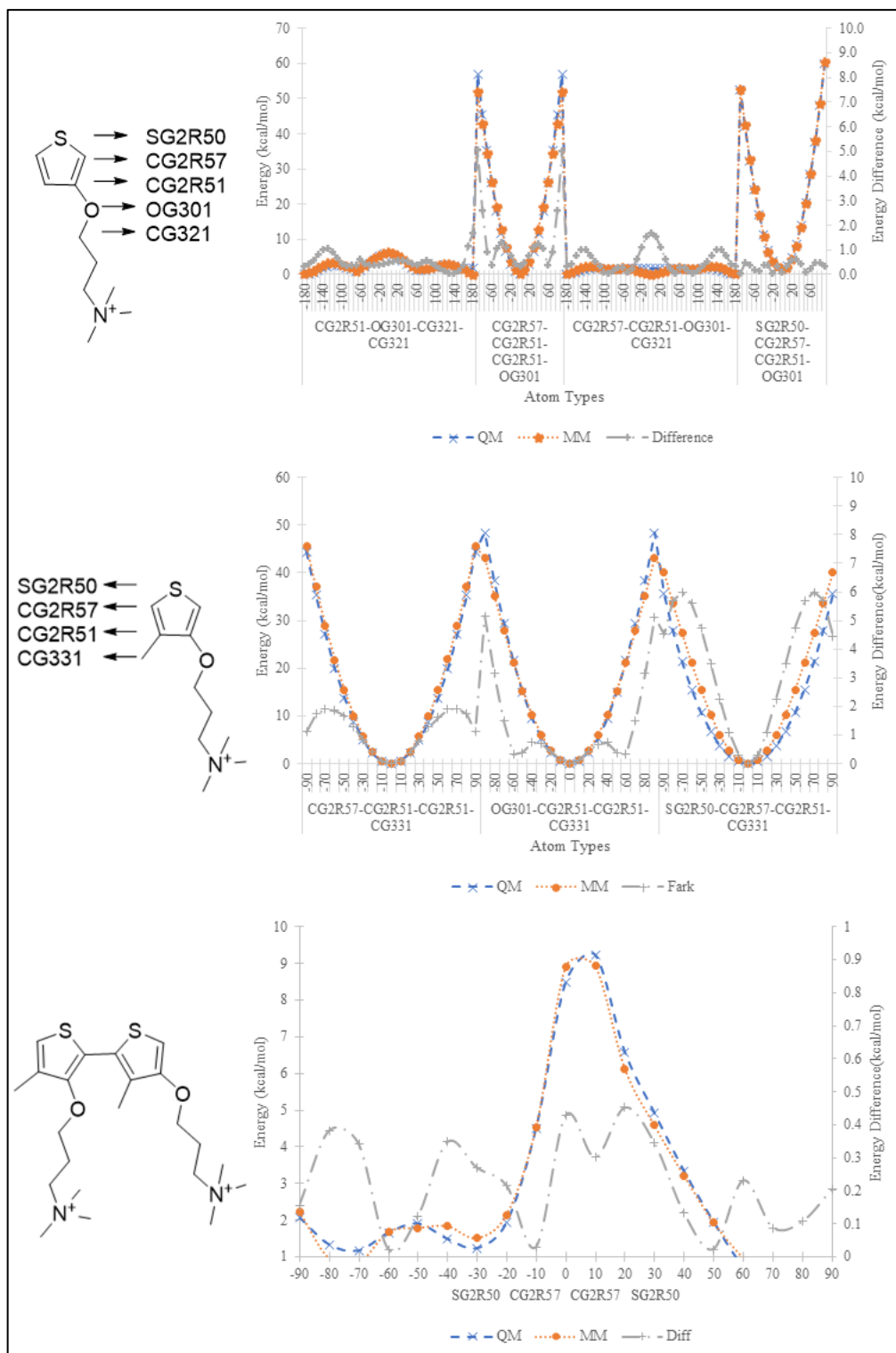
Figure 3.5. PES Graphs of Dihedral (Merged Structures)

3.1.2.2. Parametrization of Poly-(3-(2-((4-methylthiophen-3-yl) oxy) ethyl)-1-methyl-4H-1λ4-imidazol-3-ium)

Imidazolium ion parameters is contained in CGenFF parameters (RESI IMIM), therefore the imidazolium ion structure was combined at previously parametrized side chain of cationic polythiophene. The optimized charges were given in the Table 3.4. The new unidentified dihedral force constants which are CG321 – CG324 – NG2R51 – CG2R51, OG301 - CG321 – CG324 – NG2R51, and CG321 – CG324 – NG2R51 – CG2R53 were calculated. According to these PES scan graphics (see Figure 3.6), the RMSE value of the dihedrals was found as nearly 0.37.

Table 3.4. The Charges of 3-(2-((4-methylthiophen-3-yl) oxy) ethyl)-1-methyl-4H-1λ4-
       imidazol-3-ium

	Names	Types	Charges	Names	Types	Charges
	C1	CG2R57	0.12	H6	HGA2	0.09
	C2	CG2R51	-0.07	O1	OG301	-0.38
	C3	CG2R51	0.20	N1	NG2R52	-0.07
	C4	CG2R57	0.12	N2	NG2R52	-0.07
	S1	SG2R50	-0.10	C9	CG2R53	0.32
	C5	CG2R51	0.19	H7	HGR53	0.18
	H1	HGR52	0.13	C10	CG331	-0.27
	C6	CG2R51	0.19	C11	CG334	-0.27
	H2	HGR52	0.13	C7	CG324	-0.18
				C8	CG321	-0.07

All aliphatic hydrogens charges are +0.09
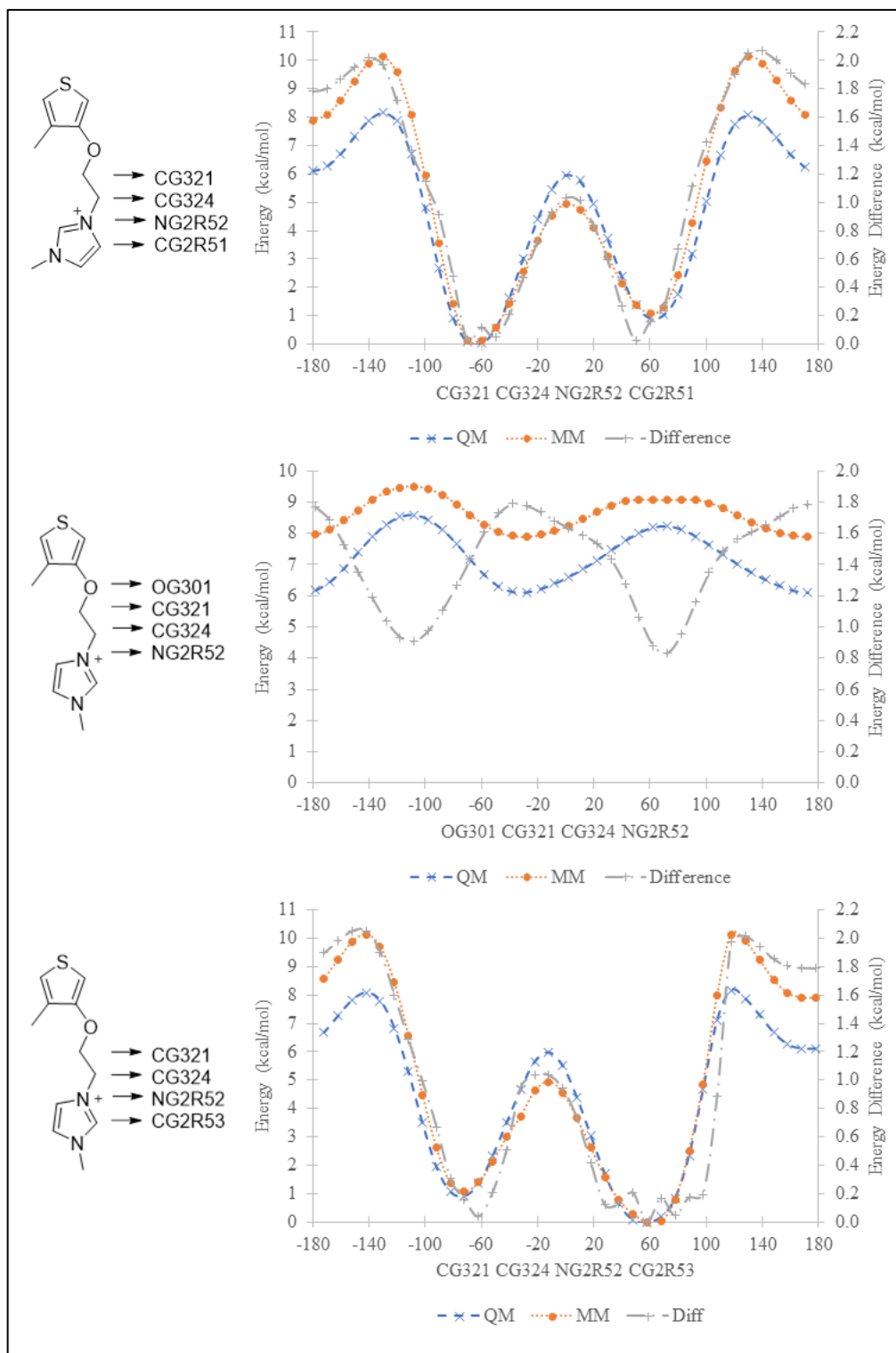
Figure 3.6. PES Graphs of Dihedrals (for Optimization of Imidazole group)

3.1.3. NBFIX Parameters

At this part, Hanif M. Khan and the study for atoms charged to CHARMM parameters. Corrections of LJ potential parameters (NonBonded FIX parameters (NBFIX)) was made using the method specified by their colleagues (Khan, MacKerell, and Reuter 2019). First about portions optimized using BLYP-D3/cc-pVTZ with dispersion correction (D3) and then optimized interactions LJ energies with different distances SAPT2+ was scanned using MM energies at the same distances are found using NAMD and QM Scanning was continued until they matched their energies .

3.1.3.1.Trimethyl Amine Interactions (TMA)
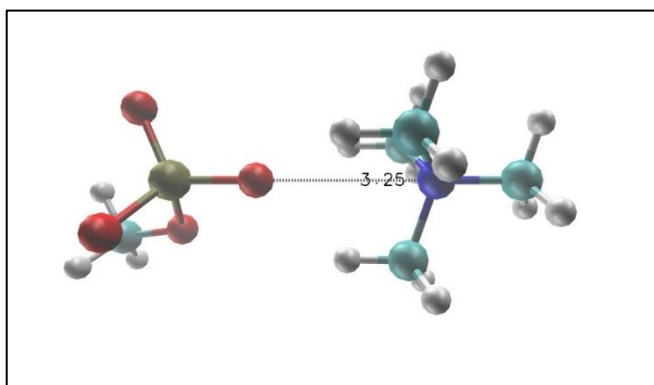
Figure 3.7. Anion (Phosphate) - Cation (TMA) Interaction

Interaction between tetramethyl ammonium (TMA) and phosphate (see Figure 3.7) was examined at Figure 3.8. In that figure, the blue lines refer to quantum mechanical calculations, and others belongs to molecular simulations. Initial molecular simulation (MM^i) data which include results of simulation before optimization of LJ (Lennard Jones) potentials are shown as orange lines. According to MM^i, the minimum distance of the interaction was calculated over 3 Å. After adding NBFIX parameter, the distance was corrected as 2.85 Å which is same for MM and QM calculations. On the other hand, the energy difference for there is nearly 14 kcal/mol.
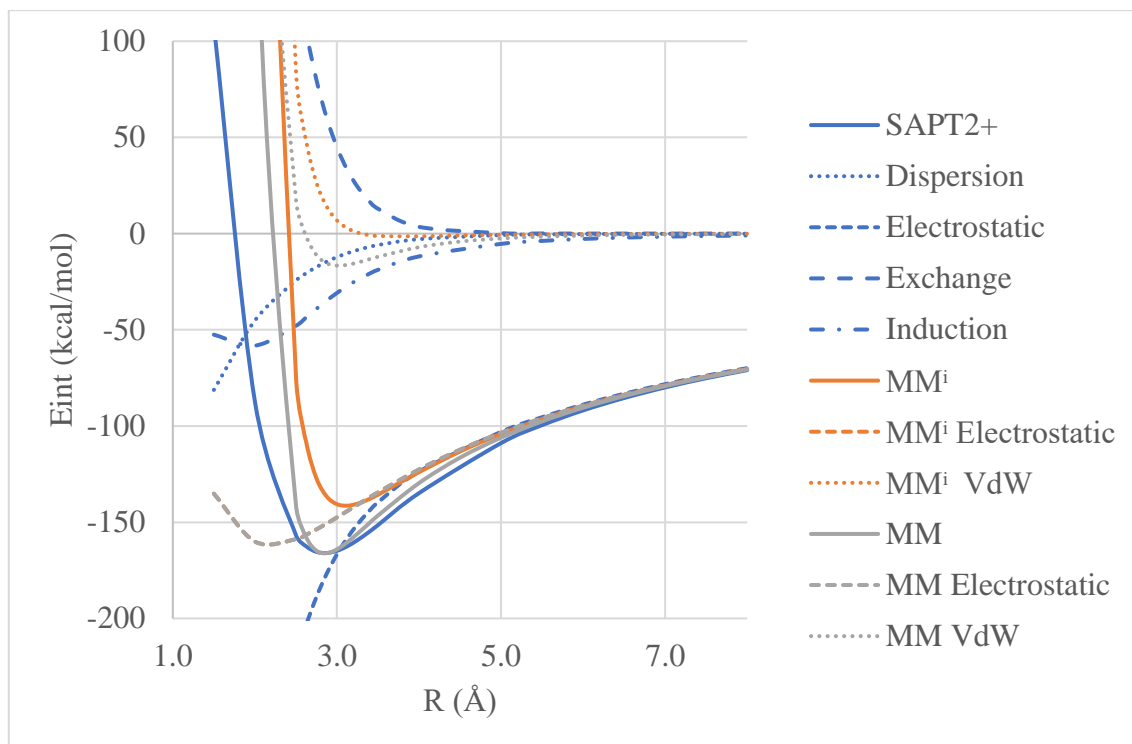
Figure 3.8. LJ (Lennard Jones) Potential of Anion (Phosphate) - Cation (TMA) Interaction

After study of phosphate, the 9H-purin-6-amine − TMA interaction was investigated to complete all adenosine phosphate structure which are used in simulations. This interaction was named as π − cation interaction (see Figure 3.9). For this correction, the distance of these groups is scanned from 2 Å to 8 Å.
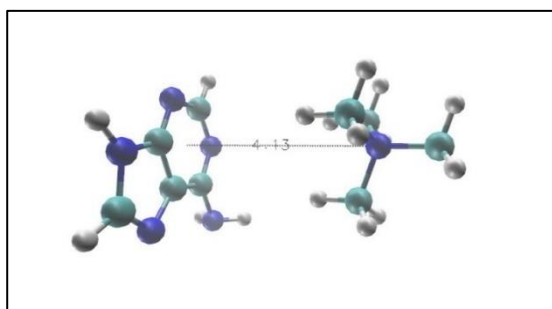
Figure 3.9. π (PUR) - Cation (TMA) Interaction

The LJ potential of π - cation (TMA) interaction graph was drawn in Figure 3.10. If the NBFIX parameter was not used, the minimum distance does not change but

the QM energy is lower than MM^i energy nearly 1.2 kcal/mol. NBFIX parameter correct this situation, and energy difference was lowered to 0.2 kcal/mol.
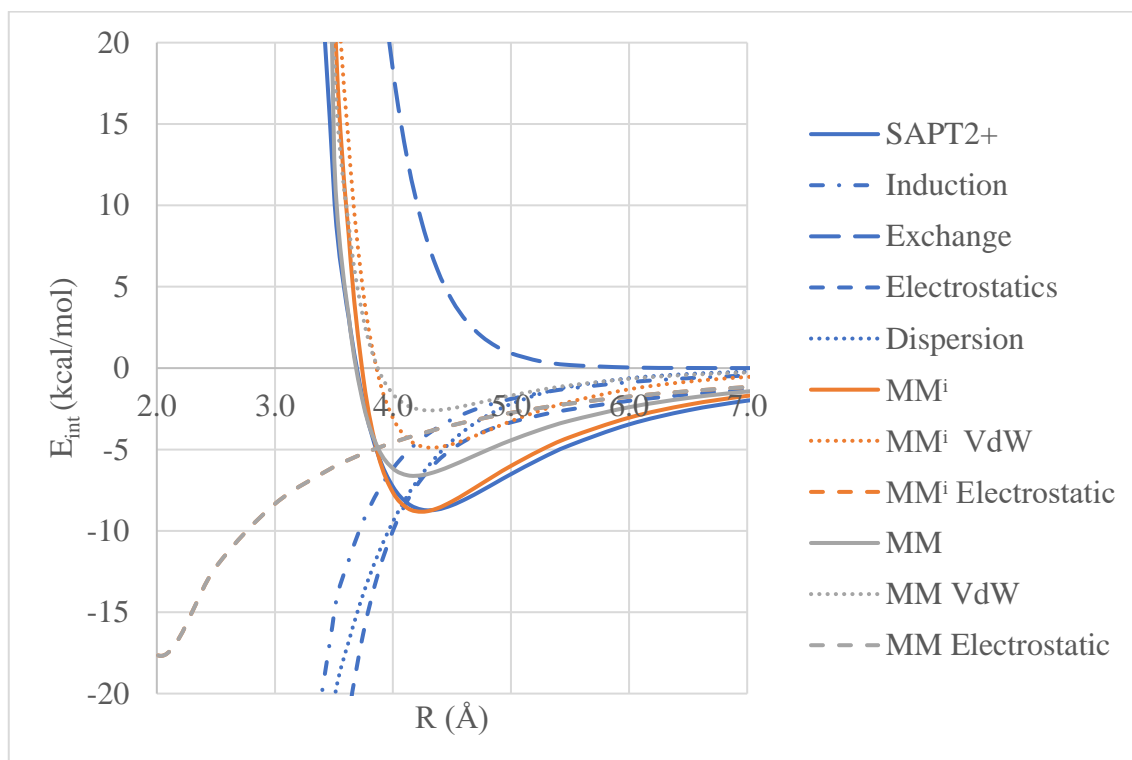
Figure 3.10. LJ (Lennard Jones) Potential of π (PUR) - Cation (TMA) Interaction
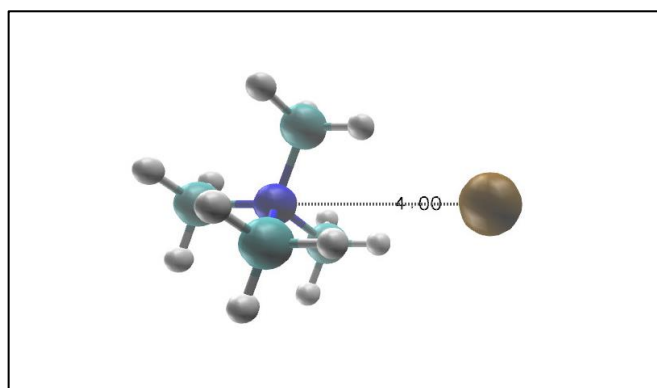
Figure 3.11. Chlorine Ion - Cation (TMA) Interaction

The last part for NBFIX for Parametrization of Poly- N, N, N-trimethyl-3-(4-methylthiophen-3-yl) oxy) propan-1-aminium, considering the simulations performed at

the presence of chlorine ion was shown in the LJ potential energy graphs (see Figure 3.11 and Figure 3.12)

As shown in Figure 3.12, NBFIX parameter effect not only the minimum energy distance but also minimum LJ potential energy of interaction between chlorine ion and TMA. After the parameter, the minimum distance of QM and MM was equalized at 3.5 Å and the energy difference was calculated as 0.5 kcal/mol.
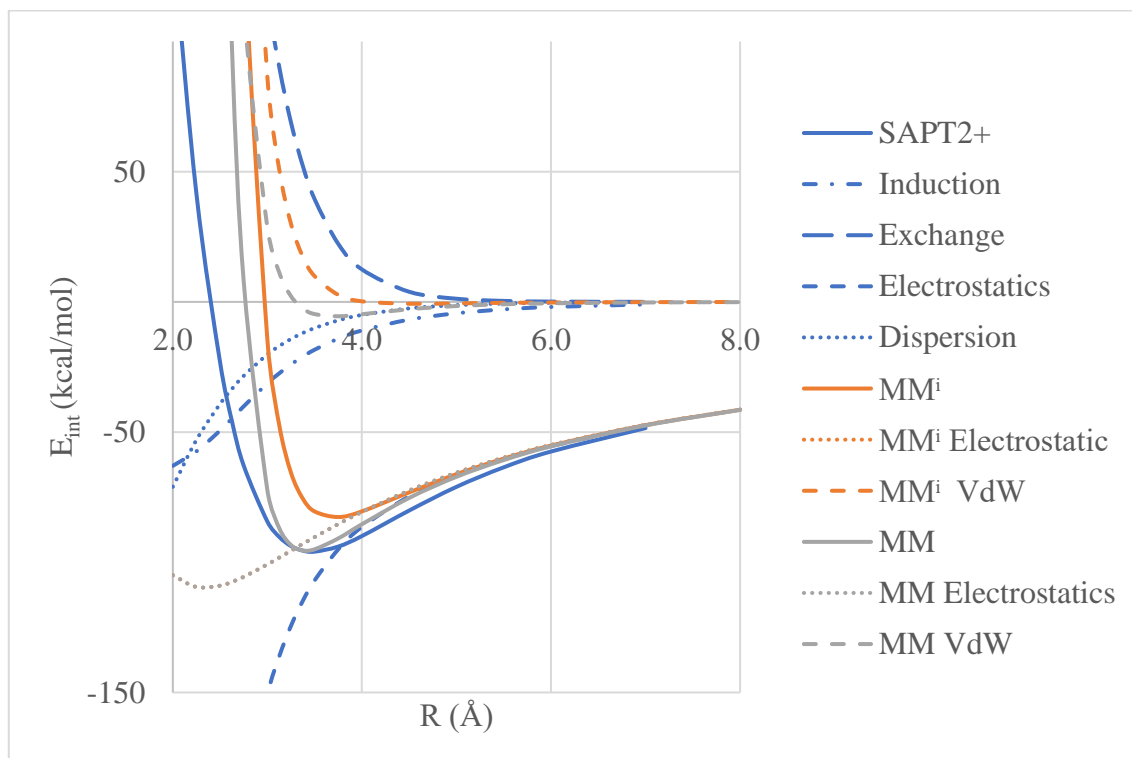
Figure 3.12. LJ (Lennard Jones) Potential of Chlorine Ion - Cation (TMA) Interaction

3.1.3.2. Imidazole Interactions (IMD)

To calculate NBFIX parameter for 3-(2-((4-methylthiophen-3-yl) oxy) ethyl)-1-methyl-4H-1λ4-imidazol-3-ium, the imidazole interactions between 1,3-dimethyl-1H-3λ^4-imidazole and phosphate, 9H-purin-6-amine and chlorine ion were considered.

The distance between oxygen atom and mass weighted center of imidazole was scanned for LJ potential. Before the NBFIX correction, the difference of minimum energy QM and MM^i was 40 kcal/mol. When the correction was used, the LJ potential

distance was calculated as 2.825 Å and it is equal to its QM value. The MM energy was found as -168 kcal/mol.
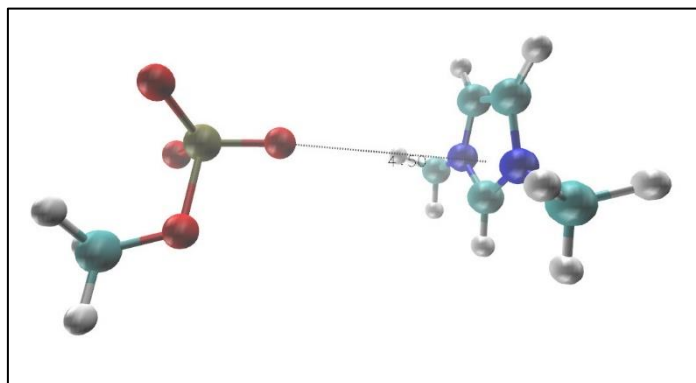
Figure 3.13. Anion (Phosphate) - Cation (IMD) Interaction
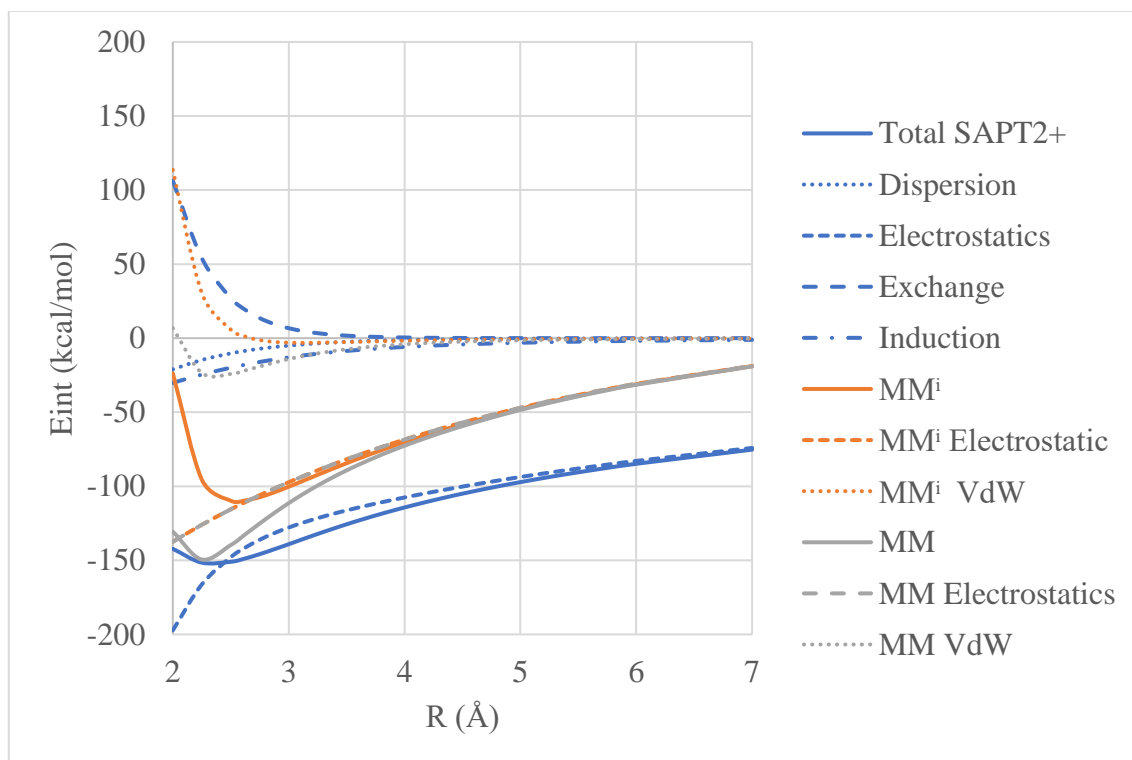
Figure 3.14. LJ (Lennard Jones) Potential of Anion (Phosphate) - Cation (IMD) Interaction
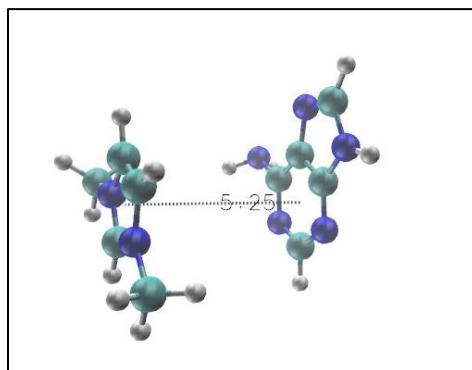
Figure 3.15. π (PUR) - Cation (IMD) Interaction

π (PUR) - cation (IMD) interaction was initialized to characterized NBFIX of adenosine part of AMP, ADP, or ATP (see Figure 3.15). At Figure 3.16, the MM^i and QM energies are not different like interaction between cation (IMD) and anion (Phosphate). After MM applied, it was seen that NBFIX is completely successful equalizing the minimum distance of QM. And also, this situation is valid for energy, and the difference is for energy for 0.2 kcal/mol.
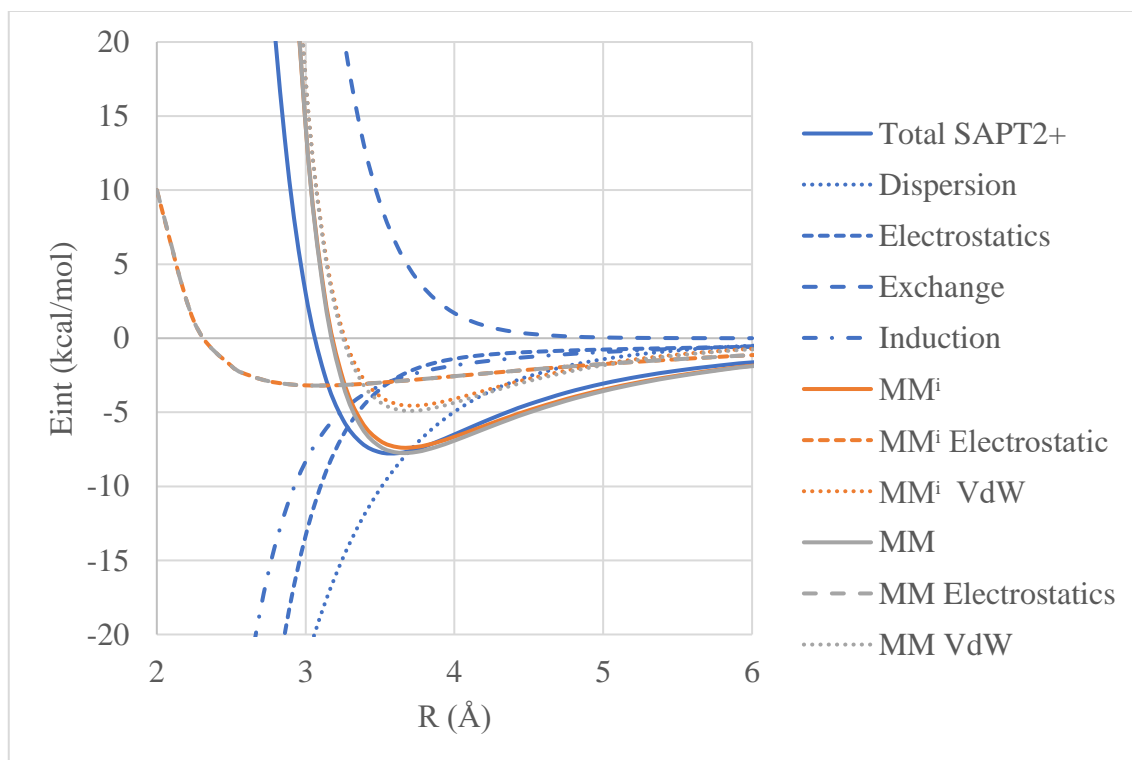
Figure 3.16. LJ (Lennard Jones) Potential of π (PUR) - Cation (IMD) Interaction
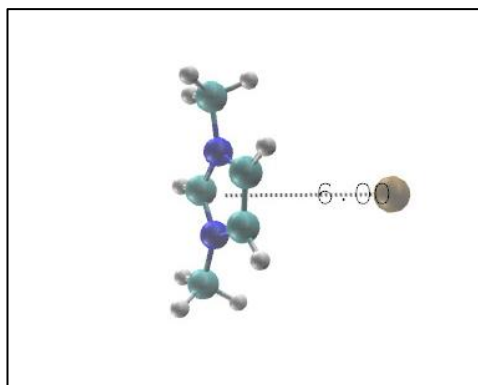
Figure 3.17. Chlorine Ion - Cation (IMD) Interaction

Like at previous title, it is shown that chlorine ion and dimethyl imidazole interaction was examined for simulation constructed with Cl ion (see Figure 3.17). The difference nearly 16 kcal/mol was adjusted by NBFIX parameter. MM and QM energy difference becomes less than one thousandth kcal/mol. The minimum distances are at 3Å (Figure 3.18).
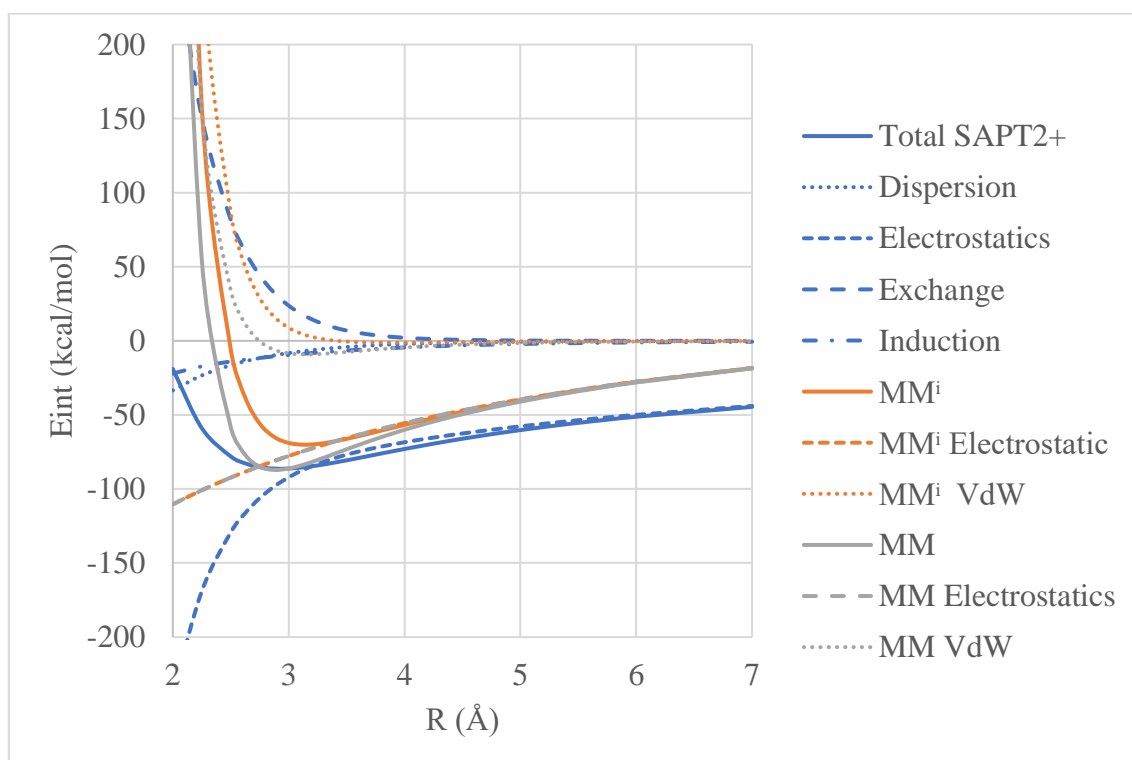
Figure 3.18. LJ (Lennard Jones) Potential of Chlorine Ion - Cation (IMD) Interaction

3.2.Molecular Dynamics Results

3.2.1.CPT parametrized using ffTK tool in VMD

Table 3.5. The computational and experimental UV-VIS absorption λ_{max}

	O1	O1 + AMP	O1 + ATP
λ(nm)	292	302	305
λ^*_{exp}(nm)	400	416	538

*The experimental λ_{max} (Li et al. 2006a)

In this part, MD simulations of oligomer which formed by 20 monomer of N, N, N-trimethyl-3-(4-methylthiophen-3-yl) oxy) propan-1-aminium (see in Figure 1.6. Poly- N, N, N-trimethyl-3-(4-methylthiophen-3-yl) oxy) propan-1-aminium) was performed using ffTK parameters. Three different simulations were carried out to investigate the responds of CPT to the addition nucleotides and the effect of the type of nucleotide to the complexations. One of them consist of only oligomer, others involve oligomer(20-mer) combined with nucleotides; i) 10 AMP and ii) 5 ATP. The simulation box length was arranged w.r.t the complex length with initial configuration that is placed diagonally in a cubic box with one side varying between 78 and 88 A. TIP3 water molecules were added as solvent to the simulation box. Then, the initial systems were minimized. In this part, the cut-off for nonbonded interactions was set to 100 A, which is more than box dimensions. After minimization step, the timestep was given taken as 2 fs and cut-off value was lowered to 14 A. The temperature of the systems was gradually increased from 0 to 293 K. After that, equilibration step was applied as N, V, T ensemble for 10 ns. Finally, production step (N, P, T) was performed for 100 ns, and the energies and coordinates of system were saved every 0.05 ns.
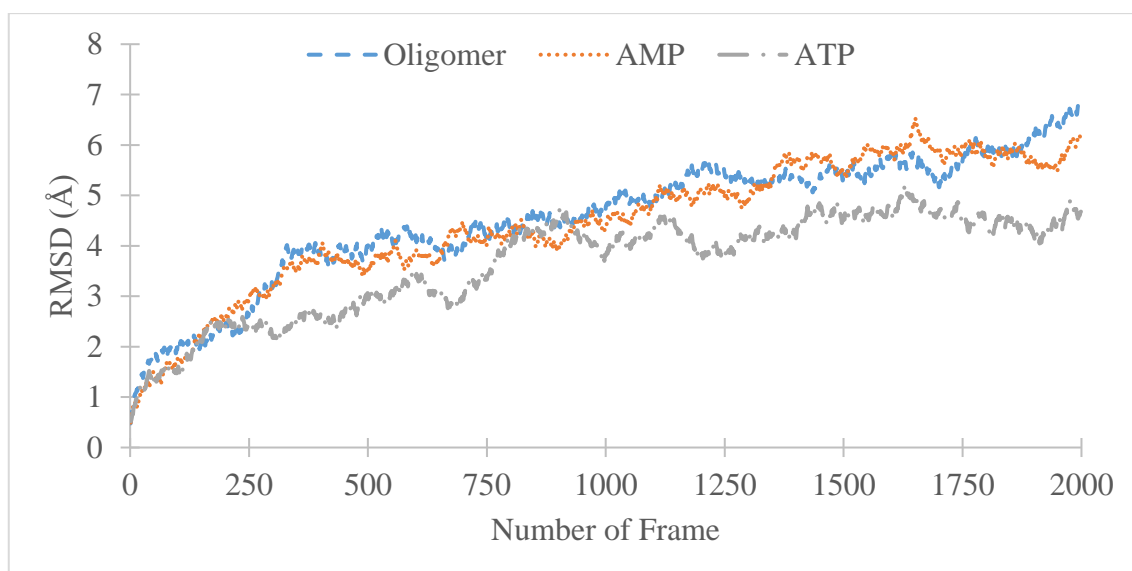
Figure 3.19. Time evolution of RMSD of 20-mer in water (blue), ATP (red) and AMP (gray) complexes

The only experimental data which can be compared to validate the generated force field of the cationic PT subject to this part of thesis is the UV-VIS spectra of the complexes with biological molecules (ATP and AMP). There are no X-RAY or NMR data available in the literature to our knowledge for this system. The UV-VIS calculations have been performed for the conformer of the backbone of the complex and oligomer composed of 20 monomers which has an average radius of gyration and end to end distance given in Table 3.5 at TD/HF/3-21G level of theory in water. Both experimental and theoretical results showed that, the oligomer responded as a red shift in the absorption spectra upon the complexation with AMP and ATP. However, the simulation results provided a small red shift. The errors in absorption wavelength calculations can be explained by the accounts; the calculations involve only one 20mer with 5 ATP or 10 AMP molecules but in experiments stacking of complexes were supposed to form, also due to the size of the system and computational demands a low level of theory was used in the UV-VIS calculations.

To observe the effect of the number of phosphate groups on CPT complexes, two different systems were prepared with ten AMP, and five ATP molecules. These molecules have the same adenine group but the number of phosphate sides linking to adenine is different.

The equilibration of simulations is achieved as shown in Figure 3.19 which has time evolution of root mean square deviations (RMSD) calculated by using equation 2.3 where N and $\vec{r}$ are number of atoms, and position vector of these atom, respectively. The small RMSD values illustrates that the structural changes w.r.t the initial configuration ($\overrightarrow{r_{0,i}}$) at the propagation part of the simulation does not alter much.
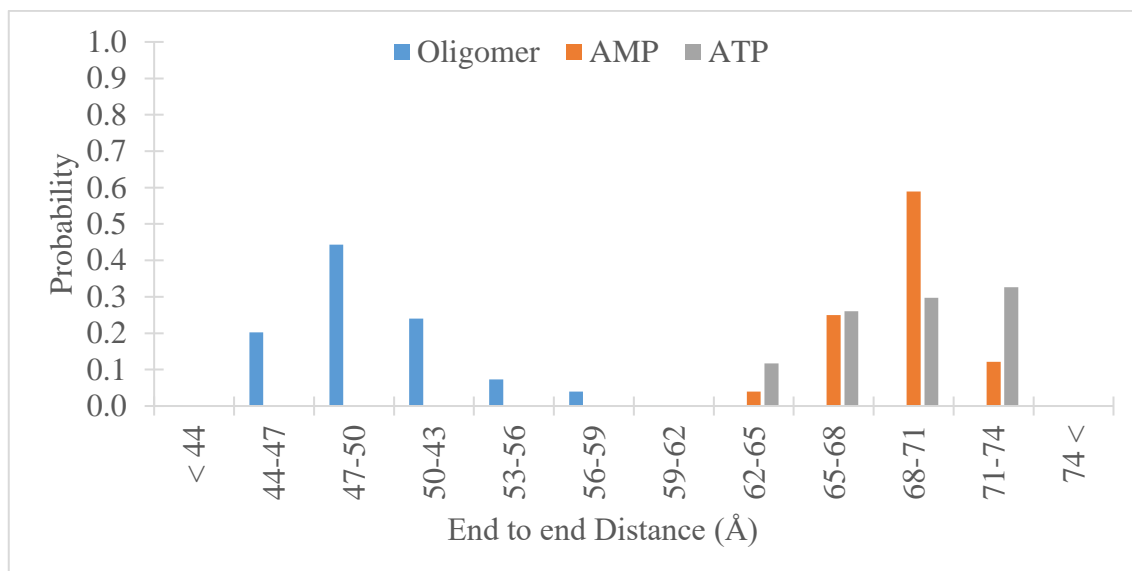
Figure 3.20. R_{ee} distributions(normalized) of 20-mer in water (blue), ATP (red) and AMP (green) complexes

The distribution of end to end distance (R_{ee}, the distance between H-atoms on the first and the last thiophene of 20-mer) which will be used as a measure of spatial extent of the CPT backbone and the oligomer (20-mer) radius of gyration (R_g) calculated by using equation 2.4 to indicate compactness of the system were given Figure 3.20, Figure 3.21 and, Figure 3.2 respectively. The complexes with ATP and AMP have the longer average (69 Å) and most probable end to end distances than 20-mer in water (49 Å) Based on our simulation results, it can be concluded that, the backbone of oligomer gets stretched with the addition of AMP and ATP.

Figure 3.20 shows that, there is a correlation between the number of phosphate groups on adenine and the compactness of the backbone structure of the oligomer in the complex. The most probable/average value of R_g increases with increasing number of phosphate groups. 20-mer in water have more compact structure than both complexes.

The initial configuration at the very beginning of the simulation and position at average R_g at the production part snapshots of 20-mer and its complexes are given in Figure 3.22. These structures reflect the findings obtained from R_g and R_{ee} analyses, the most elongated one is ATP complex, the least one is 20-mer.
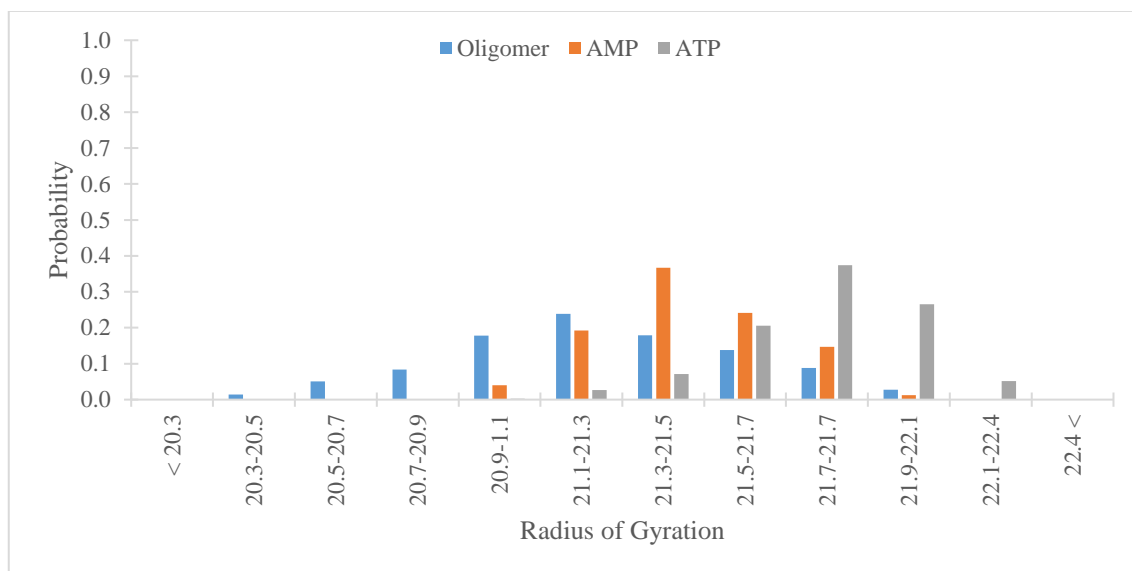
Figure 3.21. Distributions (normalized) of radius of gyration of 20-mer in water (blue), ATP (red) and AMP (green) complexes
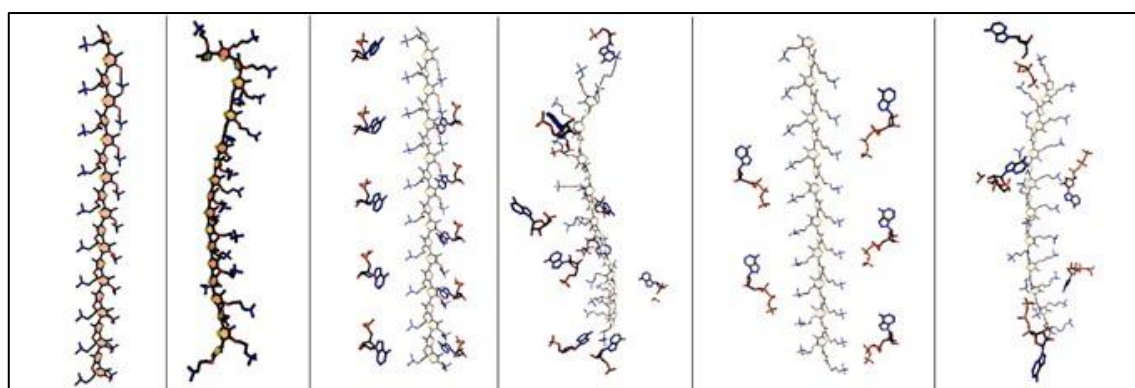
Figure 3.22. The snapshots of initial(left) and average R_g positions(right) of a) 20-mer, b) ATP complex and c) AMP complex

We have examined cation - anion and π - cation interaction in order to achieve the dominant interaction present in the complexes or to answer if there is a specific interaction for ATP, so that it can be attributed to spectroscopic behavior of its complex.

The cation - anion interaction and π-cation interaction was calculated using the distance between nitrogen atom of CPT and O atom on phosphate group of adenine molecule and between adenine six-membered ring and nitrogen atom of CPT, respectively (see Figure 3.23). The threshold distance was taken as 6.5Å.
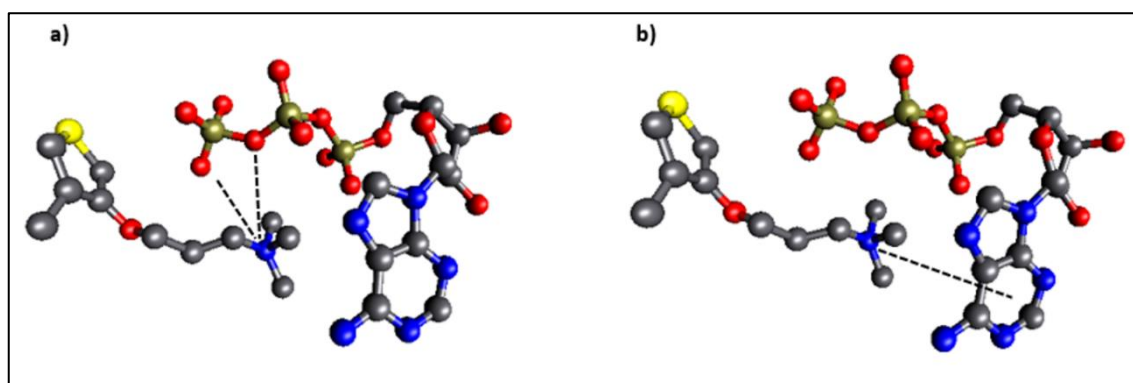
Figure 3.23. The representation of a) the cation - anion interaction, and b) π - cation interaction between 20-mer and phosphate group of adenine molecules.

The normalized cation anion interactions were computed by counting the distances which are less than the threshold value and dividing this value by the total number frames and corresponding number of possible interactions. According to Figure 3.24, ATP complex has higher cation-anion interaction strength than AMP complex. On the contrary, AMP complex which shows a minor shift in the experimental absorption spectra have stronger π - cation interaction. It seems that both electrostatic interactions play an important role on the structural and spectroscopic behavior of complexes, ATP complex have weak π- cation interaction which might be connected to strong red shift of CPT in UV-VIS spectra with the addition of ATP.
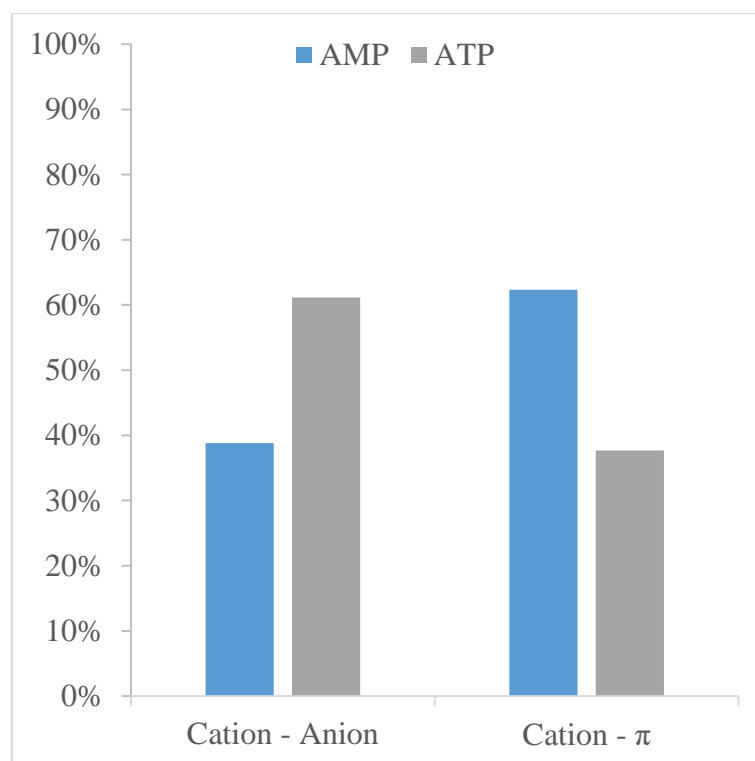
Figure 3.24. Normalized cation - anion and π - cation interactions between 20-mer and AMP, ATP along the simulations

We have also considered hydrogen atoms of ATP and AMP close to N, O and S atom on the backbone of the oligomer and H atoms on the oligomer near to O and N atoms on the adenine phosphates moieties to quantify interactions (the threshold distance in our calculations was taken as 3.5 Å). ATP and AMP have different numbers of oxygen atoms (5 ATP and 10 AMP were used in the complexations) and so the number of H-interactions are different in each complex. We have corrected this effect by dividing the normalized hit number by probability of H-interaction in each case. It should be noted that, we did not mention these interactions as hydrogen bonds since the angles were not considered. Hydrogens on the side groups and on the backbones of oligomer were considered separately to differentiate their contributions to these interactions which are shown in the Figure 3.25. AMP complexes have drastically higher amounts of H-interactions than ATP in most cases. The only considerable interactions present in ATP complex is between H atoms in the side groups of oligomer and N or O atoms in ATP, which may be due to electrostatic interactions. The strong interactions in AMP complex are observed on the H at the backbone (methyl group); N

atom at AMP and S atoms of thiophene; H atoms of AMP, in other words AMP most likely interact with the backbone of oligomer through the H-interactions which is completely absent in ATP complex. Once again, the red shift in ATP complex might be explained by the presence of weak interactions with the complex constituents.
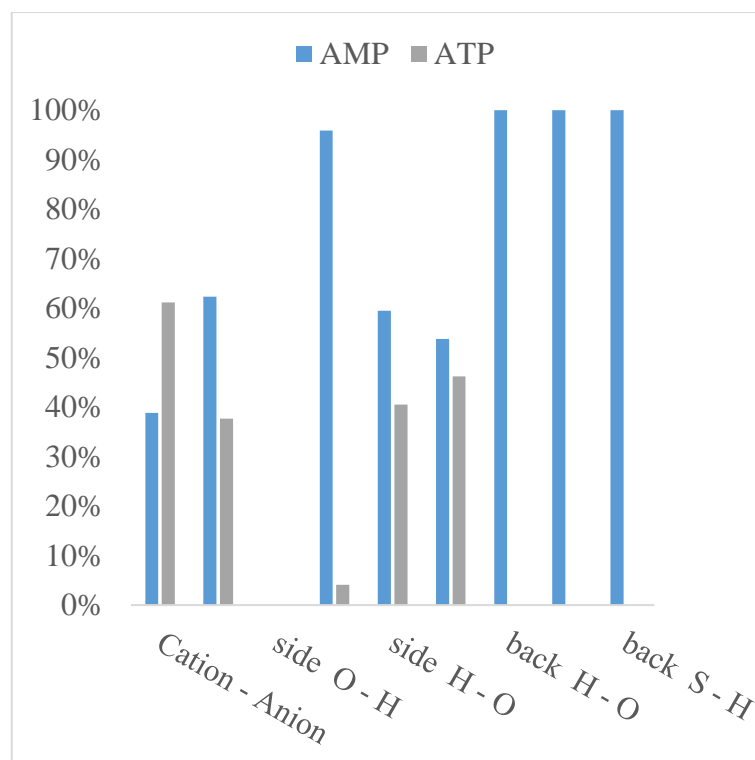
Figure 3.25. Hydrogen interactions (The first and second atoms belong to the oligomer and nucleotide groups respectively, side and back refers to side chain and backbone of the oligomer respectively.

In this part of the thesis, I have developed all-atom CHARMM compatible force field parameters sets for a cationic thiophene polyelectrolyte (N, N, N-trimethyl-3-(4-methylthiophen-3-yl) oxy) propan-1-aminium) polymer) to perform atomistic MD simulations of polyelectrolyte and its complexes with biologically active compounds. We have carried out MD simulations by using these parameter sets for the complex formation with different adenine phosphate molecules, ATP, and AMP. The structural analysis was made to understand the effect of phosphates on the spectroscopic behavior of the oligo-electrolyte. Based on the simulation results, ATP and AMP complexation make the oligomer backbone more elongated. The response of the oligomer to the

addition of ATP as a strong red shift in the absorption spectra might be explained by the weak π-cation interactions in ATP complex which prevents the complex structure from a random coil form. These simulations were done only for the validation of the force field parameters.

3.2.2. CPT parametrized using Charmm with NBFIX Parameters
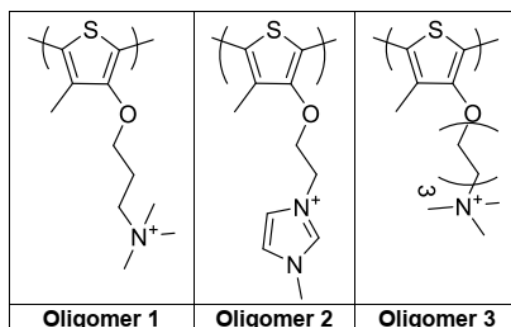
Figure 3.26. Oligomers of Simulations

Poly- N, N, N-trimethyl-3-(4-methylthiophen-3-yl) oxy) propan-1-aminium, Poly-(3-(2-((4-methylthiophen-3-yl) oxy) ethyl)-1-ethyl-4H-1λ4-imidazol-3-ium) and Poly- N,N,N-trimethyl-6-((4-methylthiophen-3-yl) oxy) hexan-1-aminium are named as O1, O2 and O3 respectively in the content of this thesis. Various simulations were performed using these oligomers and adenosine phosphates, and these are categorized as three main work groups, nucleotide trials, temperature trials and ion trials.

3.2.2.1. Nucleotide Trials

In this part, O1, O2 and O3 simulations have 70 Å x 70 Å x 70 Å box space except O1 and O3 having 10 ATP trials (90 Å x 90 Å x 90 Å). The simulations which have unbalanced charges are equalized adding sodium or chlorine ions. Oligomer – AMP, ADP, ATP and 10ATP simulations include respectively ten, six, five and ten nucleotides. The duration of all are 50 ns and for each of them snapshot was recorded every 0.05 ns. Parameters of simulations are cutoff value as 12 Å and applied Particle

Mesh Ewald. Langevin dynamics were used in order to control temperature and pressure. Temperature and pressure of nucleotide trials are respectively, 293K and 1 atm.

Before the RMSD calculations, the structures of oligomers are aligned to the first frame of the simulation with the mass weighed Kabsch algorithm. The extreme changes with this alignment were observed on RMSD, the distribution of radius of gyration and end to end distances of the oligomer structures. This situation can be easily seen on O1- ADP, O2 – ATP and O2-10ATP simulations (Figure 3.27, Figure 3.28, Figure 3.29). Except these, the displacement of oligomers during the production simulations are quite constant.
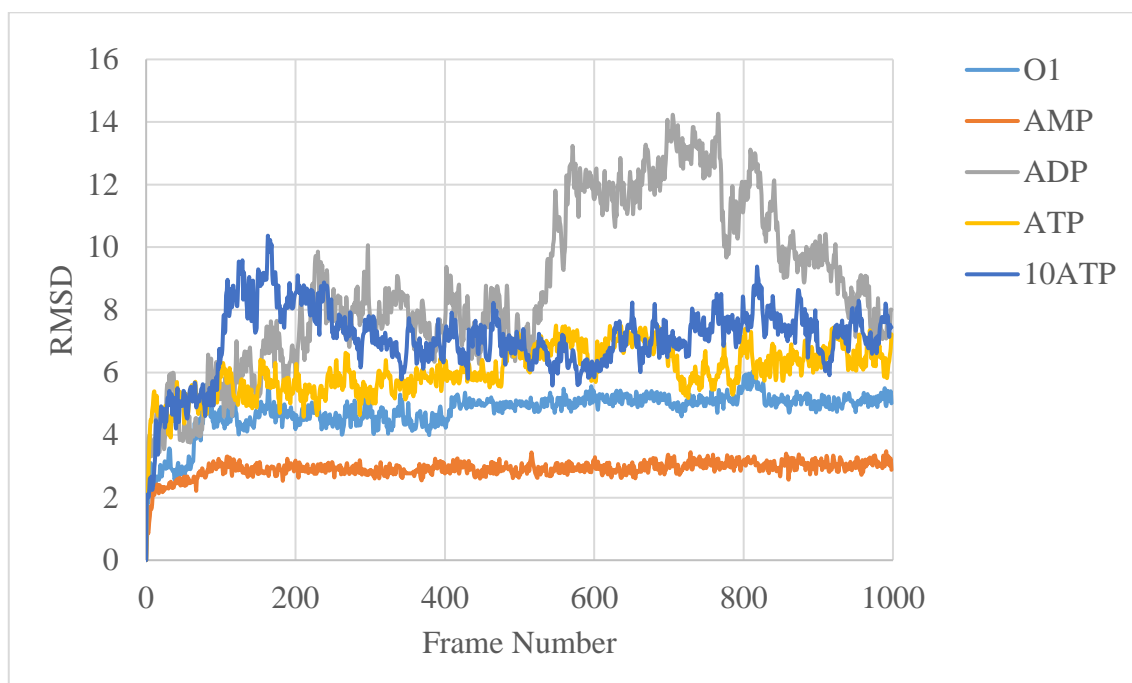
Figure 3.27. RMSD of Oligomer 1 with different Nucleotides

While the interval of radius of gyration which performed various nucleotides for ffTK parameters are narrow, for Charmm parameters they are much more different. For instance, average Rg value of AMP simulation (which performed with ffTK parameters) is 21.4 Å and its interval between ATP simulation is 0.4Å (Figure 3.20). On the other hand, when same condition simulations for Charmm were compared, the interval

between AMP and ATP simulations were calculated as 8.1 Å (Figure 3.30). This value is nearly 20 times bigger than ffTK simulations' interval.
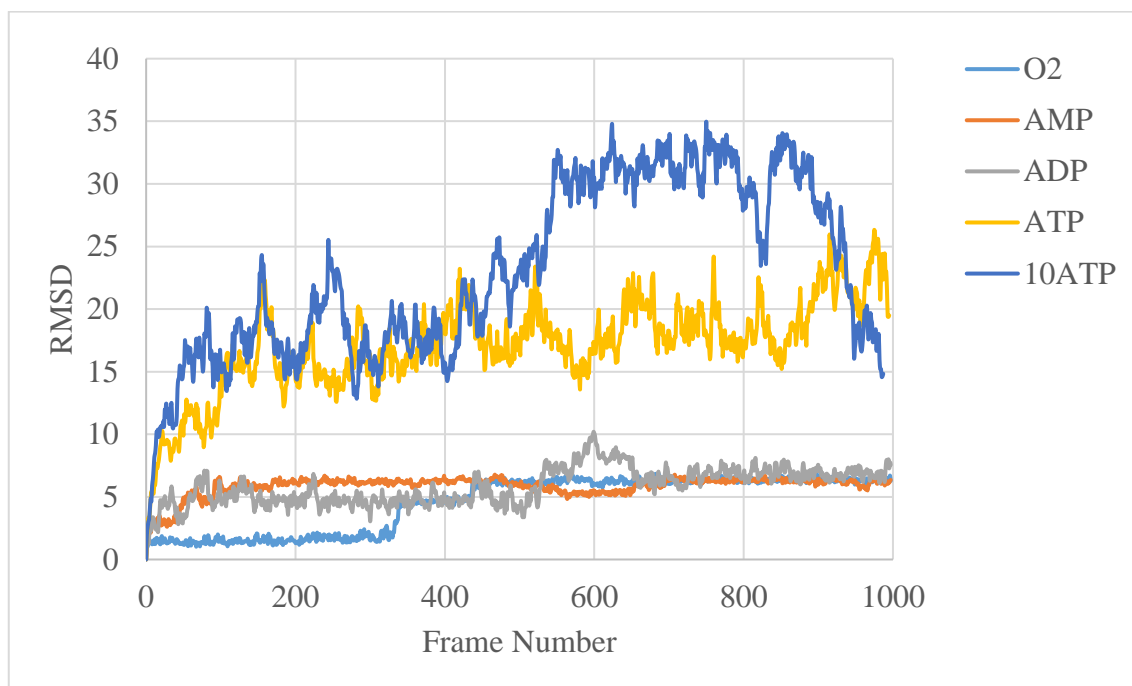
Figure 3.28 RMSD of Oligomer 2 with different Nucleotides
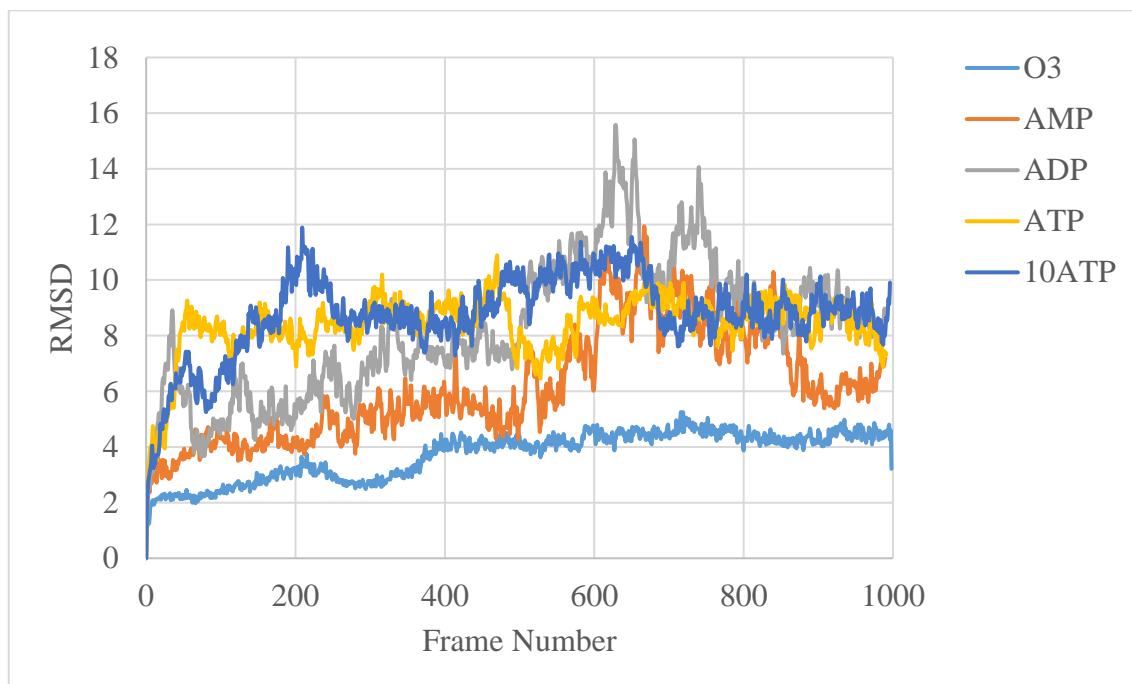
Figure 3.29. RMSD of Oligomer 3 with different Nucleotides

Additionally, the average end to end distance of AMP and ATP simulations performed ffTK are nearly same and its value longer about 21 Å than O1 simulation (Figure 3.21) which have only oligomer. But this situation were changed with Charmm parameters, the average R_{ee} of Charmm parametrized O1 simulation were calculated as 22.4 Å which is nearly half of ffTK parametrized simulation result. This value is also close to the R_g value predicted by Özenler, et.al. The notable novelty was observed as a huge difference of average R_{ee} in AMP simulations between ffTK and Charmm nearly 49 Å (Figure 3.36). That must be important for parameter choice, because according to Chun Li and coworkers (Li et al. 2006a), AMP and ATP interaction stress the oligomer structure to linearity, in consequence of that, the absorbance spectra show red shift. But Figure 1.8 could be interpreted that the AMP stress less effective than ATP stress.
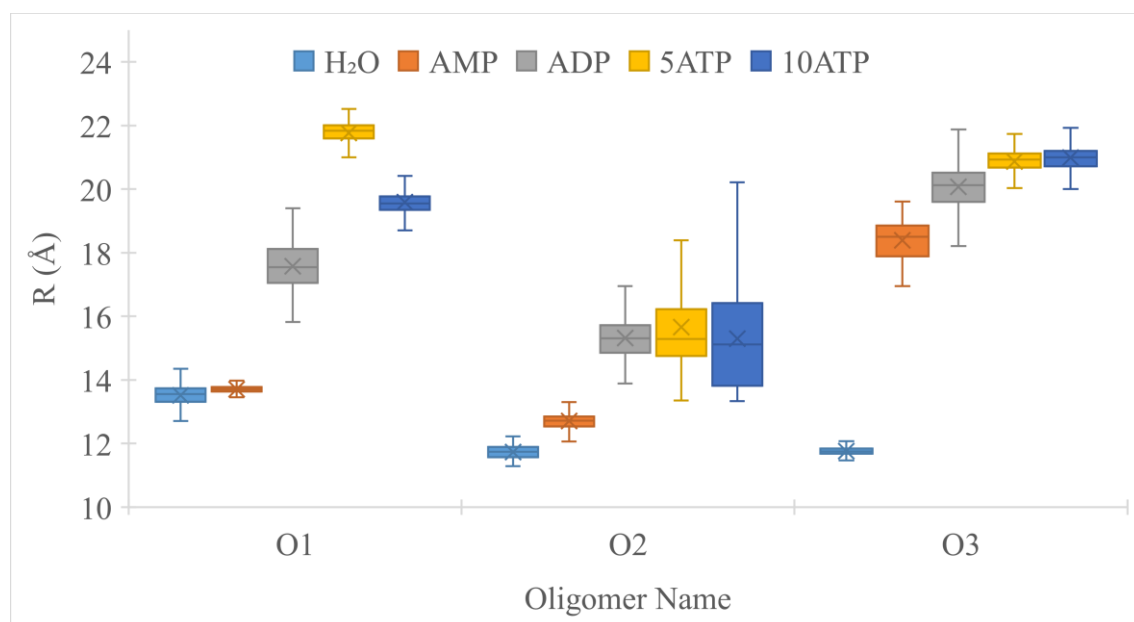
Figure 3.30. Radius of Gyration (O1: Oligomer 1, O2: Oligomer 2 and O3: Oligomer 3)

In this section, MD simulations of different adenosine nucleotides complexes with 3 different oligomer structures (see in Figure 3.26) whose parameters were created using Charmm parametrization strategy were performed. The radius of gyrations and end to end distances of oligomer's structures were analyzed from simulations' snapshots to find an explanation how the adenosine nucleotides affect the structure of oligomers. When R_g (Radius of Gyration) of O1 was investigated (Figure 3.30), It is

seen that asset of ATP decrease compactness of structure of O1. The R_g value of oligomer 1 in water and with AMP is nearly 13.5 Å. Even if double concentrated ATP interaction increase Rg of O1, generally ATP interaction increase the R_g over the 19.5 Å. That average Rg was recorded as 21.7 for ATP simulation in which ion balance was achieved. The structure of average R_g is given below and the longest O1 structure can be easily seen at Figure 3.31 d).
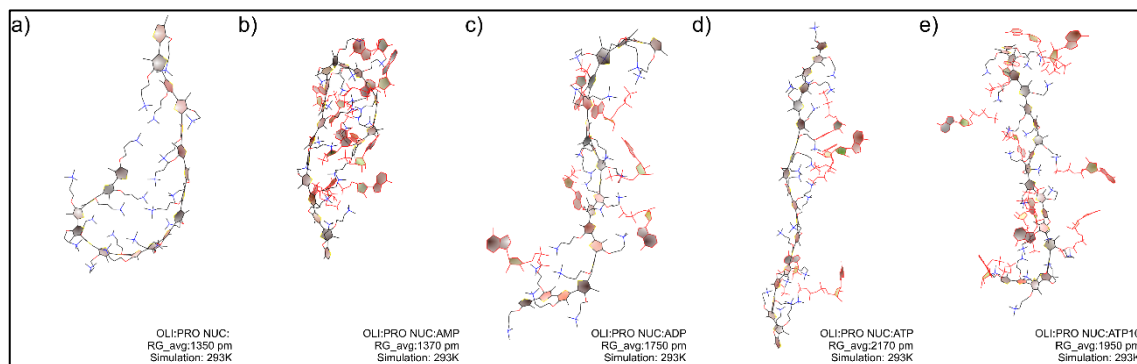
Figure 3.31. The Snapshots of O1 and Adenosine Nucleotides Complex at Average R_g of Oligomer Structure

Another structural parameter which can give an information about the size of oligomer is the end-to-end distance (R_{ee}). R_{ee} results of our simulations at various nucleotides are given in Figure 3.36. The simulations trends of R_g and R_{ee} are similar to each other, the lowest value of R_{ee} for oligomer 1 simulations belong to O1 in water as 22.3 Å and the longest structure is O1 with five ATPs (73.4 Å). At doubled concentration of ATP, the distance between first and last hydrogens on the thiophene decreased about 15.7 Å. Comparing structures of O1 and considering average R_g and R_{ee} distances at various nucleotide medium, the amount of phosphate groups are directly effective to stretch O1s structure (Figure 3.32). On the other hand, it has been seen that the number of phosphates decrease interaction between nucleotide and O1 (Figure 3.39). Despite that anion − cation interaction value for ADP and ATP (which have 5 nucleotides) are nearly same, the O1 structures compactness are very different. Addition of that, when analyzing the π − cation interactions for O1, AMP interactions are larger than doubled ADP interactions (these numbers are respectively, 4.3 x 10^{-2}, and 1.8 x 10^{-2}.) but the average R_g and R_{ee} of O1 are close to each other. Result of that,

there might be not any clue that O1 skeleton was directly affected from the count of electrostatic interactions between positive charge on the O1 and negative charge on the adenosine nucleotides. Despite of this situation, the analysis of R_g and R_{ee} of O1 simulations shows that the increasing individual charge of nucleotides enlarge the backbone of O1.
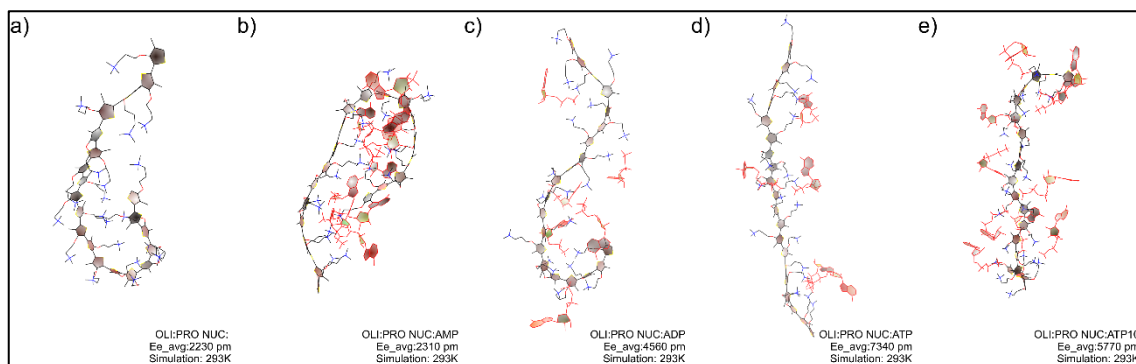
Figure 3.32. The Snapshots of O1 and Adenosine Nucleotides Complex at Average R_{ee} of Oligomer Structure
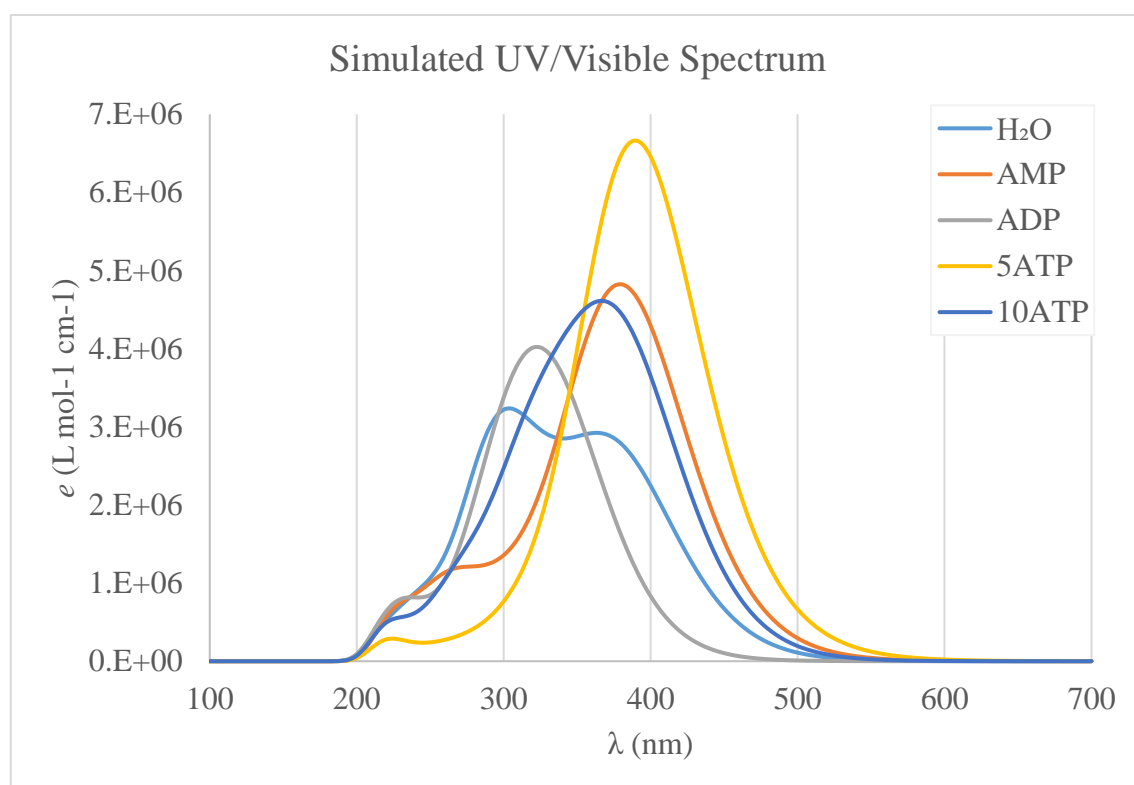
Figure 3.33. Simulated UV/Visible Spectrum of O1

As seen in Table 3.6, UV values calculated from simulations and experiments have the same trend. To be more specific, as the phosphate numbers on adenosine increase, the UV spectrums shift to red region, not only in the experimental one, but also in those calculated from the MD simulations. The simulations include only one oligomer; therefore, the aggregation effect of oligomers is ignored. But the UV spectrum of experiments having a bulk of oligomer involve aggregation stress on oligomer. This difference between experimental and simulated spectra in magnitudes can be explained as the effect of aggregation on the oligomer structure. According to Chun, Li and associate, the red shift of λ_{max} is related with the changes in the conformation and aggregation mode of O1 in which a more planar conformation induced upon noncovalent binding with ATP (Li et al. 2006a).

Table 3.6. Comparison table of UV calculated by MD simulations and experimental UV

	O1	O1 + AMP	O1 + ADP	O1 + ATP	O1+ 10ATP
λ_{avg} (nm) *	381	396	351	401	384
λ_{max} (nm) **	410	428	390	453	418
λ_{exp}(nm) ***	400	416	448	538	-

* The average value of UV calculations of 25 samples taken from MD simulations
** The maximum value of UV calculations of 25 samples taken from MD simulations
***The experimental λ_{max} (Li et al. 2006a)

Simulated UV/Vis spectrum of each simulation given in Figure 3.33 is based on TD-HF/3-21 calculations of each 25 snapshots recorded. The simulated UV-VIS spectra were obtained by using the equation 3.1, where *n* is number of states, *f* is the oscillator strength, $\tilde{v}$ is excitation energy and σ is the standard deviation in wavenumbers is used at below. At the above section, Özenler, S. et. al. mentioned that while bulk oligomer (poly [1,4-dimethyl-1- (3- ((2,4,5- trimethyl thiophen -3-yl) oxy) propyl) piperazin-1-ium bromide]) in water show double shouldered UV/Vis spectra, the single oligomer which is thought as longer conjugation length gave one shoulder spectrum. The similar trend also is seen in Figure 3.33 for O1 structures, it can be referred that the backbone distance of O1 is stretched by the number of phosphates on nucleotides (Özenler et al. 2019).

$$\sum_{i=1}^{n} \varepsilon_i(\tilde{v}) = \sum_{i=1}^{n} \left(1.30662974 \times \frac{f_i}{\sigma} \, exp\left[-\left(\frac{\tilde{v} - \tilde{v}_i}{\sigma}\right)^2 \right] \right) \qquad (3.1)$$

Oligomer called O2 simulations were performed because this structure shows experimentally optical change resulted by the interaction with DNA. In the literature, there are two studies about optical change of O2. While one was investigated how O2 structure was affected by ions in cell medium, other one is about optical detection of single-stranded DNA taking advantage from planarization and aggregation of O2 (H. A. Ho and Leclerc 2003; Hoang-A Ho, Najari, and Leclerc 2008). This research have provided that the O2 structure is optically insensitive to mono and dihydrogen phosphate ions and sensitive to nucleotides of ssDNA.

At this part, a set of MD simulation was planned to examine the effect of adenosine nucleotides upon structure of O2. The oligomer backbone parameters were taken from O1 parameters and the imidazole parameters of CGenFF (RESI IMIM) were used to produce monomer of O2. But the parameters required to merge the monomer of O1 and IMIM structure were created as described at 3.1.2.2.
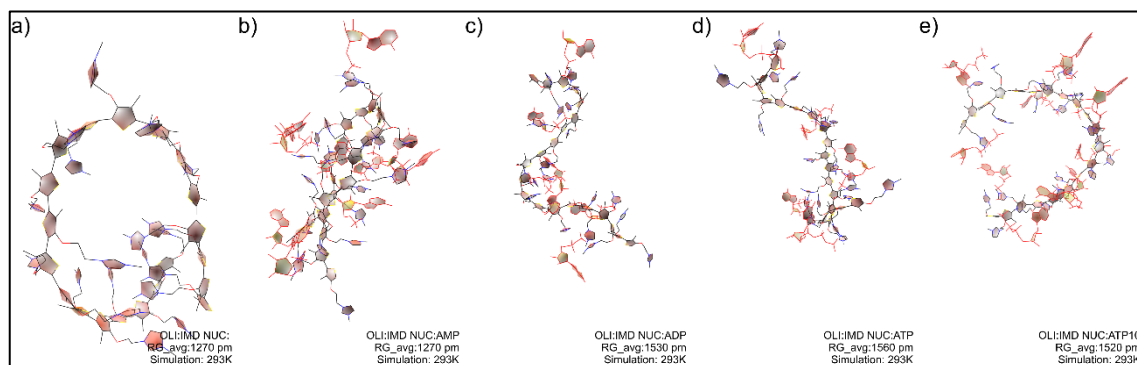
Figure 3.34. The Snapshots of O2 and Adenosine Nucleotides Complex at Average R_g of Oligomer Structure

Generally, R_g trend is similar to O1 oligomer results especially when focusing result of average of R_g. It shows increasing trend with increasing number of phosphate group on adenosine nucleotides. Average R_g of O2 in water is 11.7 Å. ATP interaction increase this value as nearly 4 Å. On the other hand, the difference between ADP and ATP is not obvious like them and it is computed as 0.3 Å. Additionally, doubling

concentration of ATP does not change the average R_g. As it was understood from RMSD graph (Figure 3.28), the diversity of structures taken ADP and ATP simulations reflect to variation of R_g. As a result of this situation, the mean radius of gyrations of ADP and ATP simulations are nearly same (15.3Å). In a summary, O2 in water has more compact structures and interaction with ATP produces a longer O2 backbone. These circumstances can be noticed in the Figure 3.34.
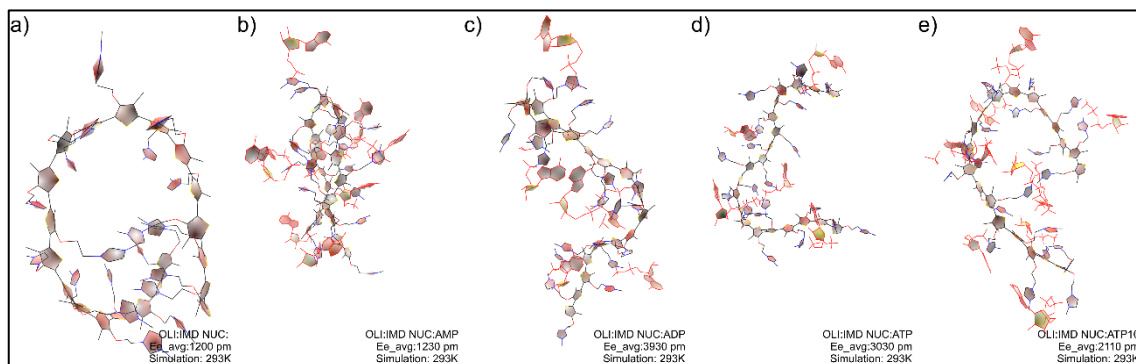
Figure 3.35. The Snapshots of O2 and Adenosine Nucleotides Complex at Average R_{ee} of Oligomer Structure

The average end to end distances of O2 at various nucleotides are displayed in Figure 3.36. AMP has no impact on O2 backbone. Whereas ADP and ATP stresses unpacked the coiled form of O2 in water without any nucleotides. Alternatively, there is a reverse trend from O1 results when evaluated the R_{ee} trend of ADP and ATP. According to the R_{ee} results, O2 with ten ATP mixture, it can be thought as if the concentration of ATP in O2 medium is doubled, the backbone of O2 has folded structure. However, it is a speculation because of variety of data due to ten ATP – O2 complexation. It can be caused from sodium ions placed for charge equivalence. Because O2 structure is more sensitive to ions than other oligomers and it will be discussed in Ion Trials section 3.2.2.3. The snapshots of O2 and nucleotides at average end to end distance is shown above Figure 3.35. the folded structures are recorded from O2 in water and O2-AMP simulations. $R_{ee(avg)}$ is nearly 12 Å for O2 and O2-AMP complex. $R_{ee(avg)}$ of the most stretched one which having ADP is found as 39Å.

At first sight of Figure 3.39 which involve interactions, the normalized π – cation and anion-cation interactions of O2 interestingly lower than other oligomers. It

can be expected due to having imidazole group. while other oligomers are formed by aliphatic ammonium group, imidazole group is consisting of aromatic structure with two nitrogen atoms. Owing to this property of imidazole, the positive charge of group disperses on the five membered ring. Although non-bonded interactions were strengthened by NBFIX parameter, the strongest energy for imidazole – phosphate interaction was calculated as nearly -149 kcal/mol. When TMA were replaced with imidazole group, this value lowered to -166 kcal/mol (Figure 3.8 and Figure 3.10). Cation - anion and π-cation interactions show similar trend with end-to-end distance. As a result of all these interactions O2 behaves distinctively from other two. It was thought that electrostatic interactions between nucleotides and O2 is directly proportional. Opposite of that, trend of radius of gyration is inversely proportional. Despite of the normalized anion - cation interactions for AMP and double concentrated ATP are close to each other (respectively, 0.48, 0,42), the structures at the average R_g and R_{ee} are very different each other. The reason of that the various backbone of O2 was recorded along ATP simulation. For example, when looking to Figure 3.36, R_{ee} of some O2 sample in ten ATP medium was enlisted as 10.6 Å. This value is also equal to some of O2 samples in AMP medium.
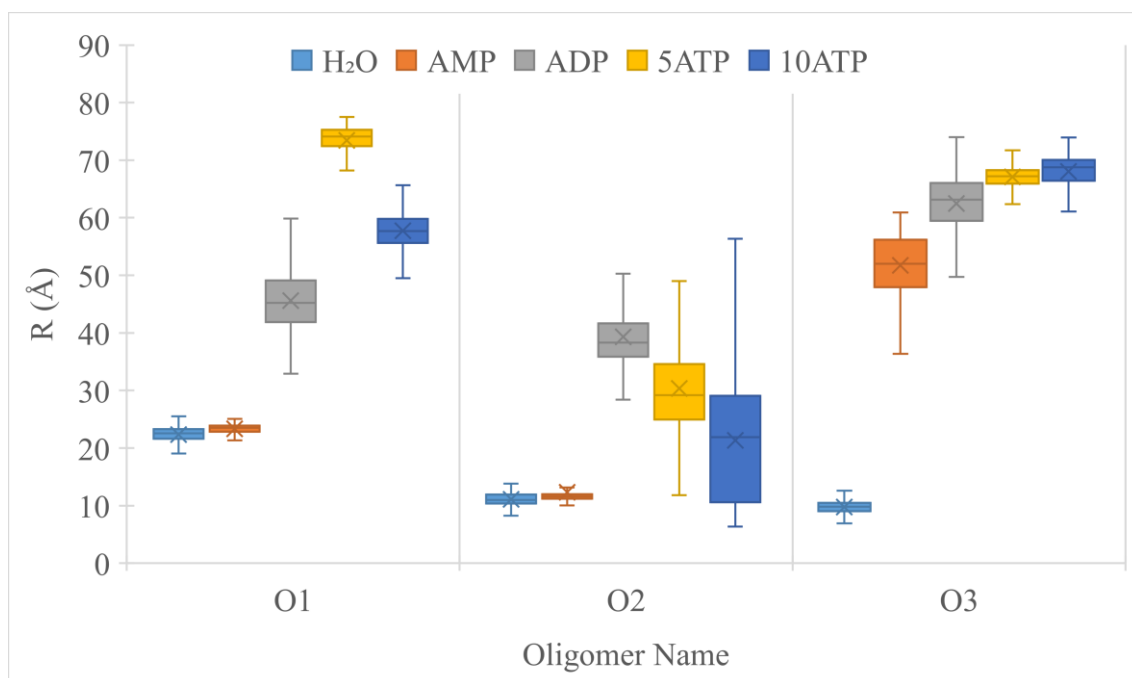

Figure 3.36. End to end Distance

Complexation between cationic polythiophene which is named poly[3-(6′-(trimethylphosphonium) hexyl) thiophene-2,5-diyl] and ssDNA is studied as not only experimentally also coarse grain MD simulation by Rubio and colleague (Rubio-Magnieto et al. 2015a). Experimentally they notice that the complex formed with CPT and ssDNA (which is constructed only thymine nucleobases) show optical change on Circular dichroism according to CPT in water medium. Also, the same impact was not detected for CPT complex with ssDNA synthesized by only adenosine nucleotides. Coarse grained MD simulation was performed to enlighten this case. Result of this simulation, it is emphasized that anion - cation and π − cation interaction between ssDNA and CPT is effective on changing backbone of CPT. As can be seen on Figure 1.12, if electrostatic and π − cation interaction of complex is more, CPT is folded and compact like ssDNA(adenosine nucleotide)/CPT complex. O3 structure was constructed to see whether our simulations will produce the similar effect or not for individual adenosine nucleotides. The only difference between CPT of Rubio and O3 is phosphorus atom on the side chain, O3 have nitrogen atom in it instead of phosphorus. We have preferred to use O3 since it does not require a new parametrized structure. When O1 parameters were supported with parameters in CGenFF database, parameters were completed for O3 simulations too.

While radius of gyration of O3 in water was calculated about 9.77Å, $R_{g(avg)}$ of the simulations with adenosine nucleotides were found greater than 18Å. Additionally, average R_g's show increasing trend with increasing number of phosphate group on adenosine. This result might be explained by similarity with O1 and O2 structures. Because the only difference between two structure is length of aliphatic side chain. But this situation reduced the gap between $R_{g\,(avg)}$ of AMP and ADP to ATP (Figure 3.30). Another remarkable case is that the concentration of ATP is not effective on the structure O3 in terms of R_g. The structures of O3 taken at average R_g snapshots are given in Figure 3.37
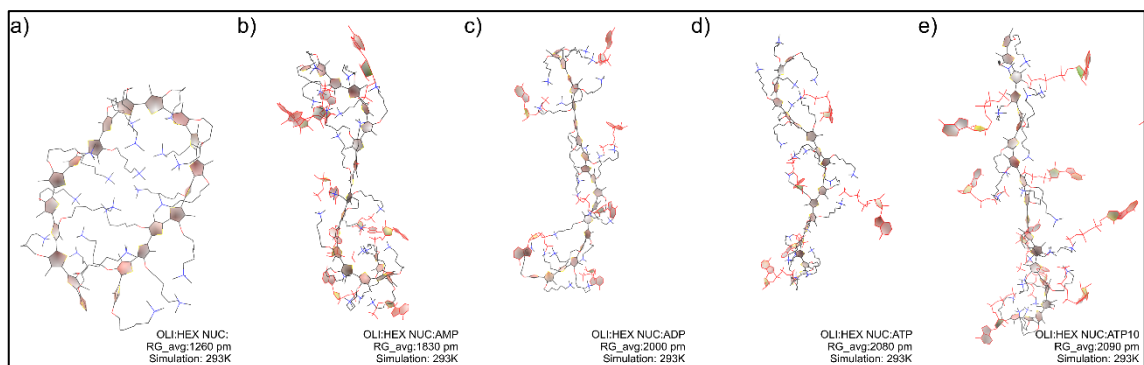
Figure 3.37. The Snapshots of O3 and Adenosine Nucleotides Complex at Average R_g of Oligomer Structure

End to end distance trend of O3 is almost same in R_g trend, the $R_{ee(avg)}$ of each simulations included nucleotides can be obtained by multiplying individual $R_{g(avg)}$ with 3.1 (Figure 3.36). When examining the snapshots (Figure 3.38), the longest backbone belongs to 10 ATP simulations. Doubling concentration of ATP increase the $R_{ee(avg)}$ only 10 nm.
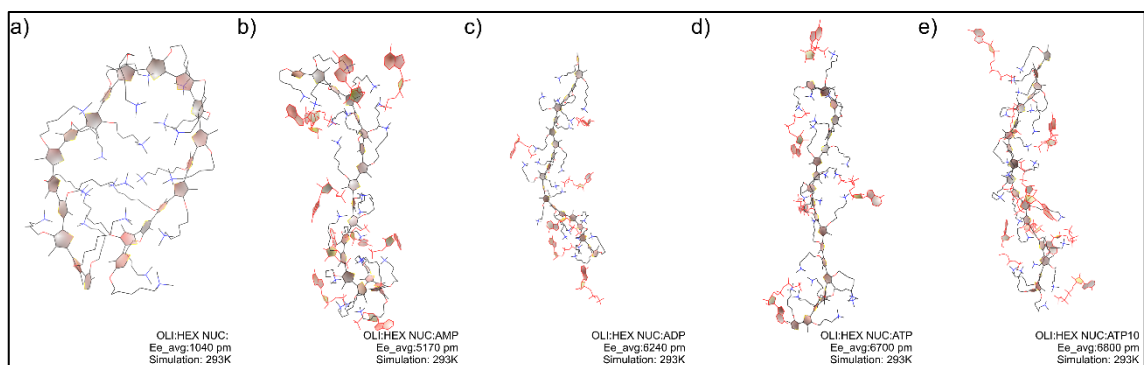
Figure 3.38. The Snapshots of O3 and Adenosine Nucleotides Complex at Average R_{ee} of Oligomer Structure
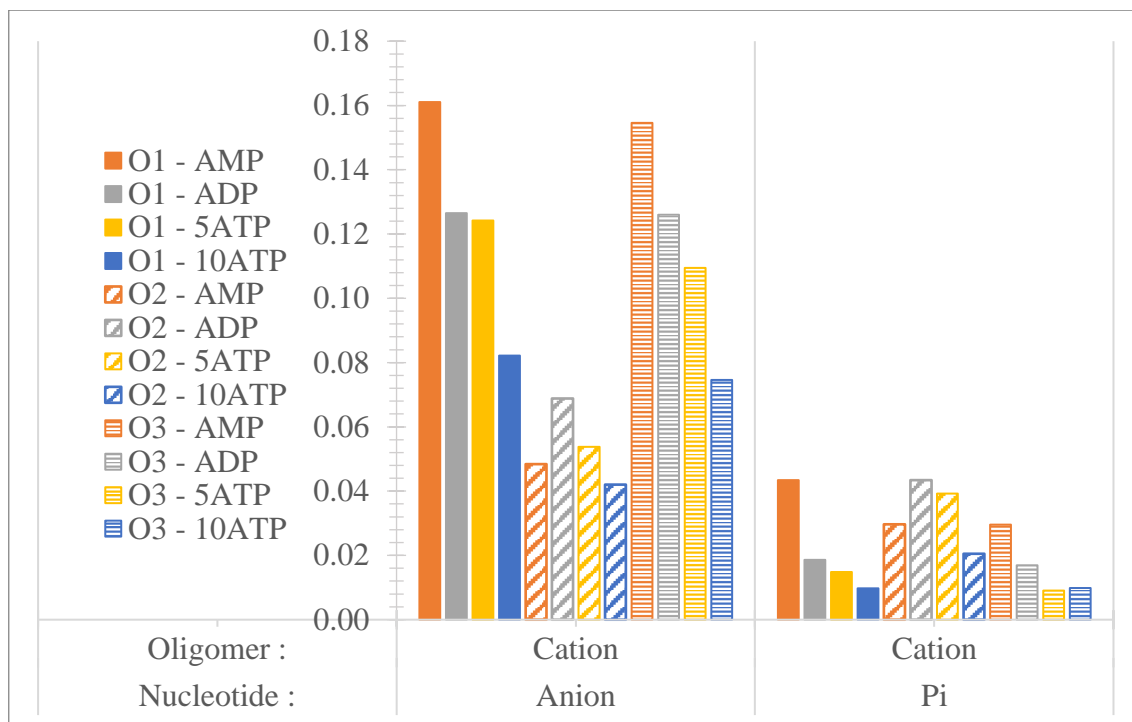
Figure 3.39. Possible Interaction Numbers of Oligomers with Various Adenosine
Nucleotides

In Figure 3.39, it is easily seen that the trend of O3 interaction number is resemble to O1′s interaction numbers. As adenosine nucleotides gaining phosphate group, the interaction numbers of anion-cation and π -cation is decreasing. This information added to structural information which are R_g and R_{ee}, it can be interpreted that the longest backbone structure has least interaction with nucleotides. At 2015, Rubio-Magnieto and coworkers make similar conclusion for DNA – CPT complexes (Rubio-Magnieto et al. 2015a).

3.2.2.2. Temperature Trials

At this section, a set of MD simulation was fictionalized how effect the backbone structure of oligomers in ATP and water medium at various temperatures.
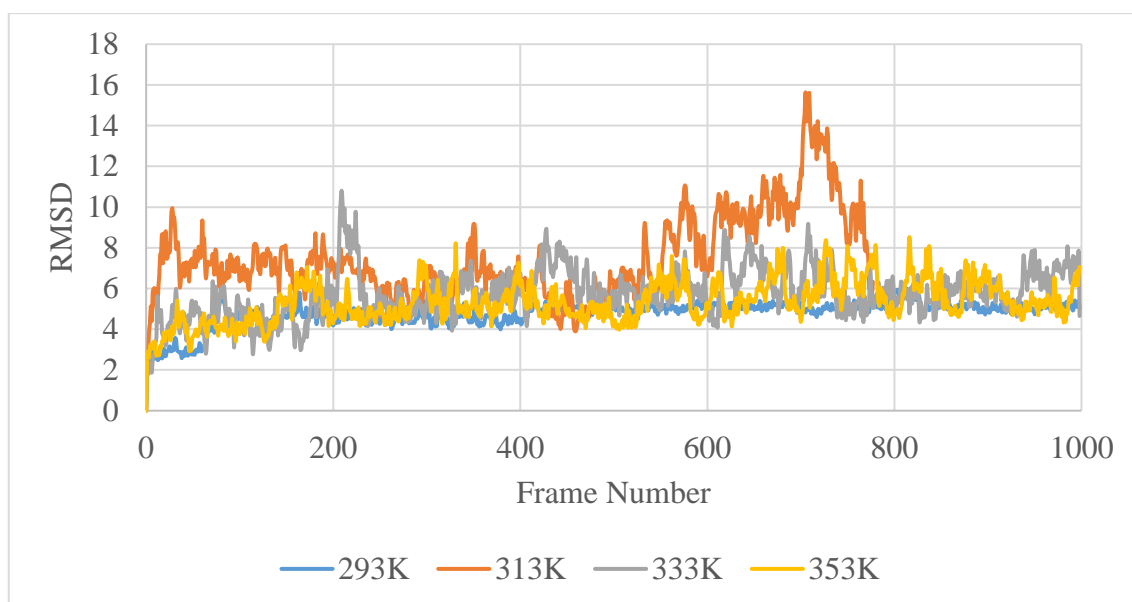
Figure 3.40. RMSD of Oligomer 1 in ATP solution at different temperatures

According to O1 results, the R_g and R_{ee} values show slight decreasing trend with increasing temperature except 353K. But all average R_g values are close to each other (Figure 3.49). On the other hand, when simulation at 353K is not part of matching, the decreasing trend of average R_{ee} can be easily seen. In literature, it was stated that when O1 − ATP solution was heated, the UV/Vis spectrum shift to blue region. And this state has been interpreted as the loosing aggregation and linearity of backbone of O1 structures (Li et al. 2006a).

Figure 3.41. The Snapshots of O1 and Adenosine Nucleotides Complex at Average R_g of Oligomer Structure at various temperatures

Figure 3.41 and Figure 3.42 can give an idea for contraction of O1 backbone at increasing temperature from 293K to 313K. The average R_{ee} at 353K was calculated as 40.8Å. Even though this $R_{ee(avg)}$ of O1 at 353K is longer than 333K, also it is half of the one at 293K (Figure 3.50).

Figure 3.42 The Snapshots of O1 and Adenosine Nucleotides Complex at Average R_{ee} of Oligomer Structure at various temperatures

The anion-cation interaction numerically shows an increasing trend while heating if the simulation result at 333K is not considered. Not only anion − cation interaction results but also the π -cation interaction results for each temperature trial are close to each other (Figure 3.47). When the relationship between interactions and structural change of oligomer was examined, it can be concluded that lowering anion - cation interactions planarize the backbone of O1.
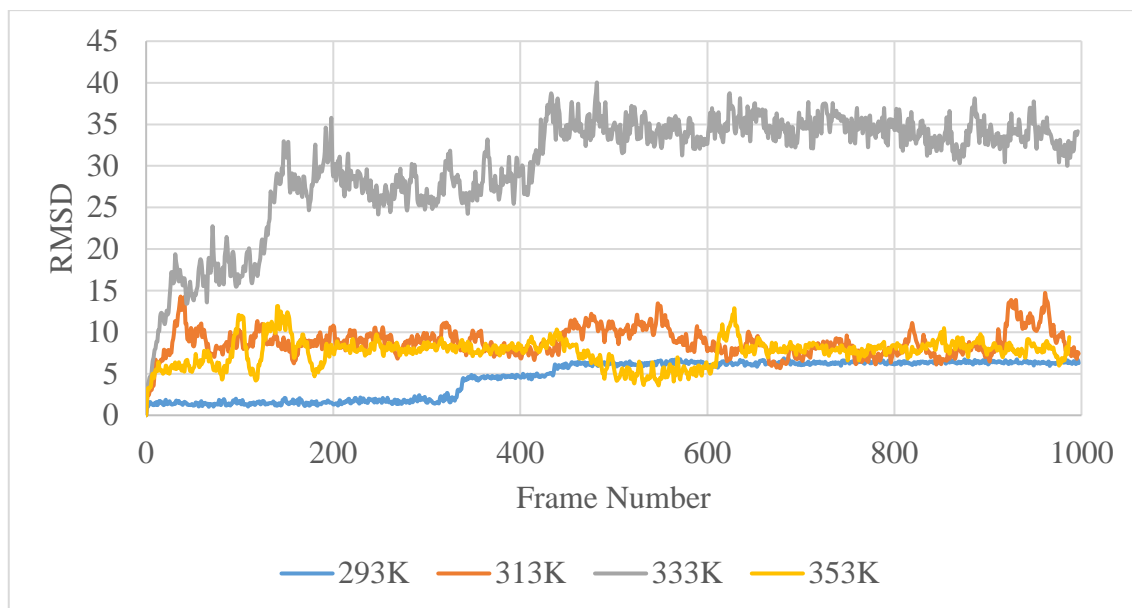
Figure 3.43. RMSD of Oligomer 2 in ATP solution at different temperatures

RMSD graph (Figure 3.43) of O2 simulations at various temperature blare out the structural change of oligomer at 333K. This structural change can be easily seen in snapshot of minimum and maximum R_g (Appendix B and Appendix C). Except for 313K data, the warm simulations have longer O2 structure than 293K. The most compact compound is recorded at 333K, its average R_g and R_{ee} is found as 13.0 Å and 22.5 Å (Figure 3.49 and Figure 3.50). If the simulation at 333 K were not considered, we can say that O2 backbone at 293K has the shortest structure.

Figure 3.44. The Snapshots of O2 and Adenosine Nucleotides Complex at Average R_g of Oligomer Structure at various temperature

According to Figure 3.44 and Figure 3.45, the order of O2 structures from lowest R_{ee} one to the most stretching one are found at 333K, 293K, 313K and 353K. These average R_g's (R_{ee}'s) were calculated as 13.0 Å (22.5 Å), 15.6 Å (30.3 Å), 18.9 Å (49.5 Å) and 20.2 Å (58.9 Å) respectively.
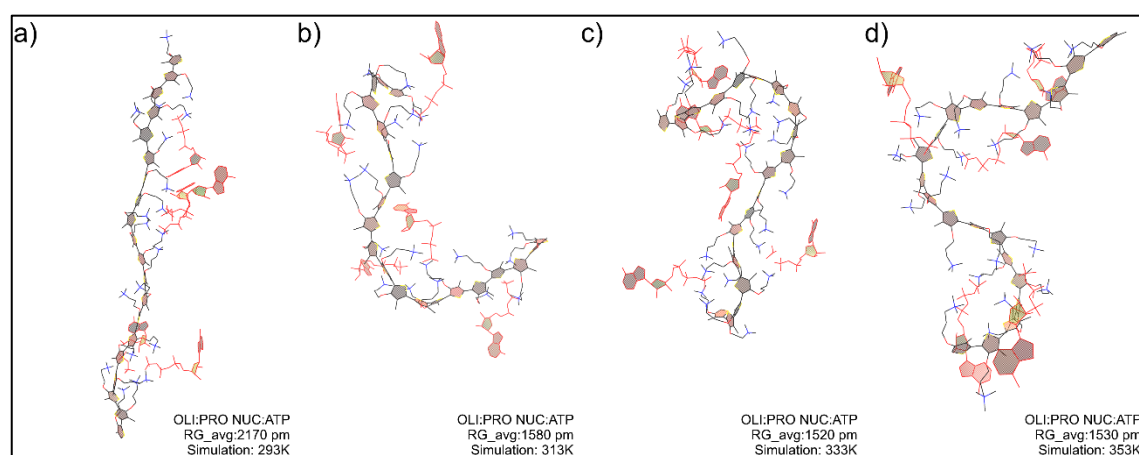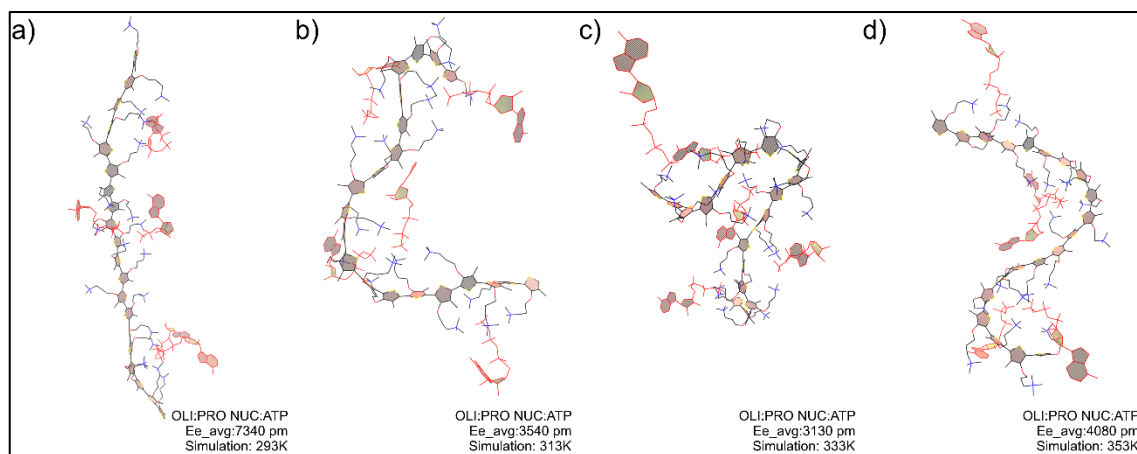

Figure 3.45. The Snapshots of O2 and Adenosine Nucleotides Complex at Average R_{ee} of Oligomer Structure at various temperature

O2 interactions results do not change the expectation made by looking R_g and R_{ee} result, for example O2 at 333K having most compact backbone show largest anion - cation interactions with nucleotides. Omitting the results of 333K simulation, the anion − cation interaction has decreasing trend with heating the ATP − O2 complex. Although π − cation interaction results have decreasing trend with heating the complex, it is not found that this trend has a connection between skeleton length of O2. On the other hand, when only the anion − cation interaction was thought, the interaction and structure analysis are in contrast with the experimental expectations. Experimentally, it was expected that the structure of oligomer must being compressed with heating up solution. Because the motion of ingredients in solution is increasing and the inter- or intra-molecular interaction is decreasing. Since this IMD moiety in O2 have distributed positive charge, the counter ion interactions might be effective and competing with interactions with adenosines and when heating the complex, they move away from O2 and cause the backbone of O2 more elongated.

Figure 3.46 is drawn to examine the change of O3 structures between the initial one and during the time evolution, the movement of O3 structures is accelerated with increasing temperature.
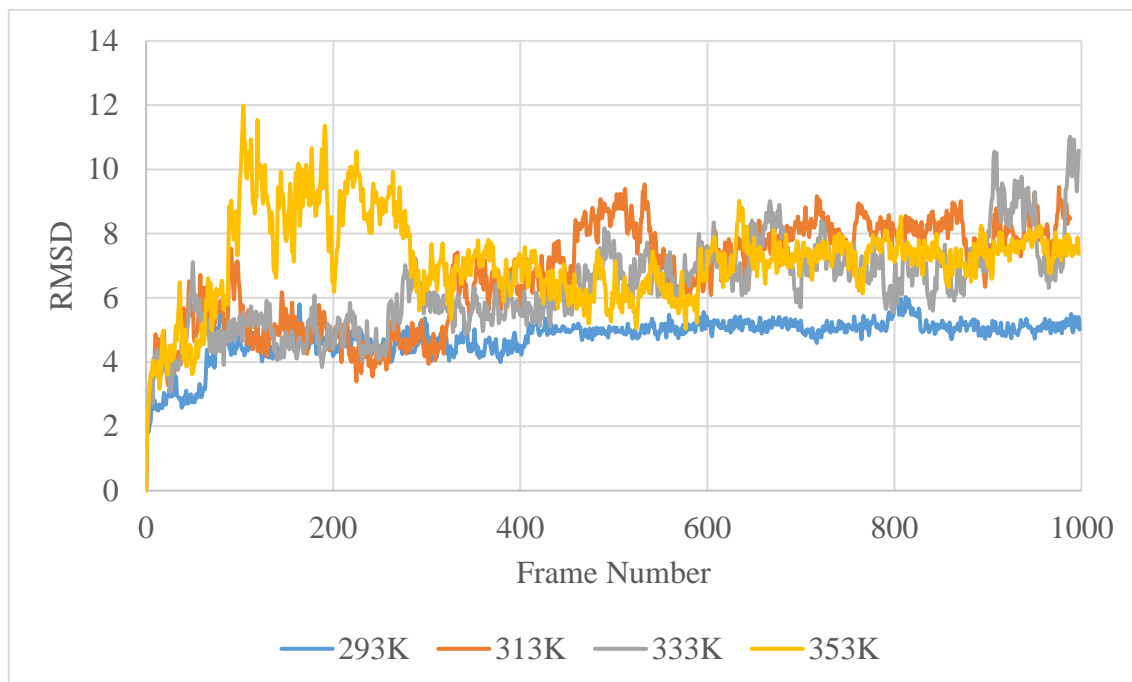
Figure 3.46. RMSD of Oligomer 3 in ATP solution at different temperatures

R_g analyses is used to find an explanation of structural depression, and there is a very slight decreasing trend with heating except the data for 353K. This trend is remarkably similar with O1 simulations data. The assumption become not wrong that the heating process is not effective on the structure of O2 when analyzed the $R_{g(avg)}$ data. These structures can be seen in Figure 3.47
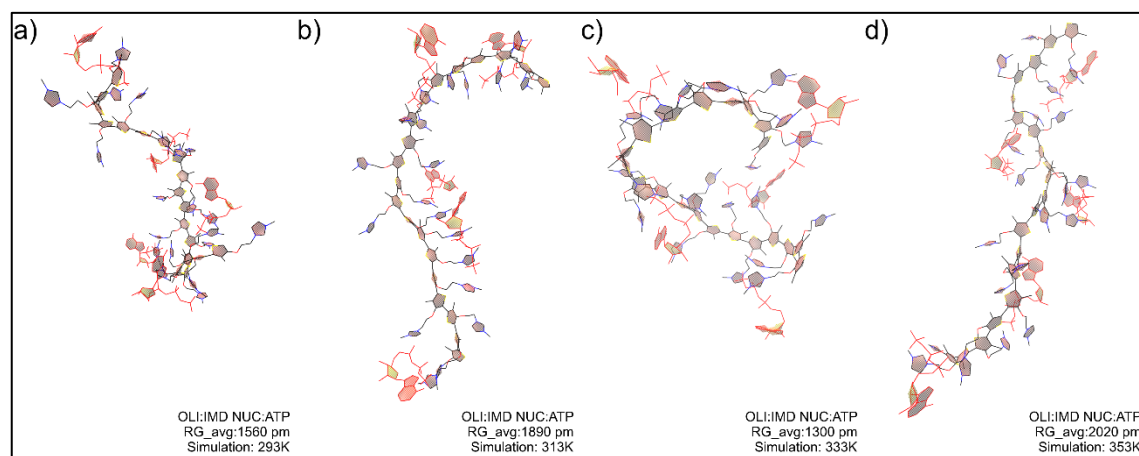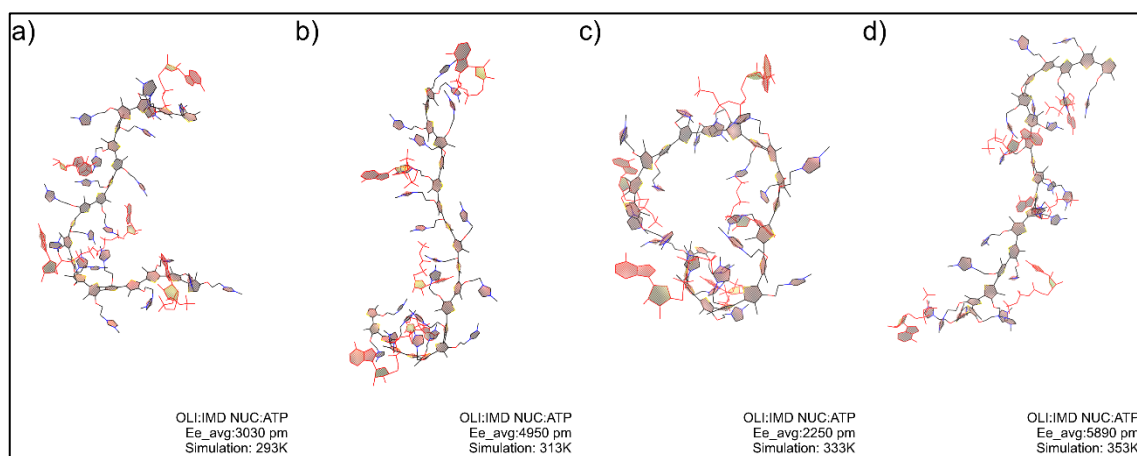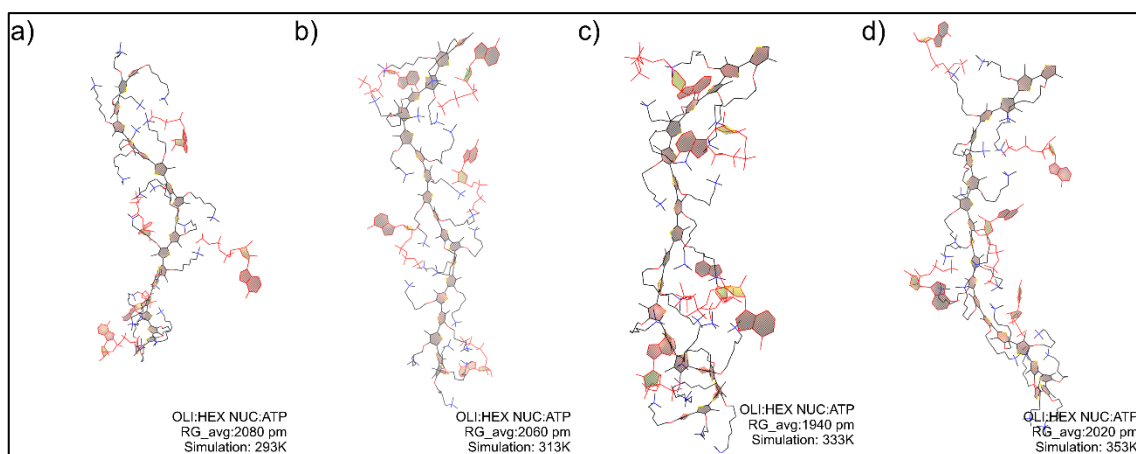
Figure 3.47. The Snapshots of O3 and Adenosine Nucleotides Complex at Average R_g of Oligomer Structure at various temperature

The trend of R_{ee} is decreasing similar trend of R_g, even the average R_{ee}/R_g ratios are calculated as respectively, 3.22, 3.14, 3.11 and 3.11 at heating process from 293K to 313K. The calculated ratio refers to deflect on backbone of O3 structure. This deflection is not noticeable in Figure 3.48Figure 3.48. The Snapshots of O3 and Adenosine Nucleotides Complex at Average R_{ee} of Oligomer Structure
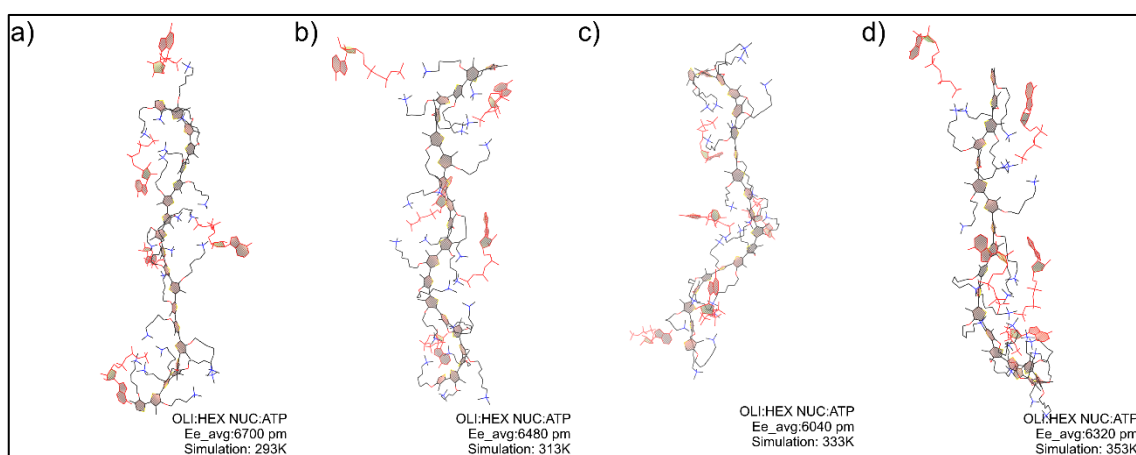
Figure 3.48. The Snapshots of O3 and Adenosine Nucleotides Complex at Average R_{ee} of Oligomer Structure at various temperature

The anion - cation and $\pi -$ cation interactions are calculated remarkably similar at various temperature; this situation explains why the R_g and R_{ee} of O3 not changing

with increasing temperature. If the smallest changes are considered, the highest possible interaction number is recorded at 333K as 0.12 for anion - cation and 0.013 for $\pi -$ cation. The average R_{ee} is smallest one at 333K, as expected (Figure 3.51).

In literature, the UV/Vis spectrum of oligomer (O1) shift to blue region with heating the solution which have ATP until absorbance of peak is nearly same with O1 in water. This temperature is 80°C for O1 $-$ ATP complex (Li et al. 2006a). Comparing between the structural data of O1 in water at 293K and in ATP $-$ water medium at 353K, the average Rg of structures are respectively, 13.52 Å (Figure 3.30) and 15.36 Å (Figure 3.49) respectively. $R_{ee(avg)}$ at 353K is found as 40.8 Å (Figure 3.50), it is twice of the value of O1 in water (Figure 3.36). It can be mentioned that the heating process in MD simulation is not effective in terms of structural change of oligomer with these parameters.
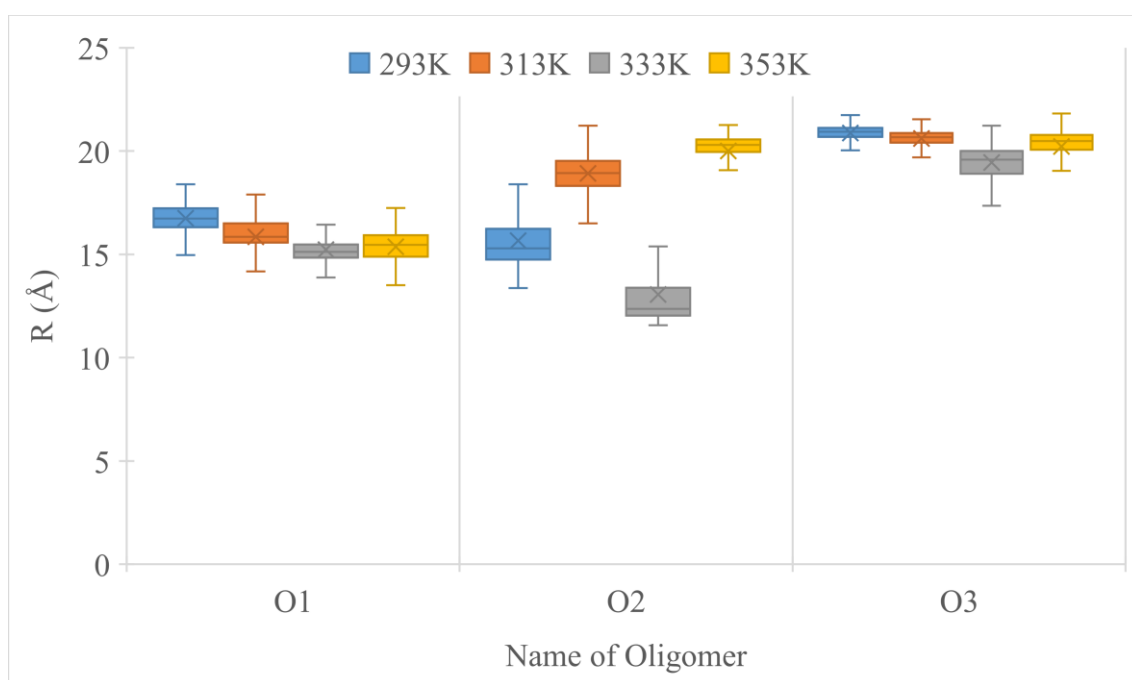
Figure 3.49. Radius of Gyration at increasing temperature
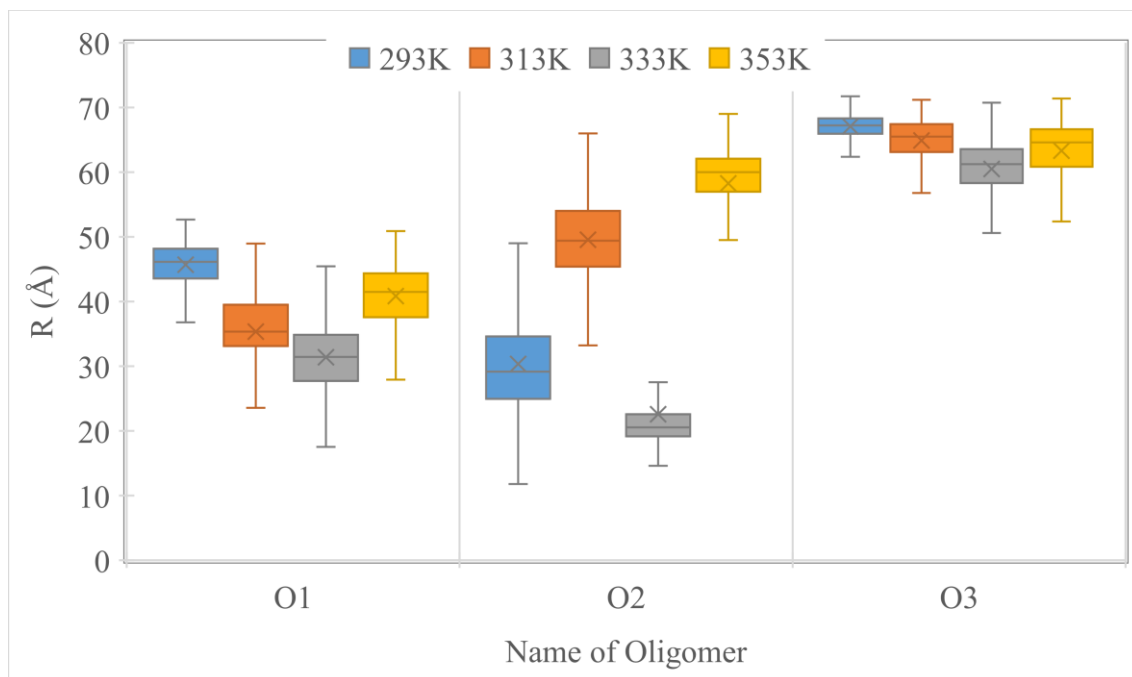
Figure 3.50. End to end distance at increasing temperature

Although there is no experimental UV/Vis spectrum of O2 and O3 in ATP –
Water solution at various temperature, it was expected that the linearity of backbone of
oligomer is decreased with increasing temperature. But this situation not seen in our
simulation. While the $R_{g(avg)}$ of O2 and O3 in water at 293K are nearly same and it is
11.7 Å, these values are found about 20.0 Å with the effect of ATP at 353K. Addition of
that situation, $R_{ee(avg)}$ of ATP complexes at 353K are six times bigger than in water at
293K. ($R_{ee(avg)}$ of O2 in water = 11.1 Å, $R_{ee(avg)}$of O3 in water = 9.8 Å)
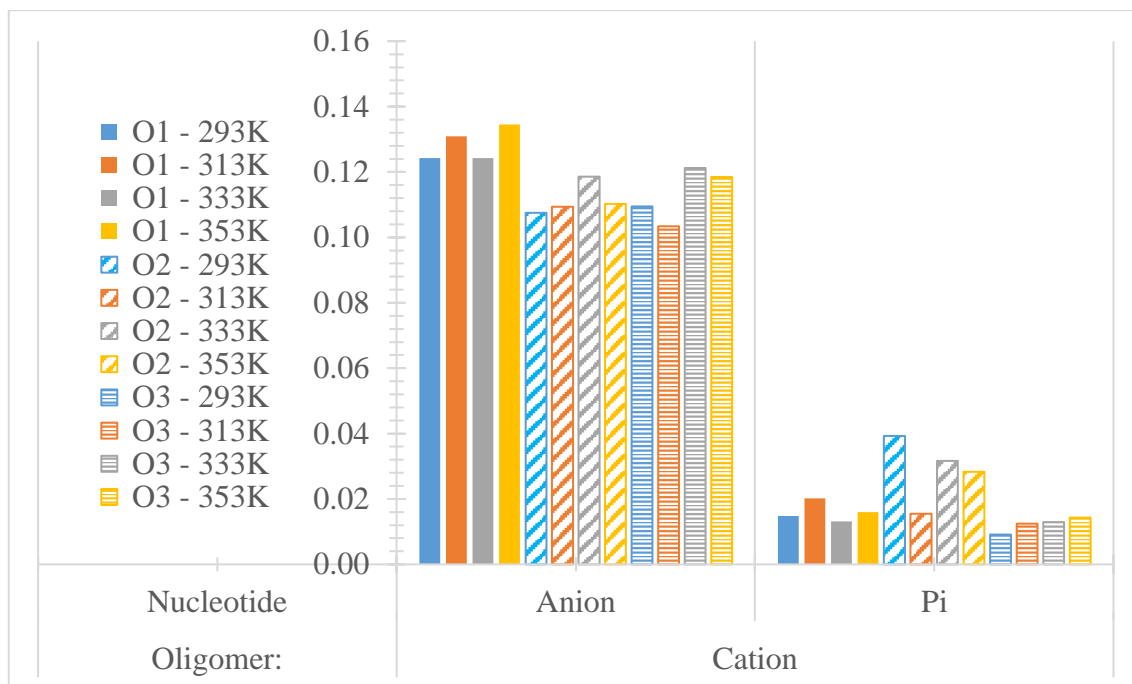
Figure 3.51. Possible Interaction Numbers of Oligomers with ATP at various Temperature

3.2.2.3. Ion Trials

The ion effect on the CPT structure is examined by Li, C., and coworkers (Li et al. 2005). It was planned that oligomer 1 and various amount of ATP was mixed in various salts which concentrated as 20 times than O1. The result of these trials, there is not noticeable effect of ions on O1 − ATP complexes. According to the relative absorbance of O1 at 535 and 400 nm (A_{535}/A_{400}) on the addition of different amount of ATP in pure water or the presence various cations, the ratio of A_{535}/A_{400} is slightly lowered by the effect of ion. For example, the highest relative absorbance was recorded for O1-ATP in water over 1.4 and the relative absorbance for alkali metals (Na^+ and K^+) is between 1.2-1.3. On the other hand, the value for alkali earth metals (Ca^{2+} and Mg^{2+}) is lower than others.
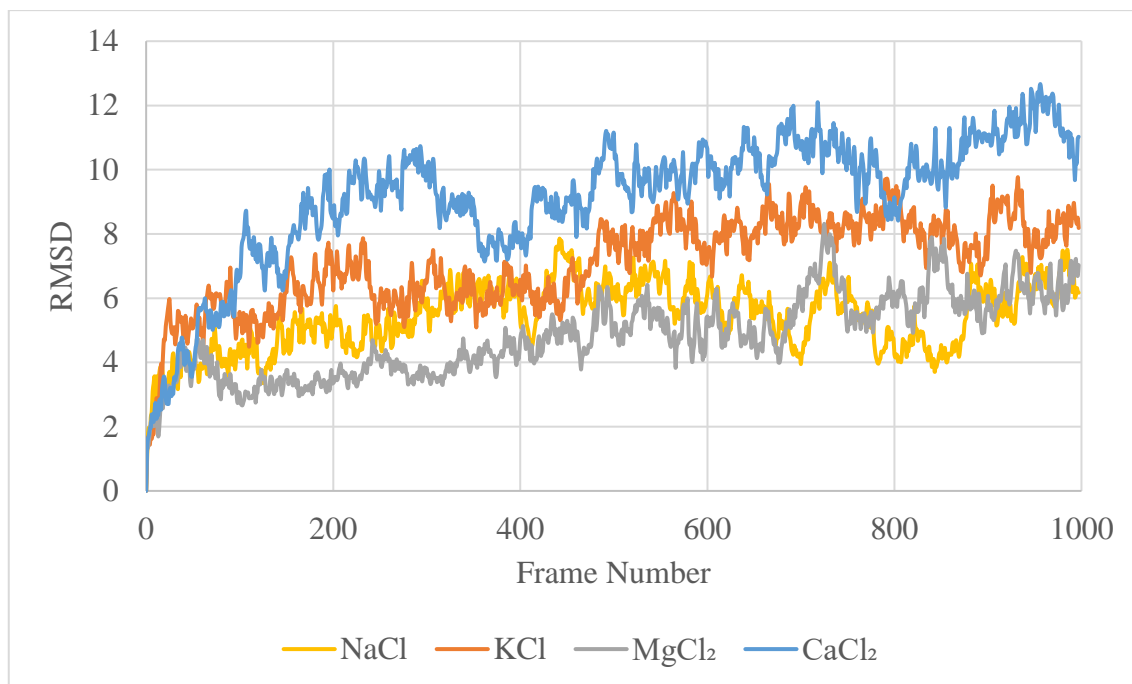
Figure 3.52. RMSD of Oligomer 1 in ATP solution in presence of monovalent and divalent ions

The simulations with 400 chlorine salt atoms were carried out. In literature, the salts concentration had 20 times bigger than the oligomer concentration, and the oligomer concentration calculated from monomer amount. For example, when an oligomer formed 20 monomer is in 1.66 nm^3, the concentration of solution is not calculated as 1 M, it must be 20 M. But on the other hand, 1200 salt atom is huge for our simulation boxes, therefore the salts of $CaCl_2$ and $MgCl_2$ was added in simulation boxes as 200 Ca^{2+} or Mg^{2+} and 400 Cl^- ions.

Based on the root mean square deviations, all oligomers at various salt medium show increasing trend in time evolution of simulation. The oligomers – ATP complexes are dynamic in sodium chloride medium for O2 and O3. O1 and O3 structure with simulation time move away from initial structure according to Figure 3.52 and Figure 3.54. But the trend of O2 RMSD can be considered stable especially after 10 ns (Figure 3.53).
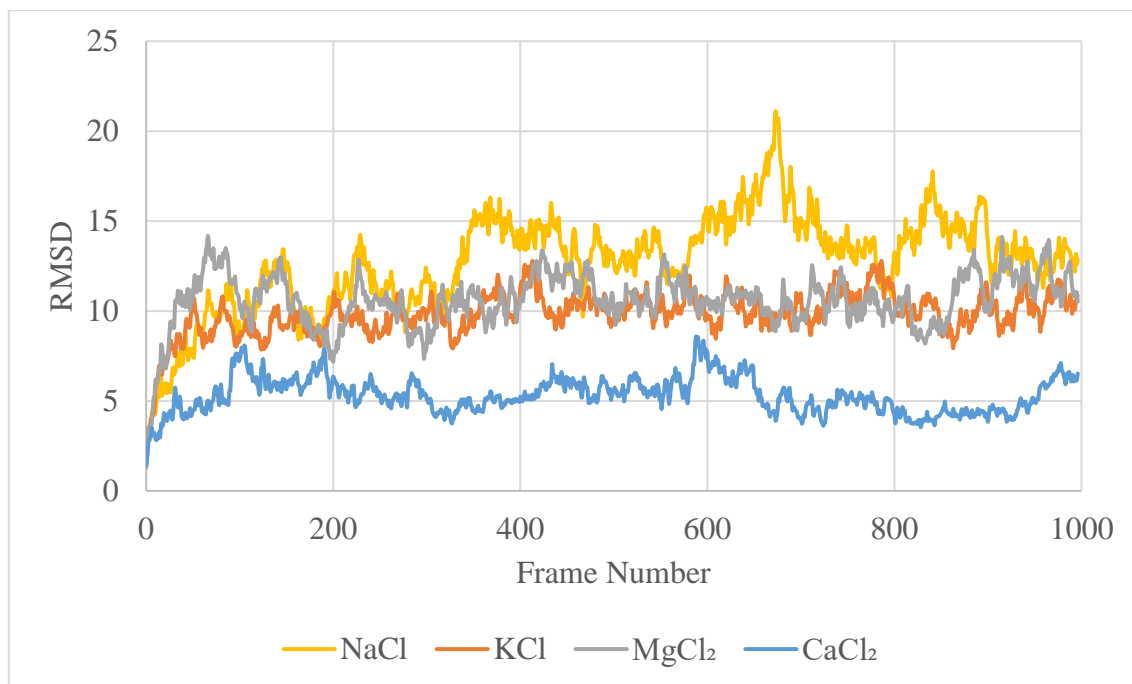
Figure 3.53. RMSD of Oligomer 2 in ATP solution in presence of monovalent and divalent ions

It can be mentioned for effect of ions in the simulation box that on O1 − ATP complex is the compression of the oligomer backbone. The presence of ion decrease the $R_{g(avg)}$ for O1 about 6 Å, the lowered $R_{g(avg)}$ values of NaCl, KCl, $MgCl_2$, and $CaCl_2$ are 15.11 Å, 15.40 Å, 16.32 Å, and 15.34 Å respectively (Figure 3.59). The backbone in non-ionic solution is calculated as 21.77 Å, and this value is remarkably higher than ionic solutions. While the presence of monovalent ions and $CaCl_2$ is similar to each other, the R_g of O1 structure in $MgCl_2$ is longer nearly 1 Å. As shown in Figure 3.55, the backbone of O1 in ion medium are remarkably close each other.

According to O1 trials with presence of ions, the monovalent ions and the $MgCl_2$ affect the O1 on $R_{ee(avg)}$. On the other hand, $CaCl_2$ ion is decreased the $R_{ee(avg)}$ from 73.4 Å to 33.7 Å (Figure 3.61). The condensed structures of oligomer with ion stress can be seen in Figure 3.56. It is clearly seen that $MgCl_2$ medium relative to presence of other ions medium stretch the O1 structure in oligomer -ATP complex considering the R_g and R_{ee} (Figure 3.61,and Figure 3.50).
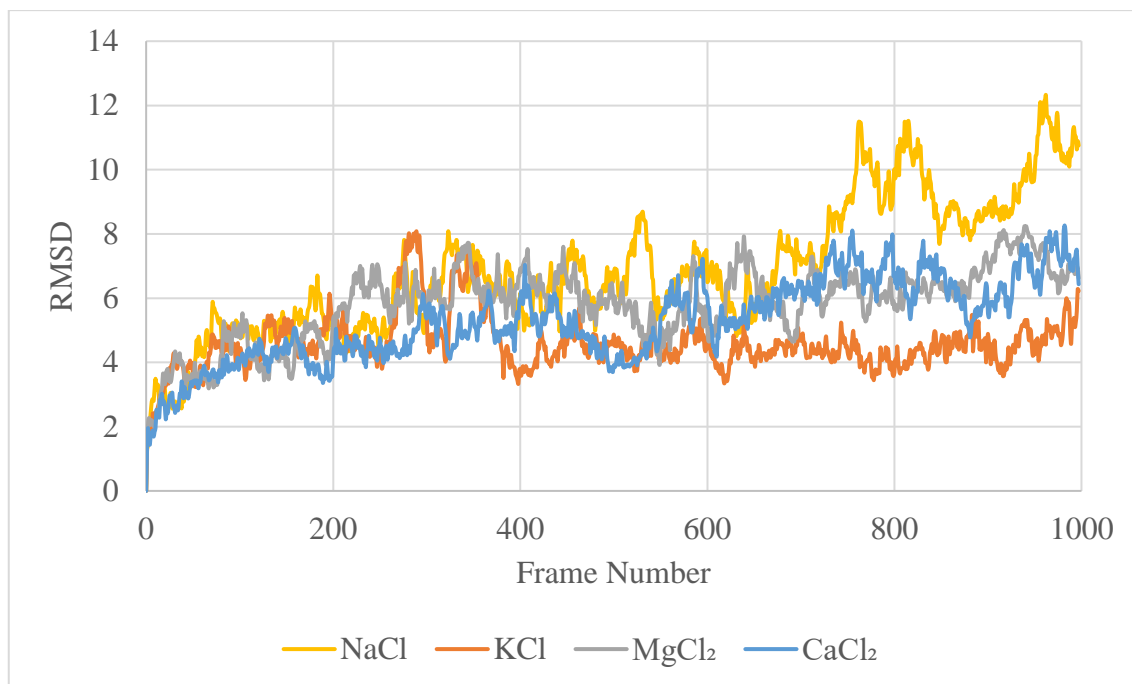
Figure 3.54. RMSD of Oligomer 3 in ATP solution in presence of monovalent and divalent ions
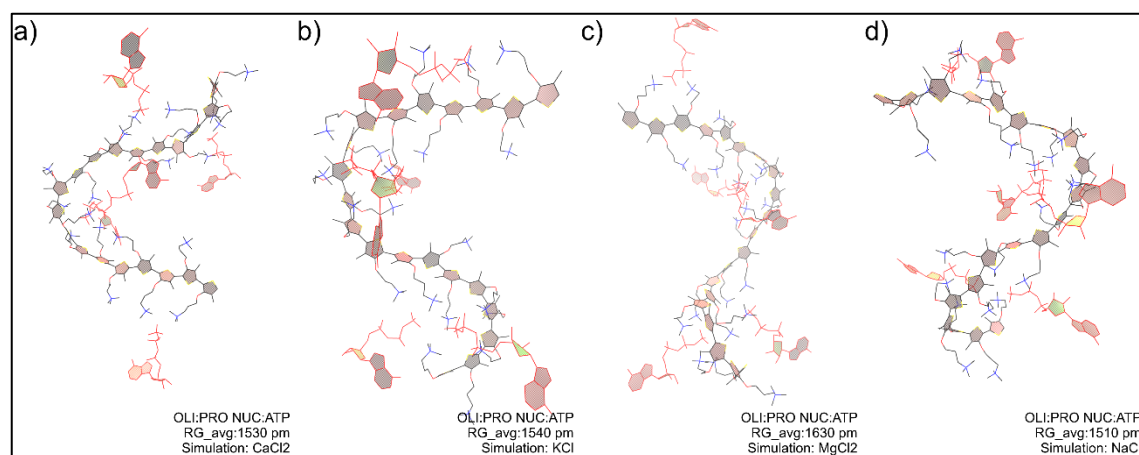
Figure 3.55. The Snapshots of O1 and Adenosine Nucleotides Complex in presence of ions at Average R_g of Oligomer Structure

The information given in previous sections, the backbone of O1 was increased by decreasing anion − cation or π -cation interaction. But this trend is not valid for in ionic medium. The interaction of anion − cation in monovalent ionic solution was calculated approximately over 0.12. This interaction for CaCl$_2$ simulation was indicated

73

as nearly 0.09 (Figure 3.63). The R_g and R_{ee} show that the O1 structure in presence of $CaCl_2$ is most compact one in salt trials. It can be concluded that anion - cation and $\pi-$ cation interaction between O1 and ATP are decreased by the presence of salts. Since the possible π -cation interaction is less than half of interaction between ATP and O1 in non − ionic solution. Ca^{2+} and oligomer competes to interact with purine and phosphates ATP and so the backbone of O1 become shrinked.

a) OLI:PRO NUC:ATP
Ee_avg:3360 pm
Simulation: CaCl2

b) OLI:PRO NUC:ATP
Ee_avg:3950 pm
Simulation: KCl

c) OLI:PRO NUC:ATP
Ee_avg:4170 pm
Simulation: MgCl2

d) OLI:PRO NUC:ATP
Ee_avg:3800 pm
Simulation: NaCl

Figure 3.56. The Snapshots of O1 and Adenosine Nucleotides Complex in presence of ions at Average R_{ee} of Oligomer Structure

The results of O2 in salt medium is interesting, the decreasing trend of O1 is not observed for O2. It can be said that the length of backbone of O2 is increasing in salt medium, especially in $CaCl_2$. Average radius of gyration and end-to-end distances in NaCl solution are respectively, 17.6 Å and 36.7 Å (Figure 3.59 and Figure 3.61) respectively. According to these results, the backbone of O2 in NaCl is the most compact one among all these salts medium. The longest structure in salt solutions were recorded as The longest structure in salt solutions were found for the O2 in $CaCl_2$ by the average of R_g and R_{ee} and their corresponding structures are given Figure 3.57 and Figure 3.58.

The interaction analysis results of salts indicate that the overall anion -cation interaction of O2 is less than O1 in salt solution, that's why the structural flattening of O2 was occured. But if the salt trial of O2 is examined individually, except $CaCl_2$ results, The anion – cation interaction between ATP and oligomer in presence of NaCl, KCl and $MgCl_2$ are very close to each other. On the other hand, π – cation interactions

of NaCl and $CaCl_2$ solutions is higher than KCl and $MgCl_2$ solutions. Although any explanation was sought for the effect of π - cation interactions on the O2 structure, no context could be found between structural compactness and this interaction. For example, according to R_g and R_{ee}, the most condense structure is recorded in NaCl, and most longest one is in $CaCl_2$. But the anaylsis show us their normalized π – cation interactions are respectively 0.18 and 0.23

Figure 3.57. The Snapshots of O2 and Adenosine Nucleotides Complex in presence of ions at Average R_g of Oligomer Structure

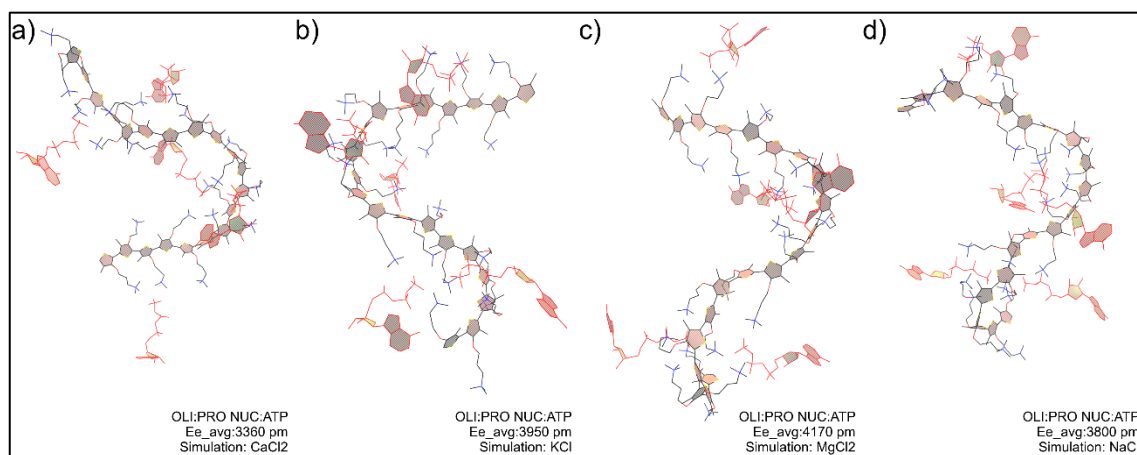Figure 3.58. The Snapshots of O2 and Adenosine Nucleotides Complex in presence of ions at Average R_{ee} of Oligomer Structure

When examining results of O3 - ATP complexes in presence of various salts, it is first remarked that the trend of end-to-end distance and radius of gyration is remarkably similar to O1 results although the values are different. The average R_g and R_{ee} for results of in $MgCl_2$ medium and none salts case are calculated as 20.9Å, 66.5Å, 21.0Å and 66.3Å, respectively (Figure 3.59 and Figure 3.61). The chlorine salts including monovalent cations influence identically the structure of O3 in ATP complexes. The simulations in NaCl and KCl medium produced the same O3 backbone since their average radius of gyrations was measured about 19.7Å. The structural change of O3 in $CaCl_2$ medium resembles more in presence of monovalent cations than in $MgCl_2$. The structures of O3 in various cation ions medium at average R_g and R_{ee} are given in Figure 3.60 and Figure 3.62 respectively. The most elongated structure in presence of cations is found in as $MgCl_2$ medium according to R_g and R_{ee}.
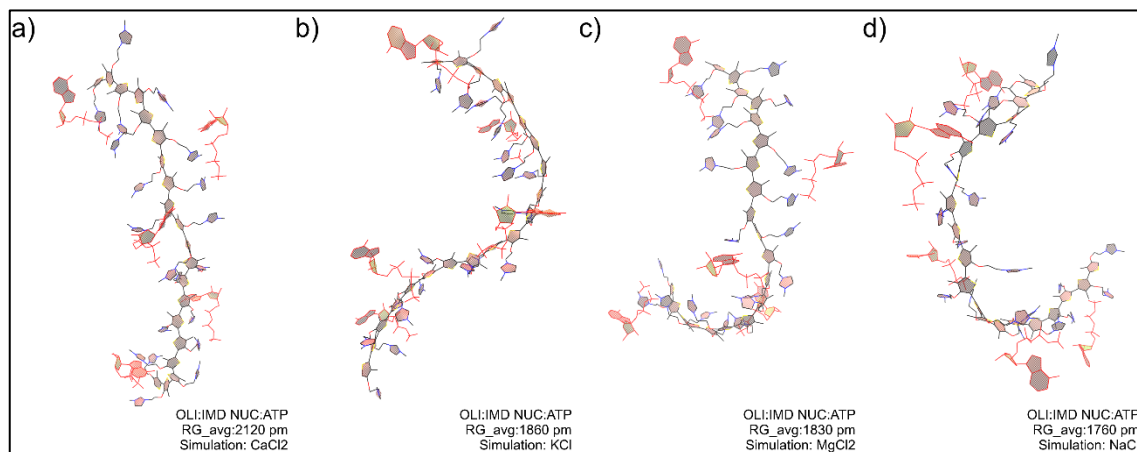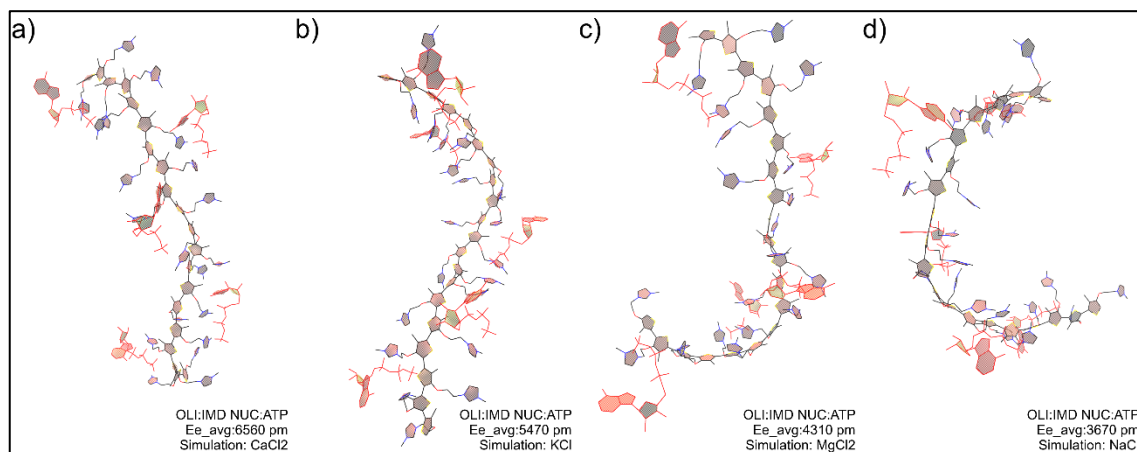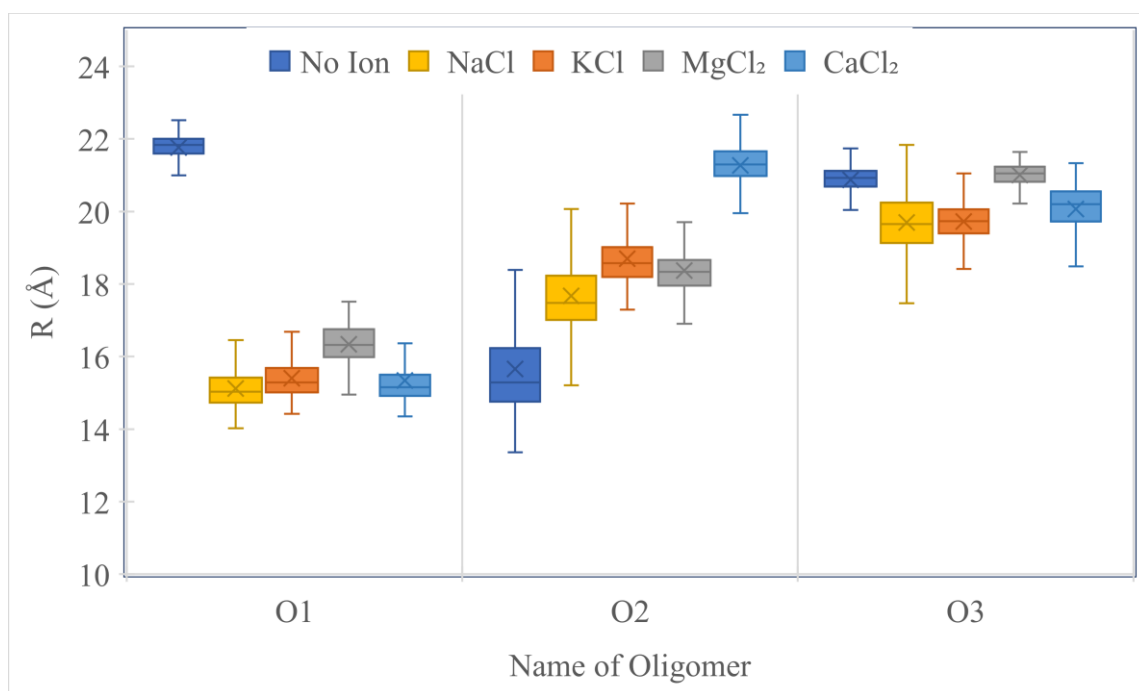

Figure 3.59. Radius of Gyration in presence of various salts

Figure 3.60. The Snapshots of O3 and Adenosine Nucleotides Complex in presence of ions at Average R_g of Oligomer Structure

Figure 3.61. End to end Distance in presence of various salts

The possible interaction values in various salt medium show that the most anion-cation interaction is counted for $MgCl_2$. On the other hand, that simulation having fewest $\pi -$ cation interaction. The possible interactions values in the absence of salts are 0.109 for anion -cation and 0.009 for $\pi -$ cation. These values also are close to the values calculated for $MgCl_2$. Therefore, it is not suprising that the O3 structure in

MgCl2 and absence of ions is similar according to structural analysis (R_g and R_{ee}). But that the interactions between O3 and ATP in salt medium does not explain the structural change of O3. For example, difference of anion – cation interaction in NaCl and MgCl$_2$ is up to 5 x 10^{-3}, but the R_g difference between their simulations is measured as 1.4 Å.
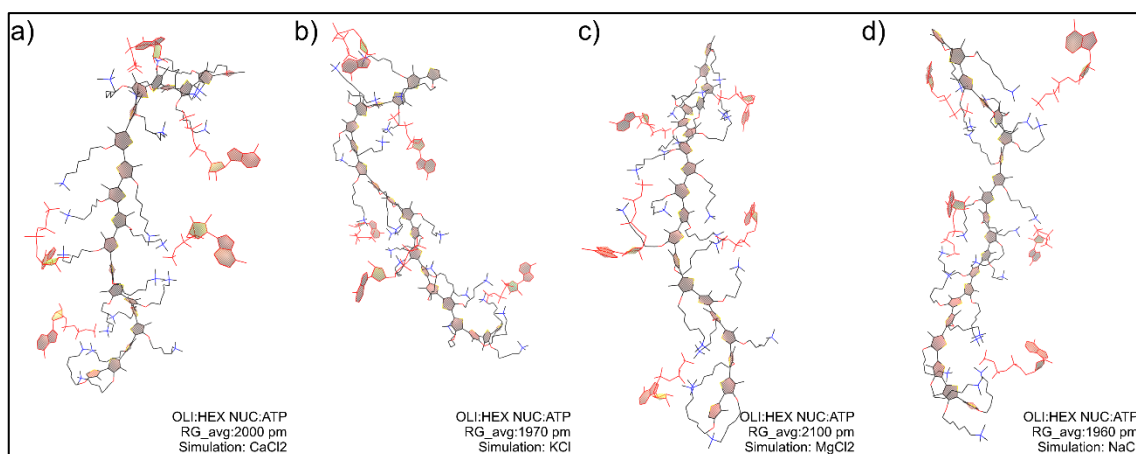

Figure 3.62. The Snapshots of O3 and Adenosine Nucleotides Complex in presence of ions at Average R_{ee} of Oligomer Structure

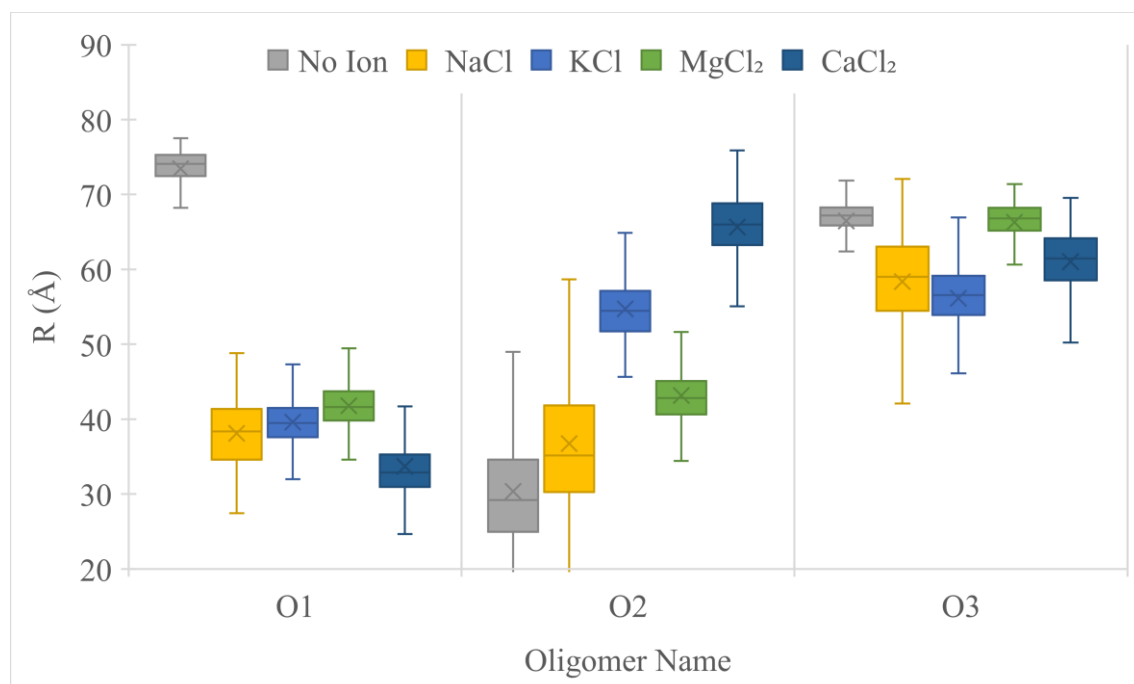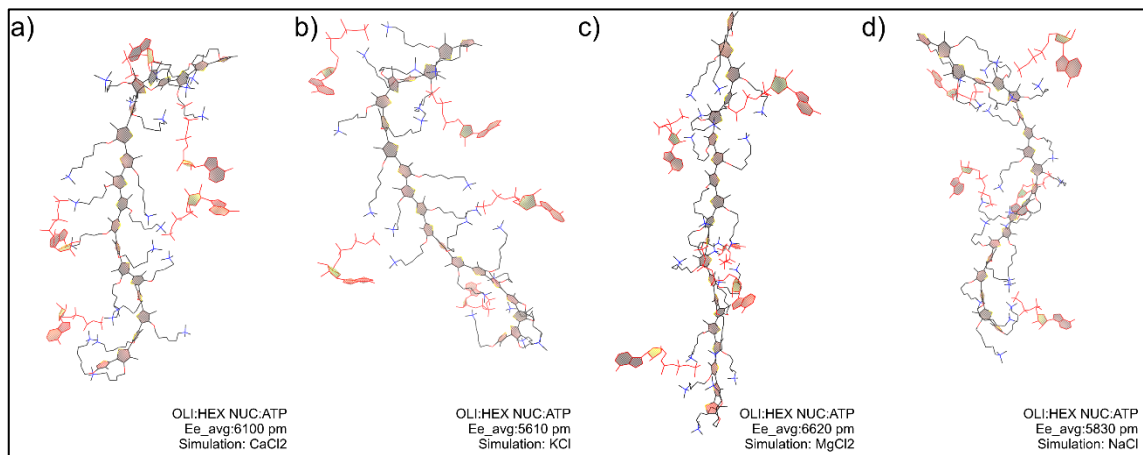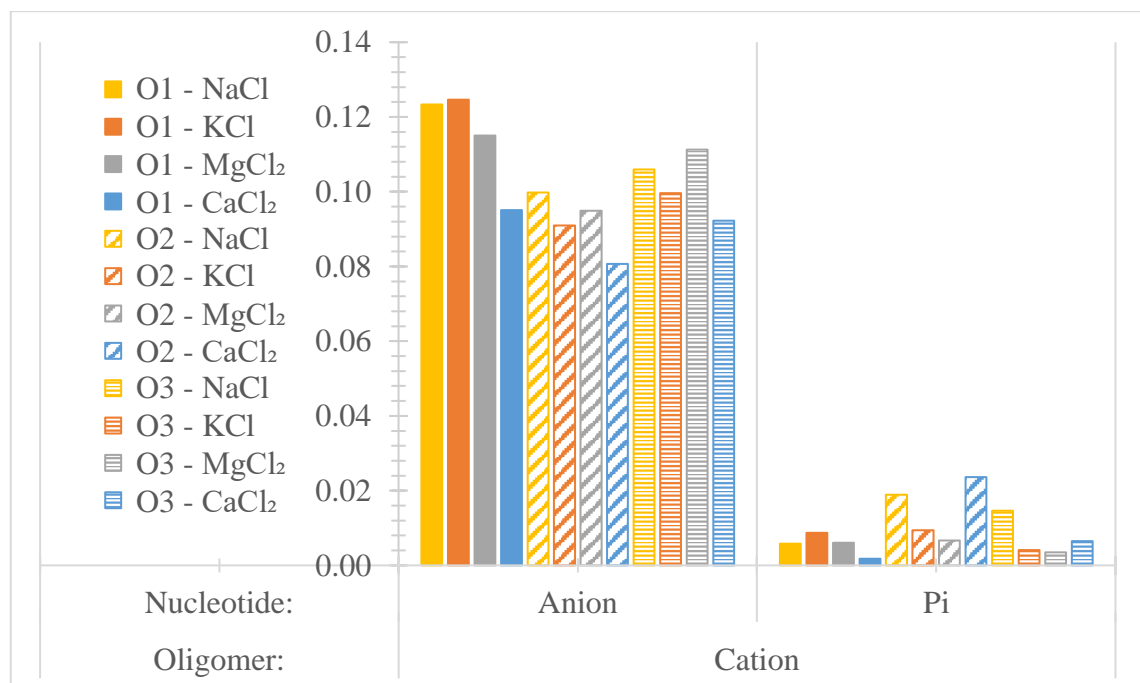Figure 3.63 Interactions

CHAPTER 4

CONCLUSION

In this thesis, Poly- N, N, N-trimethyl-3-(4-methylthiophen-3-yl) oxy) propan-1-aminium named O1 was parametrized for MD simulations using ffTK and CHARMM program. Although the parametrization step in ffTK is successful for RMSE values of bond, angle, and dihedral, it is obvious that the structural change on oligomer is not satisfying in ATP medium when examining the R_g and R_{ee} values. For better simulation results, the same missing parameters of O1 were generated by Charmm program, and also NBFIX parameters were created in order to correct intermolecular interactions between adenosine nucleotides and oligomer. The experimental data of UV/Vis spectrum indicate that the structural flattening on oligomer is occurred by increasing phosphate group on adenosine nucleotide. This case is also reflected well with the structural analysis of MD simulations performed with Charmm parameters. The red-shift on simulated UV/Vis spectrum has verified the simulation parameters. The intermolecular interactions; anion-cation and π-cation were examined to explain how nucleotides affect the backbone structure of oligomer.

O1 simulations results with various adenosine nucleotides agreed well with the experimental UV-VIS spectrum, the structures which can be used for similar purposes is than parametrized for O2 and O3. The results of O2 in ADP and ATP medium show that the structural change on oligomer have remarkably similar compactness. Therefore, this oligomer cannot be stated any optical difference for these nucleotides. However, the oligomer with the aliphatic hexyl side group (O3) can separate the nucleotide environments optically. Phosphate interaction energy for imidazole group stronger than TMA by 17 kcal/mol. It has lower cation - anion and some little bit higher π-cation interactions than O1 and O3. As a result of all these O2 behaves distinctively from the other two.

Experimentally, O1 which have linear backbone in ATP medium loses its stretched structure with increasing temperature and compacting w.r.t. backbone in water

medium. When the computational results at different temperatures was examined, MD simulations was not reflected good experimental statement at increasing temperature.

At the final stage of this thesis, the effect of salts on the structure of oligomers were examined. We observed that the presence the monovalent or divalent cations do not affect linearity of oligomers structure in ATP medium for O3 remarkably. However, O1 and O2 have a great respond to ATP with Mg^{2+}, K^+ and Ca^{2+}(most sensed) ions, O2 has almost no reactions to ATP without these ions. Ca^{2+} is a key ion which regulates ATP production by mitochondria. O2 might take part in a biosensor design for ATP in the presence of Ca^{+2} .

REFERENCES

Brooks, Bernard R., Robert E. Bruccoleri, Barry D. Olafson, David J. States, S. Swaminathan, and Martin Karplus. 1983. "CHARMM: A Program for Macromolecular Energy, Minimization, and Dynamics Calculations." *Journal of Computational Chemistry* 4 (2): 187–217. https://doi.org/10.1002/jcc.540040211.

Dennis, Patrick B. 2001. "Mammalian TOR: A Homeostatic ATP Sensor." *Science* 294 (5544): 1102–5. https://doi.org/10.1126/science.1063518.

Gourine, Alexander V., Enrique Llaudet, Nicholas Dale, and K. Michael Spyer. 2005. "ATP Is a Mediator of Chemosensory Transduction in the Central Nervous System." *Nature* 436 (7047): 108–11. https://doi.org/10.1038/nature03690.

Ho, Hoang A., and Mario Leclerc. 2003. "New Colorimetric and Fluorometric Chemosensor Based on a Cationic Polythiophene Derivative for Iodide-Specific Detection." *Journal of the American Chemical Society* 125 (15): 4412–13. https://doi.org/10.1021/ja028765p.

Ho, Hoang-A, Ahmed Najari, and Mario Leclerc. 2008. "Optical Detection of DNA and Proteins with Cationic Polythiophenes." *Accounts of Chemical Research* 41 (2): 168–78. https://doi.org/10.1021/ar700115t.

Ho, Hoang-Anh, Maïté Béra-Abérem, and Mario Leclerc. 2005. "Optical Sensors Based on Hybrid DNA/Conjugated Polymer Complexes." *Chemistry - A European Journal* 11 (6): 1718–24. https://doi.org/10.1002/chem.200400537.

Huang, Bing-Huan, Zhi-Rong Geng, Xiao-Yan Ma, Cui Zhang, Zhi-Yang Zhang, and Zhi-Lin Wang. 2016. "Lysosomal ATP Imaging in Living Cells by a Water-Soluble Cationic Polythiophene Derivative." *Biosensors and Bioelectronics* 83 (5): 213–20. https://doi.org/10.1016/j.bios.2016.04.064.

Khan, Hanif M., Alexander D. MacKerell, and Nathalie Reuter. 2019. "Cation-π Interactions between Methylated Ammonium Groups and Tryptophan in the

CHARMM36 Additive Force Field." Rapid-communication. *Journal of Chemical Theory and Computation* 15 (1): 7–12. https://doi.org/10.1021/acs.jctc.8b00839.

Li, Chun, Munenori Numata, Masayuki Takeuchi, and Seiji Shinkai. 2005. "A Sensitive Colorimetric and Fluorescent Probe Based on a Polythiophene Derivative for the Detection of ATP." *Angewandte Chemie International Edition* 44 (39): 6371–74. https://doi.org/10.1002/anie.200501823.

Ma, Tai, Chun Li, and Gaoquan Shi. 2007. "Optically Active Supramolecular Complex Formed by Ionic Self-Assembly of Cationic Perylenediimide Derivative and Adenosine Triphosphate." *In Final Form*, no. 33: 751–56. https://doi.org/10.1021/la702559m.

MacKerell, A. D., D Bashford, M Bellott, R L Dunbrack, J D Evanseck, M J Field, S Fischer, et al. 1998. "All-Atom Empirical Potential for Molecular Modeling and Dynamics Studies of Proteins †." *The Journal of Physical Chemistry B* 102 (18): 3586–3616. https://doi.org/10.1021/jp973084f.

Mayne, Christopher G., Jan Saam, Klaus Schulten, Emad Tajkhorshid, and James C. Gumbart. 2013. "Rapid Parameterization of Small Molecules Using the Force Field Toolkit." *Journal of Computational Chemistry* 34 (32): 2757–70. https://doi.org/10.1002/jcc.23422.

Miranda, Oscar R., Chang Cheng You, Ronnie Phillips, Ik Bum Kim, Partha S. Ghosh, Uwe H.F. Bunz, and Vincent M. Rotello. 2007. "Array-Based Sensing of Proteins Using Conjugated Polymers." *Journal of the American Chemical Society* 129 (32): 9856–57. https://doi.org/10.1021/ja0737927.

Özenler, Sezer, Muge Yucel, Özge Tüncel, Hakan Kaya, Serdar Özçelik, and Umit Hakan Yildiz. 2019. "Single Chain Cationic Polymer Dot as a Fluorescent Probe for Cell Imaging and Selective Determination of Hepatocellular Carcinoma Cells." *Analytical Chemistry* 91 (16): 10357–60. https://doi.org/10.1021/acs.analchem.9b02300.

Phillips, James C, Rosemary Braun, Wei Wang, James Gumbart, Emad Tajkhorshid, Elizabeth Villa, Christophe Chipot, Robert D Skeel, Laxmikant Kalé, and Klaus Schulten. 2005. "Scalable Molecular Dynamics with NAMD." *Journal of Computational Chemistry* 26 (16): 1781–1802. https://doi.org/10.1002/jcc.20289.

Pulay, Péter, Géza Fogarasi, Frank Pang, and Janies E. Boggs. 1979. "Systematic AB Initio Gradient Calculation of Molecular Geometries, Force Constants, and Dipole Moment Derivatives." *Journal of the American Chemical Society* 101 (10): 2550–60. https://doi.org/10.1021/ja00504a009.

Rubio-Magnieto, Jenifer, Elias Gebremedhn Azene, Jérémie Knoops, Stefan Knippenberg, Cécile Delcourt, Amandine Thomas, Sébastien Richeter, et al. 2015a. "Self-Assembly and Hybridization Mechanisms of DNA with Cationic Polythiophene." *Soft Matter* 11 (32): 6460–71. https://doi.org/10.1039/c5sm01484k.

Rubio-Magnieto, Jenifer, Amandine Thomas, Sébastien Richeter, Ahmad Mehdi, Philippe Dubois, Roberto Lazzaroni, Sébastien Clément, and Mathieu Surin. 2013. "Chirality in DNA–π-Conjugated Polymer Supramolecular Structures: Insights into the Self-Assembly." *Chemical Communications* 49 (48): 5483. https://doi.org/10.1039/c3cc42108b.

Shirakawa, Hideki, Alan McDiarmid, and Alan Heeger. 2003. "Focus Article: Twenty-Five Years of Conducting Polymers." *Chemical Communications*, no. 1 (December): 1–4. https://doi.org/10.1039/b210718j.

Sun, Han, and Kirk S. Schanze. 2022. "Functionalization of Water-Soluble Conjugated Polymers for Bioapplications." *ACS Applied Materials & Interfaces* 14 (18): 20506–19. https://doi.org/10.1021/acsami.2c02475.

Swager, Timothy M. 2017. "50th Anniversary Perspective: Conducting/Semiconducting Conjugated Polymers. A Personal Perspective on the Past and the Future." *Macromolecules*. American Chemical Society. https://doi.org/10.1021/acs.macromol.7b00582.

Thomas, Samuel W., Guy D. Joly, and Timothy M. Swager. 2007. "Chemical Sensors Based on Amplifying Fluorescent Conjugated Polymers." *Chemical Reviews* 107 (4): 1339–86. https://doi.org/10.1021/cr0501339.

Vanommeslaeghe, K., E. Hatcher, C. Acharya, S. Kundu, S. Zhong, J. Shim, E. Darian, et al. 2009a. "CHARMM General Force Field: A Force Field for Drug-like Molecules Compatible with the CHARMM All-Atom Additive Biological Force Fields." *Journal of Computational Chemistry* 31 (4): NA-NA. https://doi.org/10.1002/jcc.21367.

Wang, X Y, Q L Feng, L Wang, M S Pei, J J Zhao, and G Y Zhang. 2014. "A Novel Polythiophene Derivative as a Sensitive Colorimetric and Fluorescent Sensor for the Detection of ATP." *Designed Monomers and Polymers* 17 (1): 26–32. https://doi.org/Doi 10.1080/15685551.2013.771315.

Yao, Zhiyi, Xueling Feng, Wenjing Hong, Chun Li, and Gaoquan Shi. 2009. "A Simple Approach for the Discrimination of Nucleotides Based on a Water-Soluble Polythiophene Derivative." *Chemical Communications* 405 (31): 4696. https://doi.org/10.1039/b904975d.

Zhu, Chunlei, Libing Liu, Qiong Yang, Fengting Lv, and Shu Wang. 2012. "Water-Soluble Conjugated Polymers for Imaging, Diagnosis, and Therapy." *Chemical Reviews* 112 (8): 4687–4735. https://doi.org/10.1021/cr200263w.

APPENDIX A

SNAPSHOTS OF OLIGOMERS AT AVERAGE R_g

Figure A. 1. Snapshots of O1 in water and different adenosine nucleotides medium at average R_g

Figure A. 2. Snapshots which are recorded average R_g of O1 in ATP medium at increasing temperature

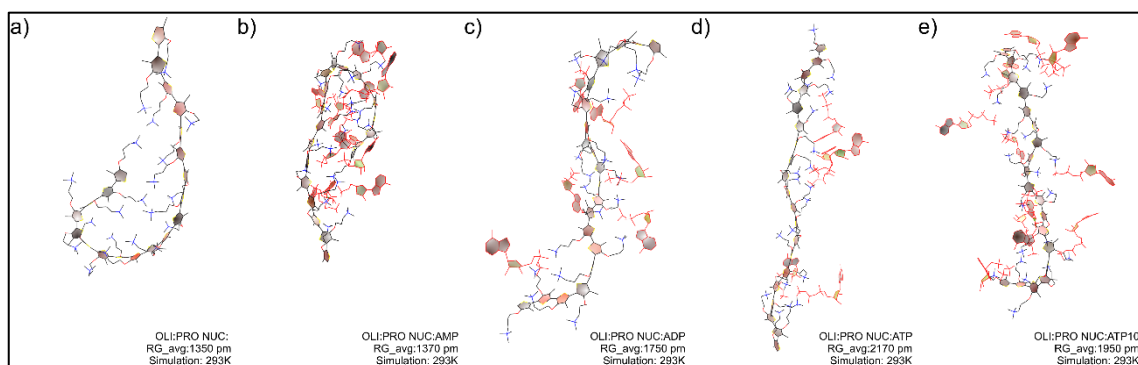Figure A. 3. Snapshots which is recorded average R_g of O1 in ATP medium at presence of different salts

Figure A. 4. Snapshots of O2 in water and different adenosine nucleotides medium at average R_g
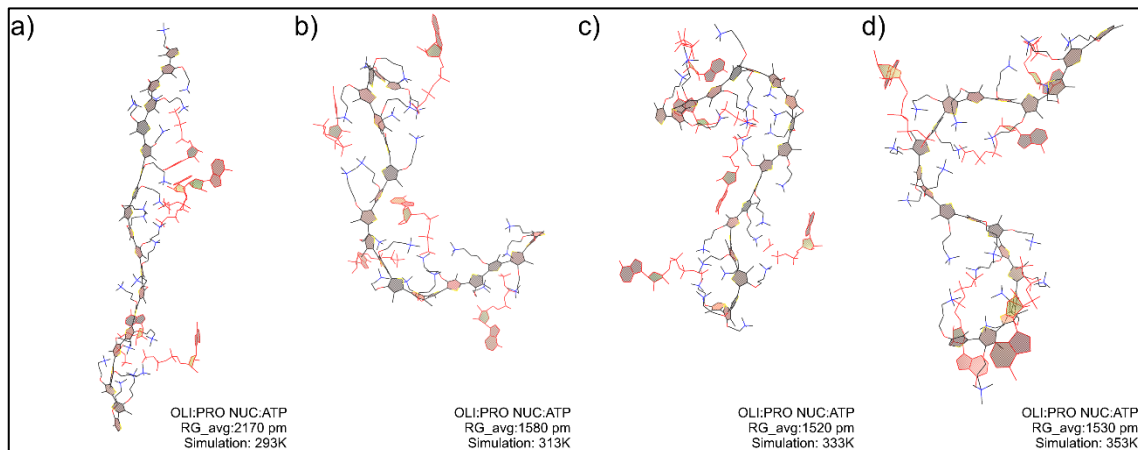
Figure A. 5. Snapshots which is recorded average R_g of O2 in ATP medium at increasing temperature
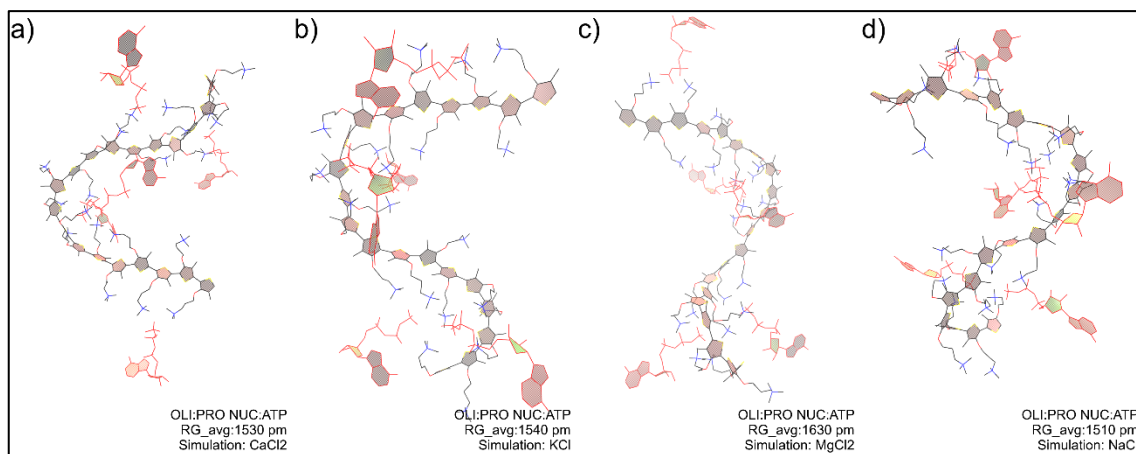

Figure A. 6. Snapshots which is recorded average R_g of O2 in ATP medium at presence of different salts
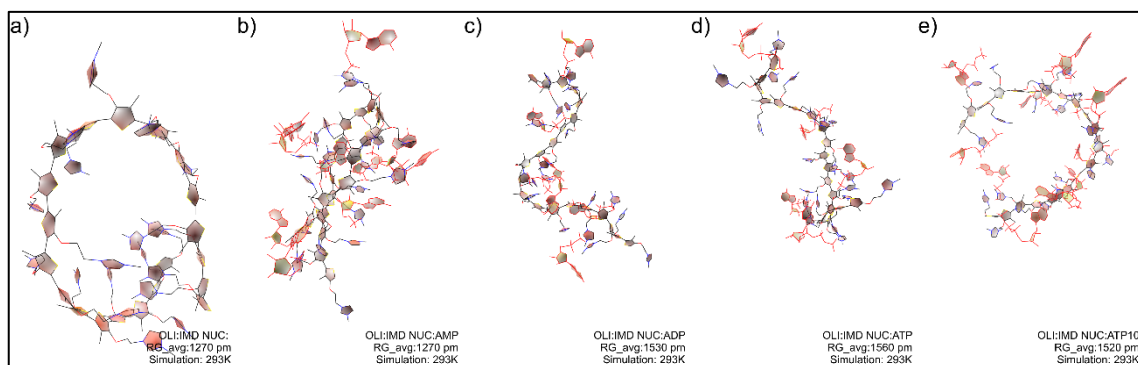
Figure A. 7. Snapshots of O3 in water and different adenosine nucleotides medium at average R_g
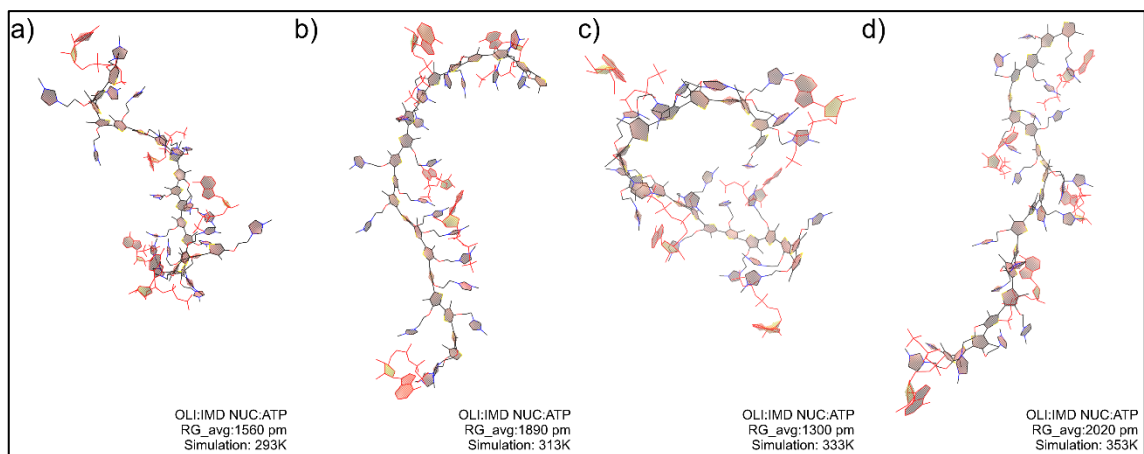

Figure A. 8. Snapshots which is recorded average R_g of O3 in ATP medium at increasing temperature

Figure A. 9. Snapshots which is recorded average R_g of O3 in ATP medium at presence of different salts

APPENDIX B

SNAPSHOTS OF OLIGOMERS AT MINIMUM R$_g$

Figure B. 1. Snapshots of O1 in water and different adenosine nucleotides medium at minimum R$_g$

Figure B. 2. Snapshots which is recorded minimum R$_g$ of O1 in ATP medium at increasing temperature
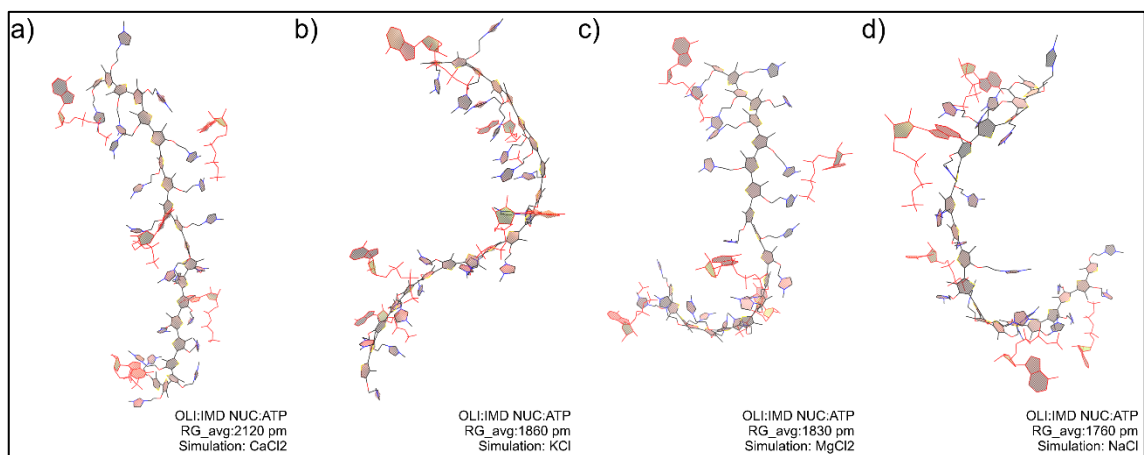
Figure B. 3. Snapshots which is recorded minimum R_g of O1 in ATP medium at presence of different salts

Figure B. 4. Snapshots of O2 in water and different adenosine nucleotides medium at minimum R_g

OLI:IMD NUC:ATP
RG_min:1330 pm
Simulation: 293K

OLI:IMD NUC:ATP
RG_min:1600 pm
Simulation: 313K

OLI:IMD NUC:ATP
RG_min:1150 pm
Simulation: 333K

OLI:IMD NUC:ATP
RG_min:1730 pm
Simulation: 353K

Figure B. 5. Snapshots which is recorded minimum R_g of O2 in ATP medium at increasing temperature

OLI:IMD NUC:ATP
RG_min:1940 pm
Simulation: CaCl2

OLI:IMD NUC:ATP
RG_min:1720 pm
Simulation: KCl

OLI:IMD NUC:ATP
RG_min:1690 pm
Simulation: MgCl2

OLI:IMD NUC:ATP
RG_min:1500 pm
Simulation: NaCl

Figure B. 6. Snapshots which is recorded minimum R_g of O2 in ATP medium at presence of different salts

Figure B. 7. Snapshots of O3 in water and different adenosine nucleotides medium at minimum R_g

Figure B. 8.. Snapshots which is recorded minimum R_g of O3 in ATP medium at increasing temperature
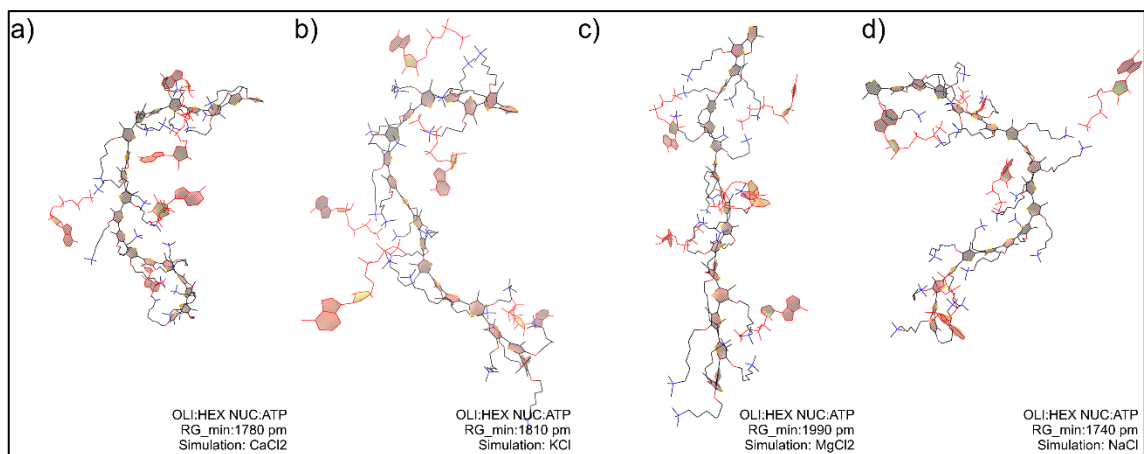
Figure B. 9. Snapshots which is recorded minimum R_g of O3 in ATP medium at presence of different salts
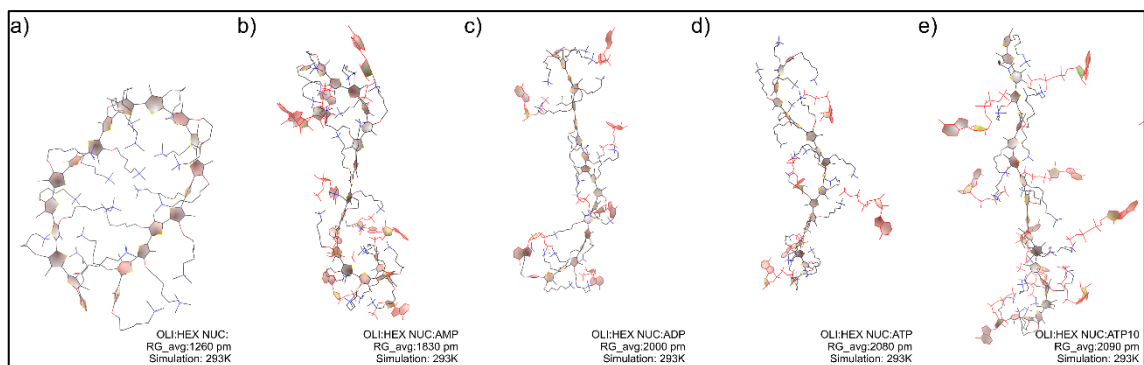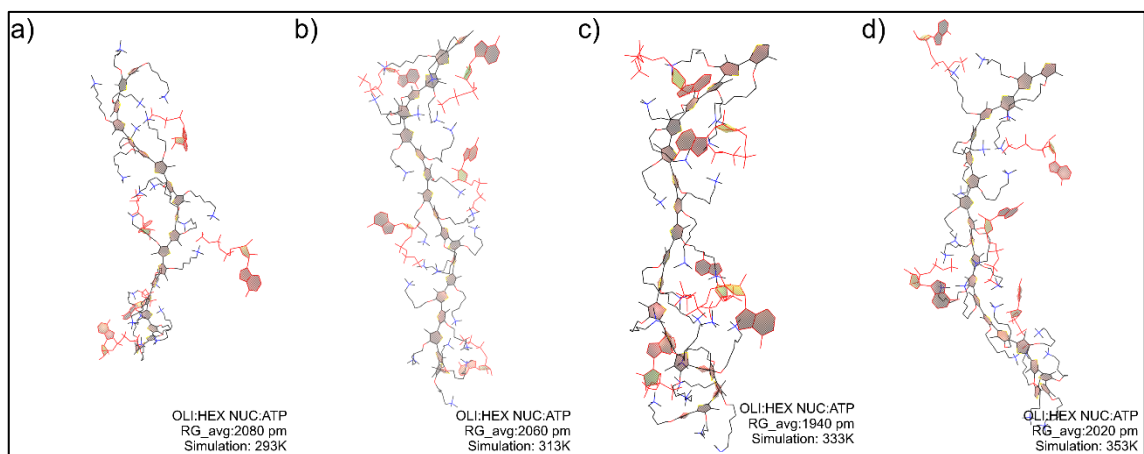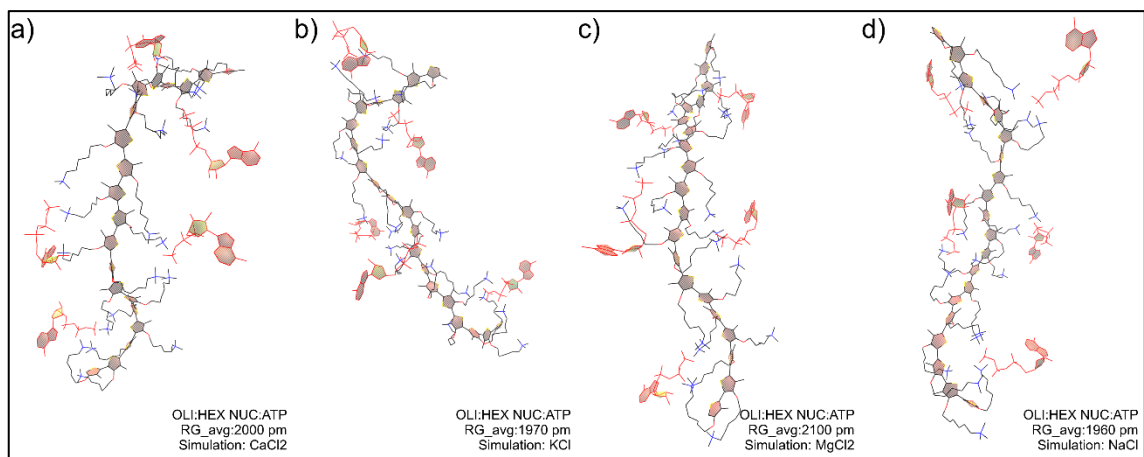
APPENDIX C

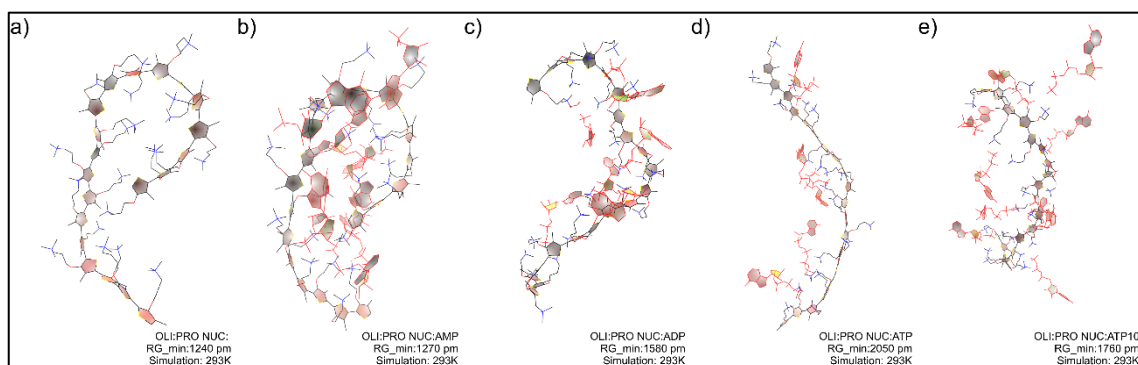# SNAPSHOTS OF OLIGOMERS AT MAXIMUM R_g

Figure C. 1. Snapshots of O1 in water and different adenosine nucleotides medium at maximum R_g
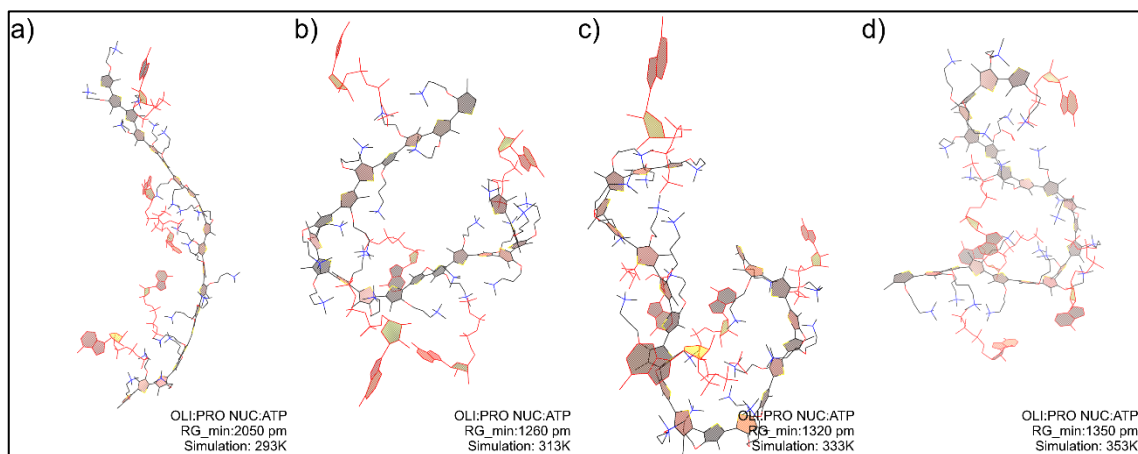

Figure C. 2. Snapshots which is recorded maximum R_g of O1 in ATP medium at increasing temperature
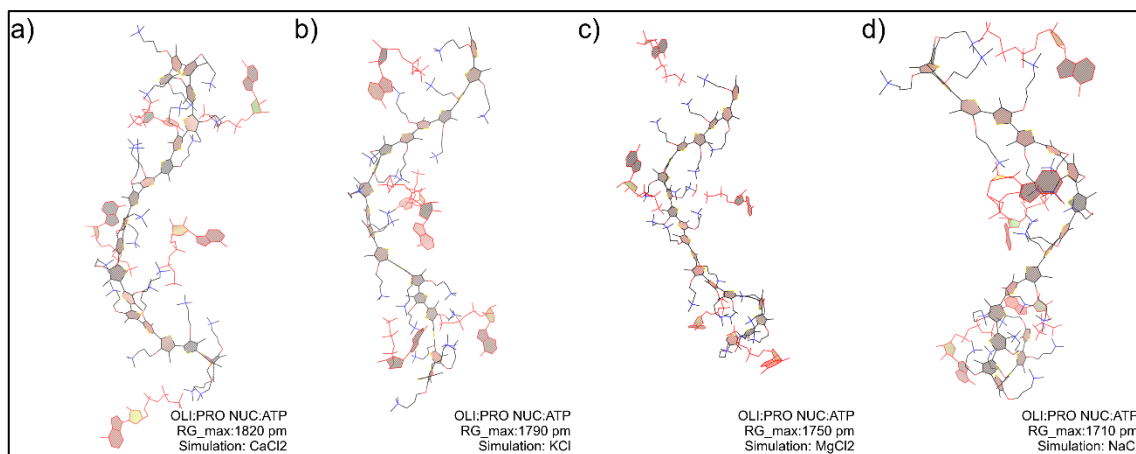
Figure C. 3. Snapshots which is recorded maximum R_g of O1 in ATP medium at presence of different salts

Figure C. 4.. Snapshots of O2 in water and different adenosine nucleotides medium at maximum R_g

Figure C. 5. Snapshots which is recorded maximum R_g of O2 in ATP medium at increasing temperature
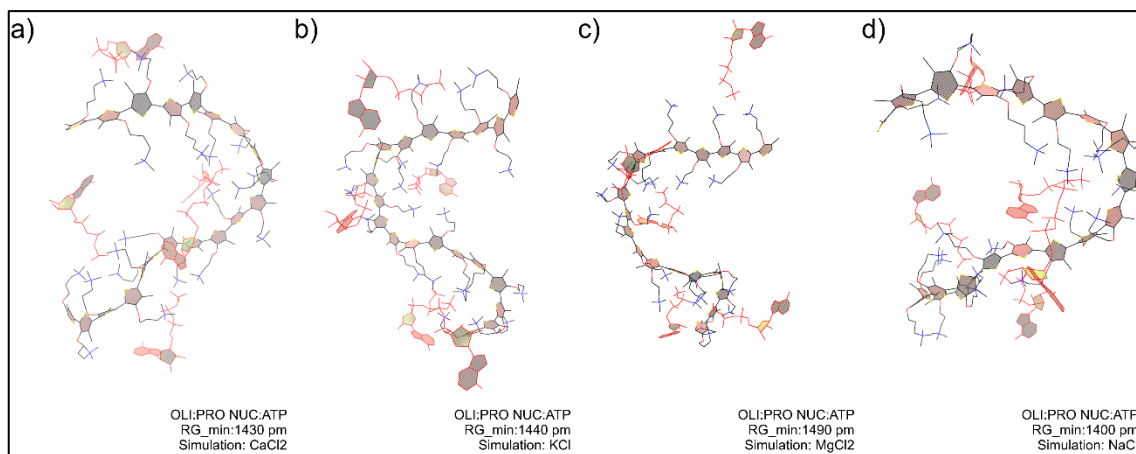

Figure C. 6. Snapshots which is recorded maximum R_g of O2 in ATP medium at presence of different salts
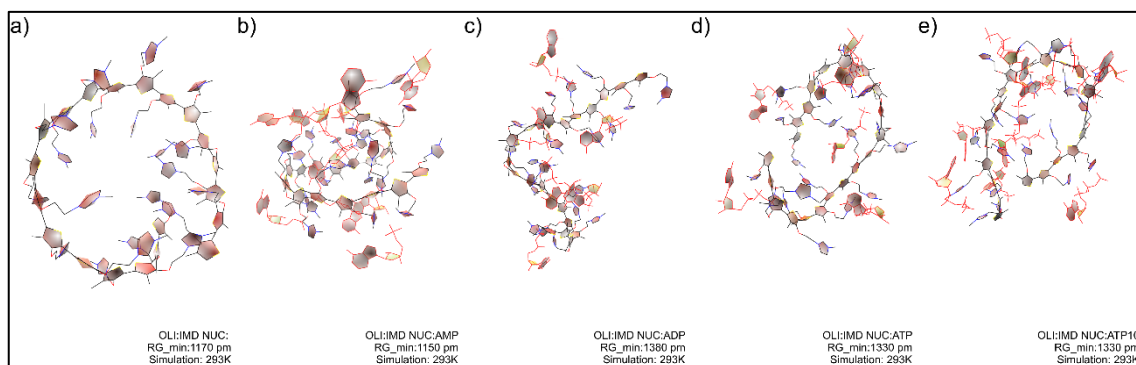
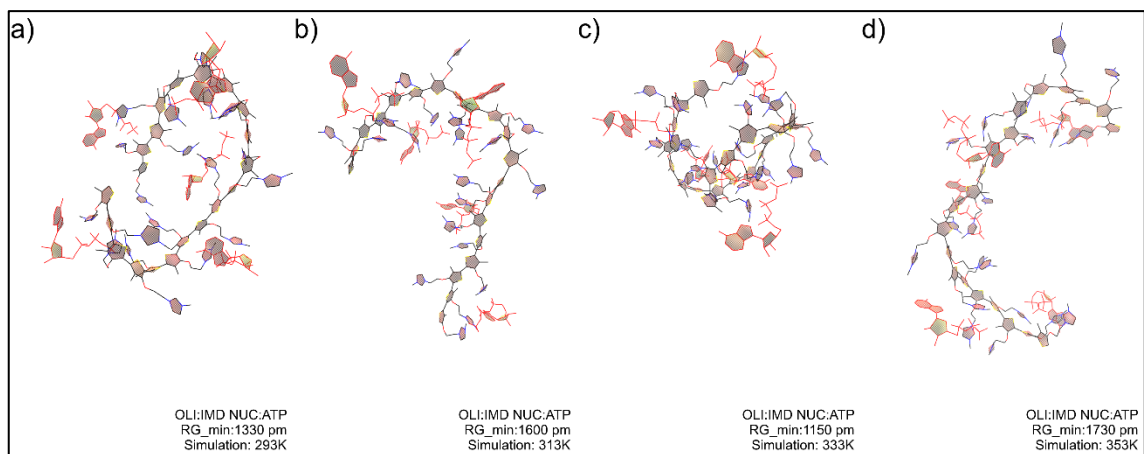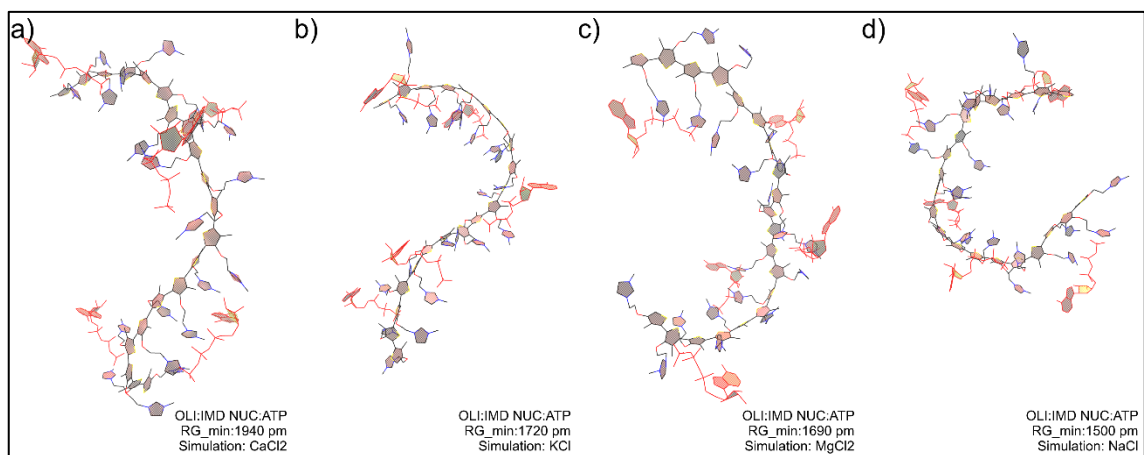Figure C. 7. Snapshots of O3 in water and different adenosine nucleotides medium at maximum R_g

Figure C. 8. Snapshots which is recorded maximum R_g of O3 in ATP medium at increasing temperature

98

a)
OLI:HEX NUC:ATP
RG_max:2130 pm
Simulation: CaCl2

b)
OLI:HEX NUC:ATP
RG_max:2100 pm
Simulation: KCl

c)
OLI:HEX NUC:ATP
RG_max:2160 pm
Simulation: MgCl2

d)
OLI:HEX NUC:ATP
RG_max:2190 pm
Simulation: NaCl

Figure C. 9. Snapshots which is recorded maximum R_g of O3 in ATP medium at presence of different salts

APPENDIX D

SNAPSHOTS OF OLIGOMERS AT AVERAGE R$_{ee}$

Figure D. 1. Snapshots of O1 in water and different adenosine nucleotides medium at average R$_{ee}$

Figure D. 2. Snapshots which is recorded average R$_{ee}$ of O1 in ATP medium at increasing temperature

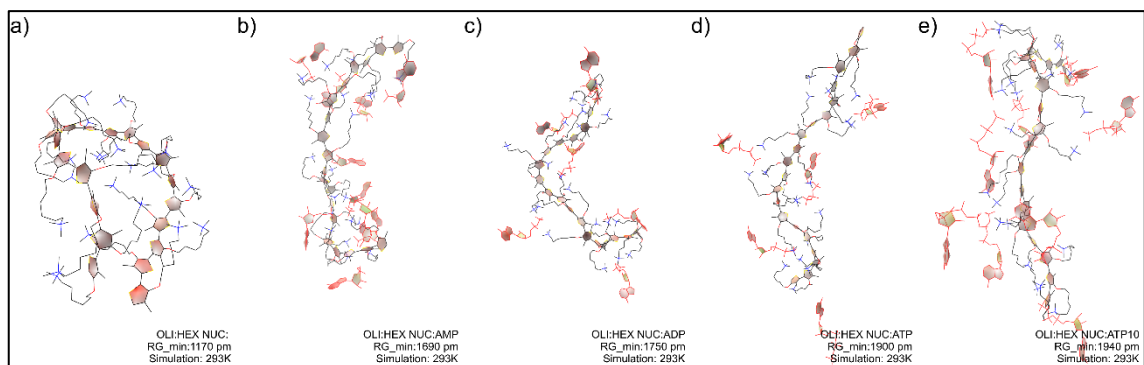Figure D. 3. Snapshots which is recorded average R_{ee} of O1 in ATP medium at presence of different salts

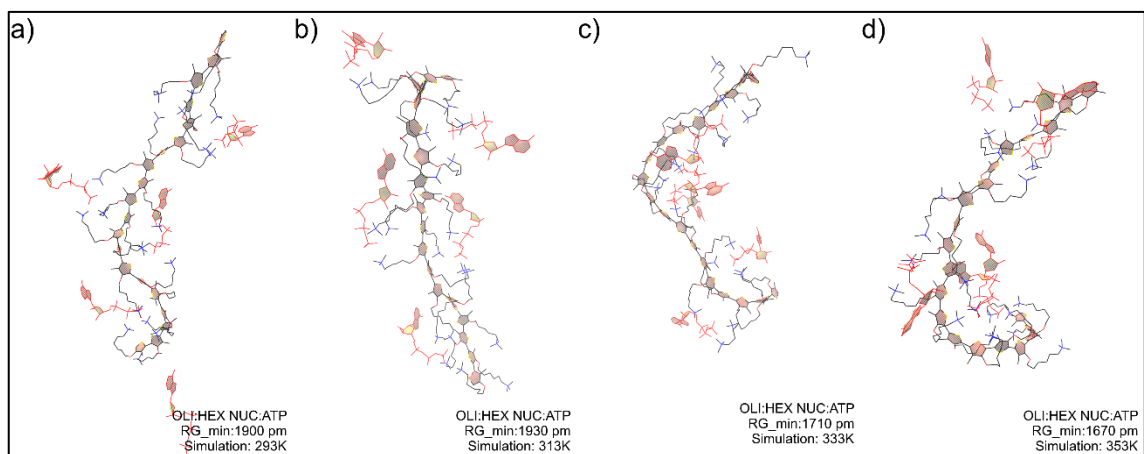Figure D. 4. Snapshots of O2 in water and different adenosine nucleotides medium at average R_{ee}

Figure D. 5. Snapshots which is recorded average R_{ee} of O2 in ATP medium at increasing temperature

Figure D. 6. Snapshots which is recorded average R_{ee} of O2 in ATP medium at presence of different salts

a) OLI:HEX NUC:
Ee_avg:1040 pm
Simulation: 293K

b) OLI:HEX NUC:AMP
Ee_avg:5170 pm
Simulation: 293K

c) OLI:HEX NUC:ADP
Ee_avg:6240 pm
Simulation: 293K

d) OLI:HEX NUC:ATP
Ee_avg:6700 pm
Simulation: 293K

e) OLI:HEX NUC:ATP10
Ee_avg:6800 pm
Simulation: 293K

Figure D. 7. Snapshots of O3 in water and different adenosine nucleotides medium at average R_{ee}

a) OLI:HEX NUC:ATP
Ee_avg:6700 pm
Simulation: 293K

b) OLI:HEX NUC:ATP
Ee_avg:6480 pm
Simulation: 313K

c) OLI:HEX NUC:ATP
Ee_avg:6040 pm
Simulation: 333K

d) OLI:HEX NUC:ATP
Ee_avg:6320 pm
Simulation: 353K

Figure D. 8. Snapshots which is recorded average R_{ee} of O3 in ATP medium at increasing temperature

a) OLI:HEX NUC:ATP
Ee_avg:6100 pm
Simulation: CaCl2

b) OLI:HEX NUC:ATP
Ee_avg:5610 pm
Simulation: KCl

c) OLI:HEX NUC:ATP
Ee_avg:6620 pm
Simulation: MgCl2

d) OLI:HEX NUC:ATP
Ee_avg:5830 pm
Simulation: NaCl

Figure D. 9. Snapshots which is recorded average R_{ee} of O3 in ATP medium at presence of different salts
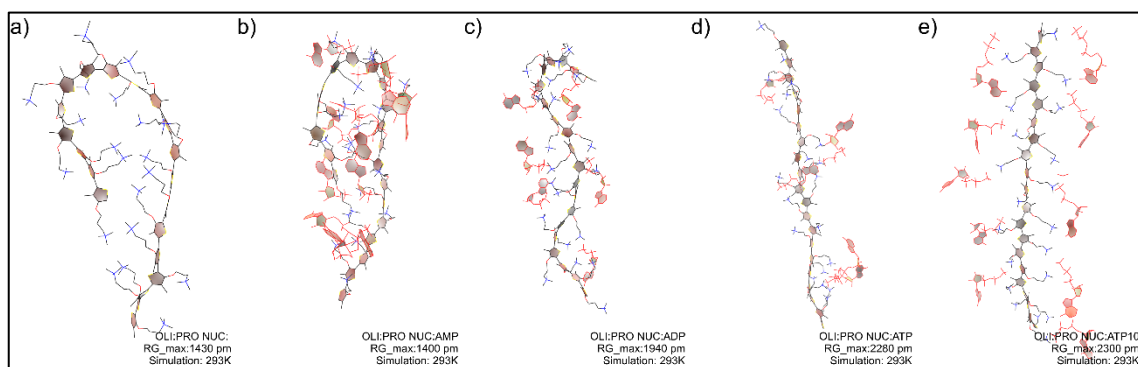
APPENDIX E

SNAPSHOTS OF OLIGOMERS AT MINIMUM R$_{ee}$

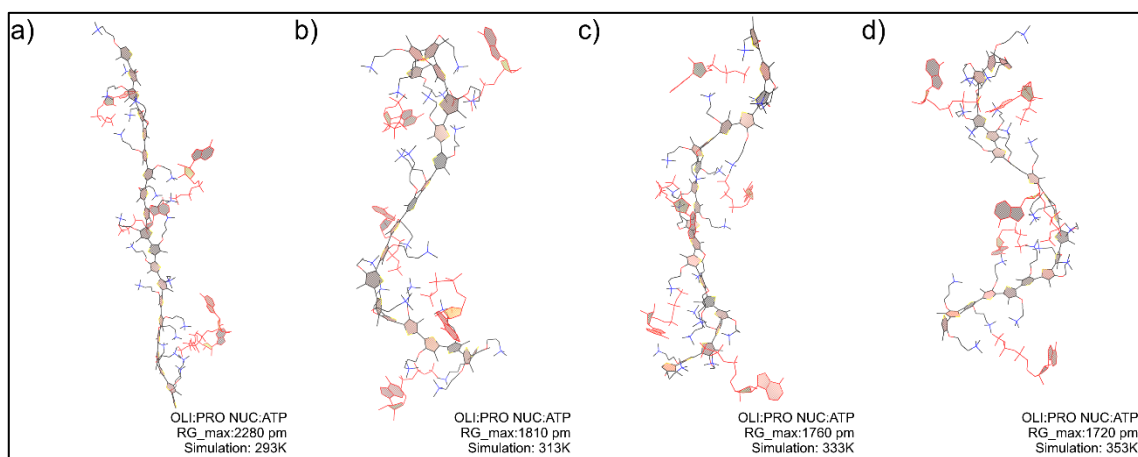Figure E. 1. Snapshots of O1 in water and different adenosine nucleotides medium at minimum R$_{ee}$

Figure E. 2.. Snapshots which is recorded minimum R$_{ee}$ of O1 in ATP medium at increasing temperature

Figure E. 3. Snapshots which is recorded minimum R_{ee} of O1 in ATP medium at presence of different salts
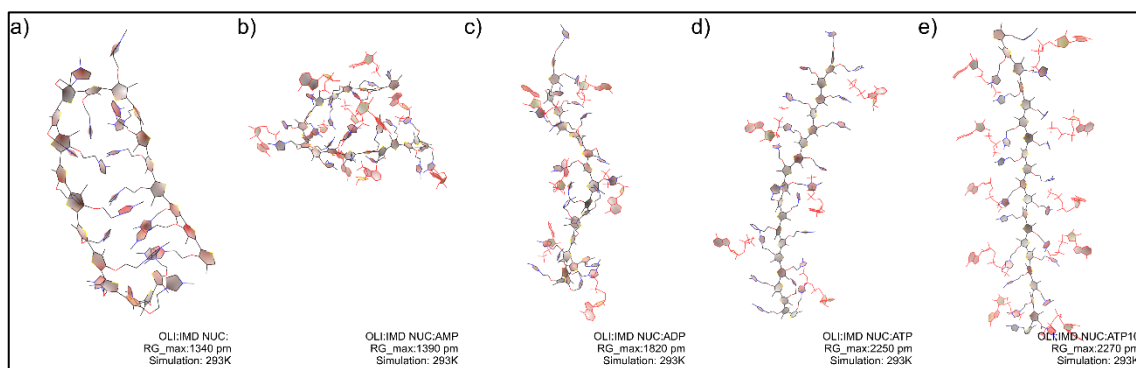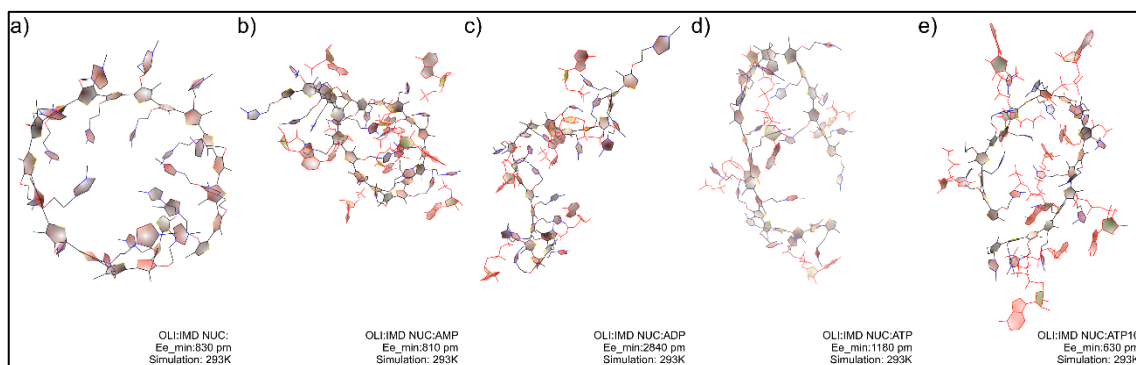

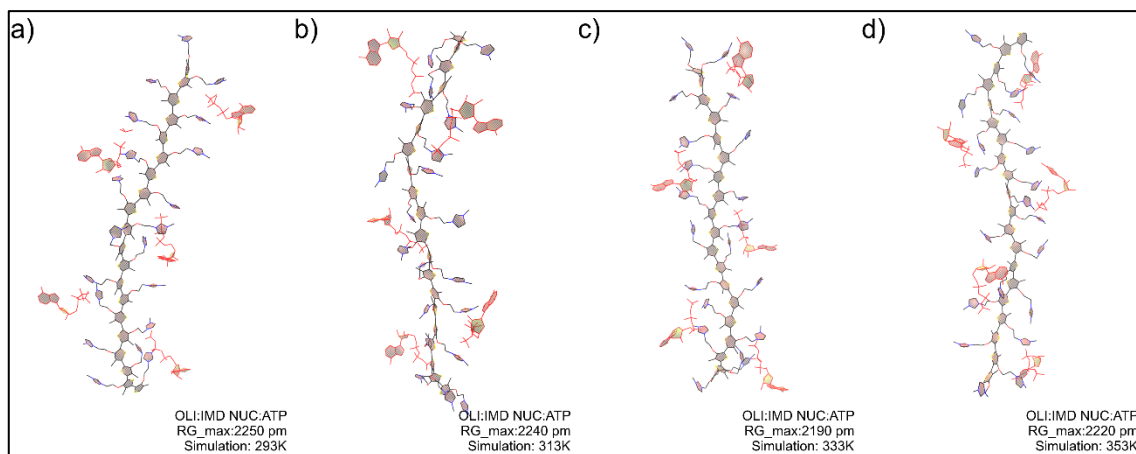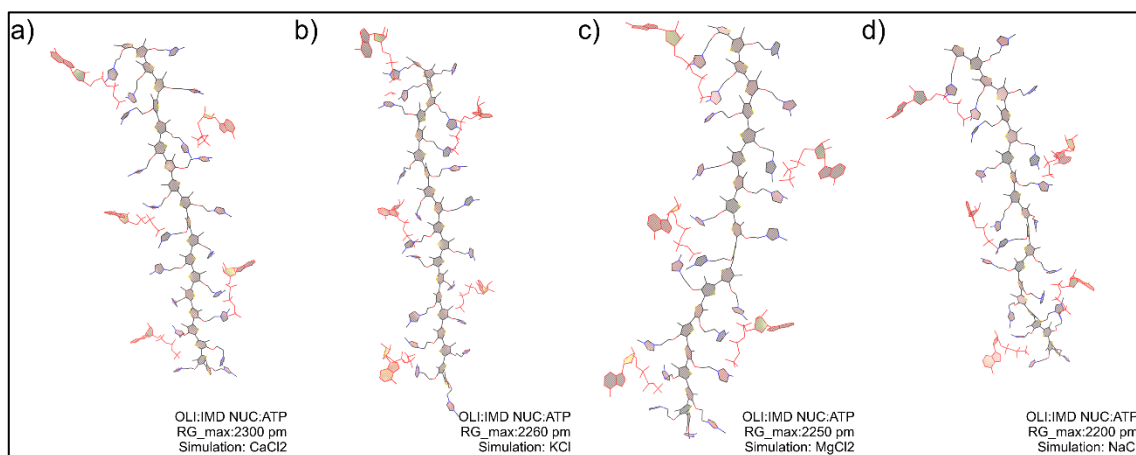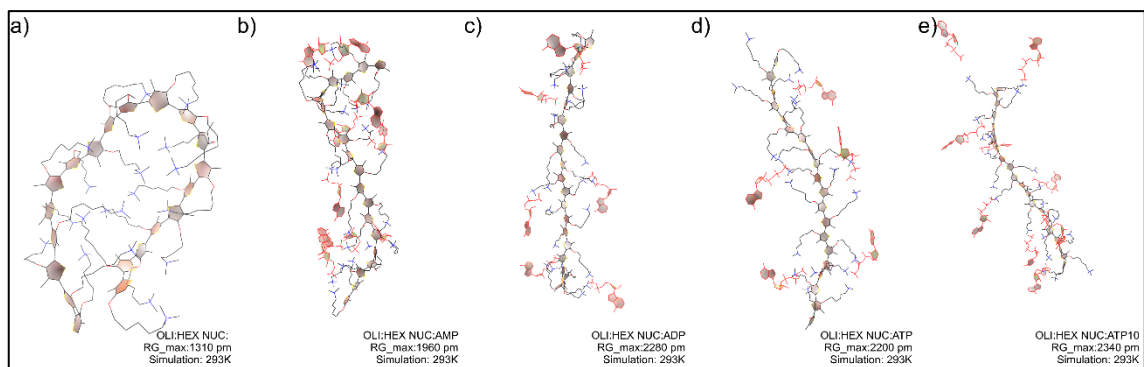Figure E. 4. Snapshots of O2 in water and different adenosine nucleotides medium at minimum R_{ee}

a) OLI:IMD NUC:ATP
Ee_min:1180 pm
Simulation: 293K

b) OLI:IMD NUC:ATP
Ee_min:3020 pm
Simulation: 313K

c) OLI:IMD NUC:ATP
Ee_min:1450 pm
Simulation: 333K

d) OLI:IMD NUC:ATP
Ee_min:3100 pm
Simulation: 353K
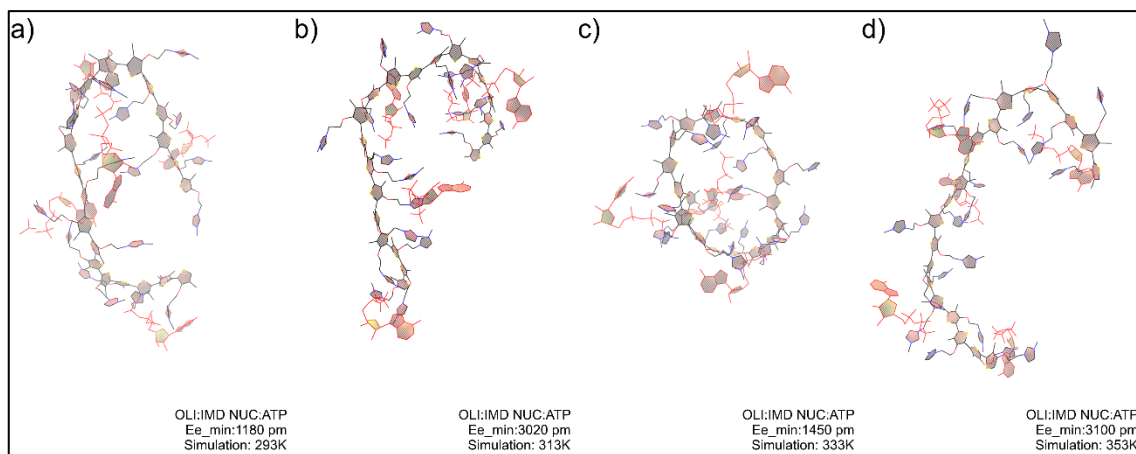
Figure E. 5. Snapshots which is recorded minimum R_{ee} of O2 in ATP medium at increasing temperature

a) OLI:IMD NUC:ATP
Ee_min:5200 pm
Simulation: CaCl2

b) OLI:IMD NUC:ATP
Ee_min:4560 pm
Simulation: KCl

c) OLI:IMD NUC:ATP
Ee_min:3100 pm
Simulation: MgCl2

d) OLI:IMD NUC:ATP
Ee_min:1380 pm
Simulation: NaCl
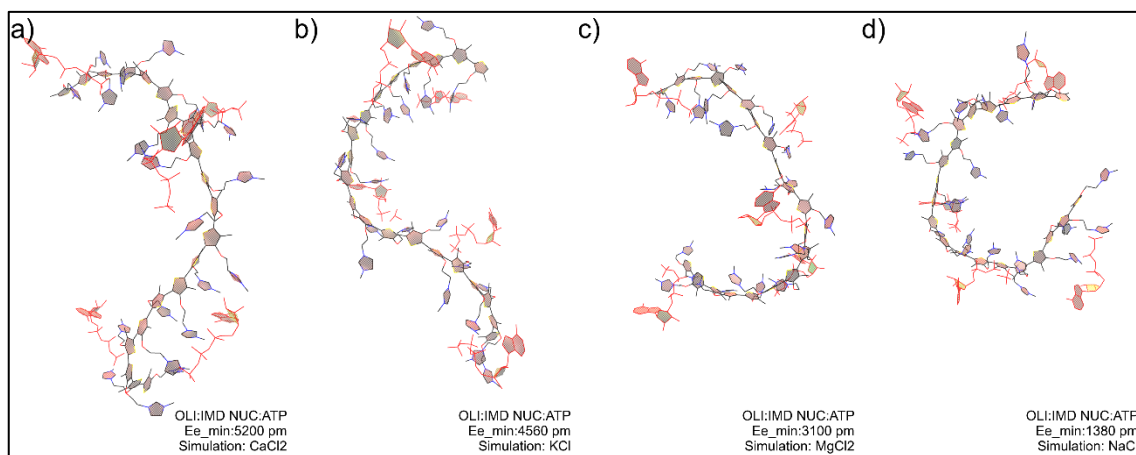
Figure E. 6. Snapshots which is recorded minimum R_{ee} of O2 in ATP medium at presence of different salts
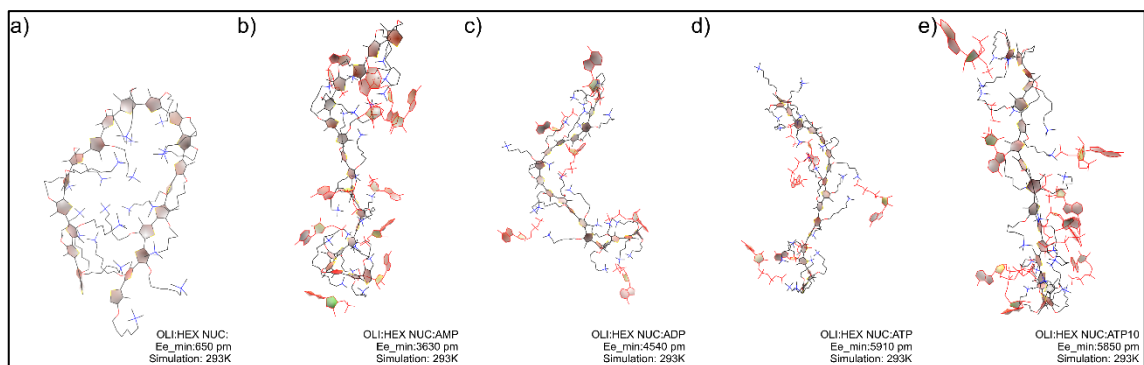
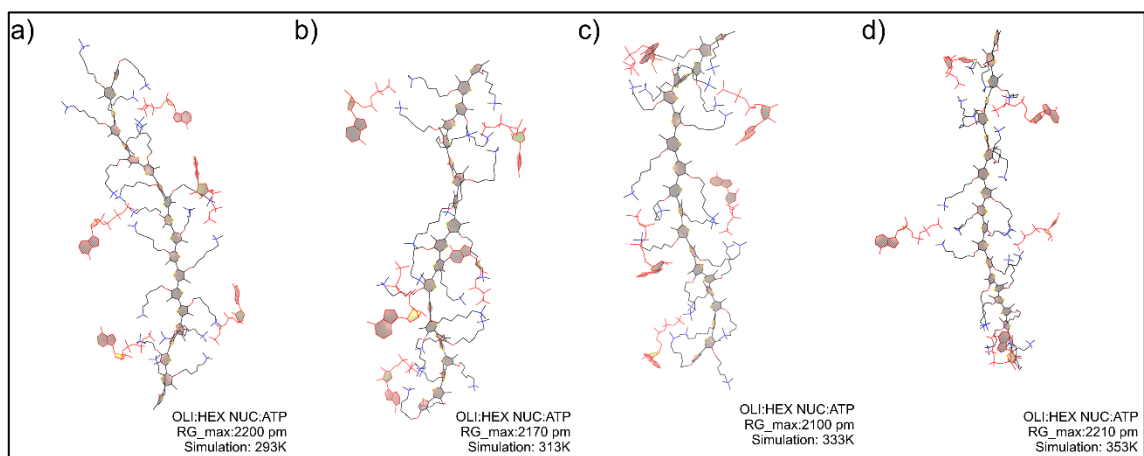Figure E. 7. Snapshots of O3 in water and different adenosine nucleotides medium at minimum R_{ee}
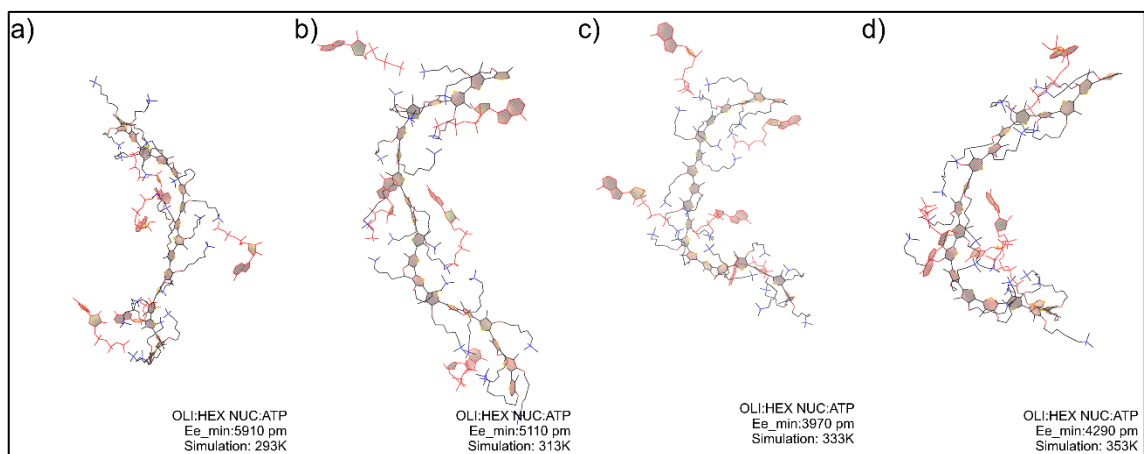
Figure E. 8. Snapshots which is recorded minimum R_{ee} of O3 in ATP medium at increasing temperature
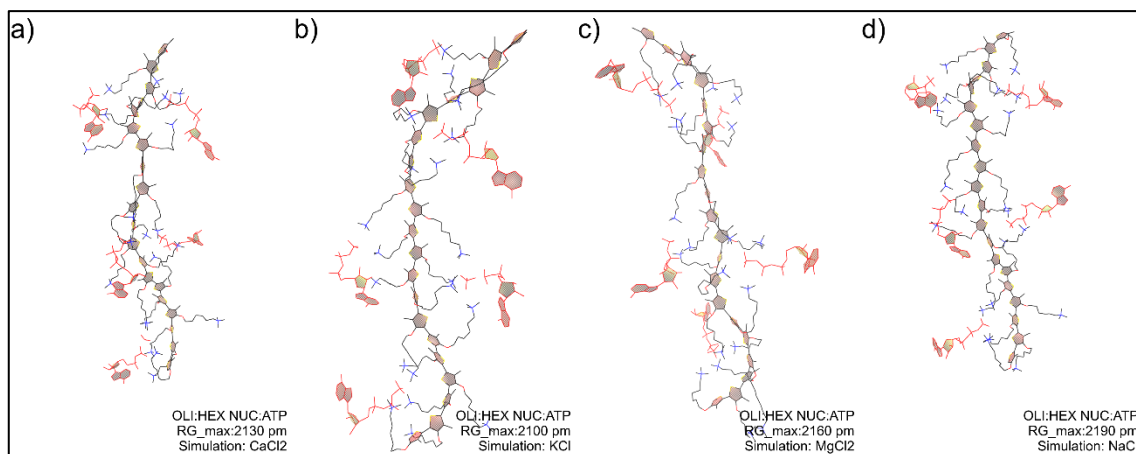
a) OLI:HEX NUC:ATP
Ee_min:4760 pm
Simulation: CaCl2

b) OLI:HEX NUC:ATP
Ee_min:3710 pm
Simulation: KCl

c) OLI:HEX NUC:ATP
Ee_min:5620 pm
Simulation: MgCl2

d) OLI:HEX NUC:ATP
Ee_min:4010 pm
Simulation: NaCl
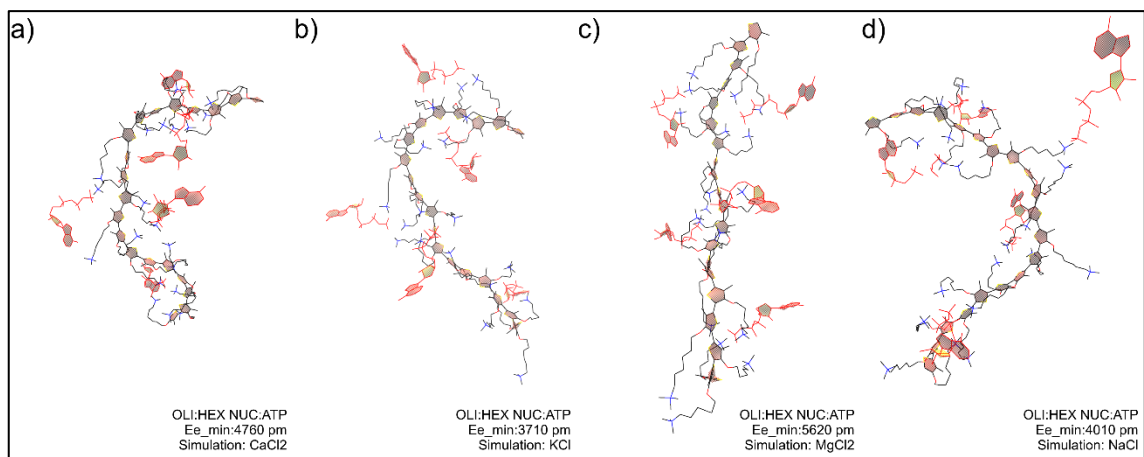
Figure E. 9. Snapshots which is recorded minimum R_{ee} of O3 in ATP medium at presence of different salts
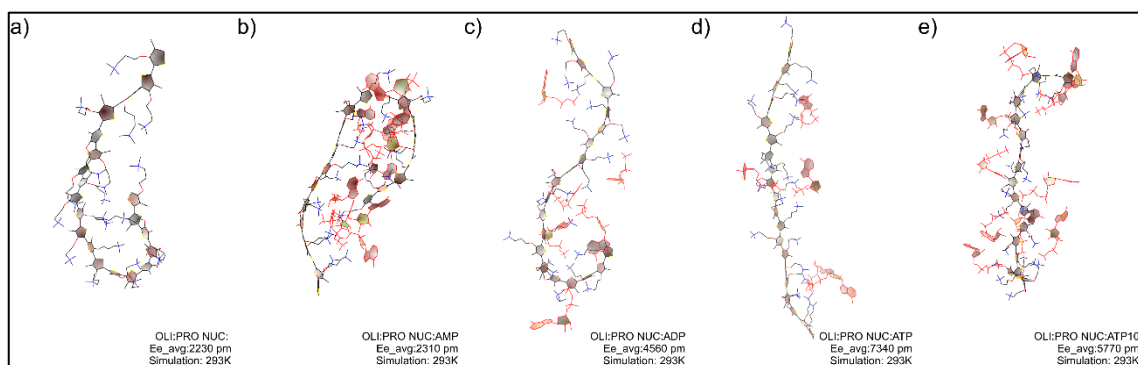
APPENDIX F

SNAPSHOTS OF OLIGOMERS AT MAXIMUM R_{ee}
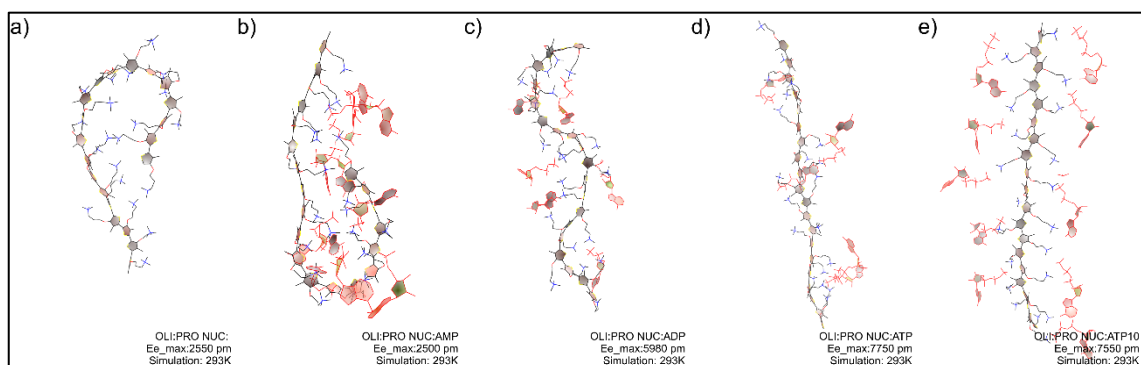
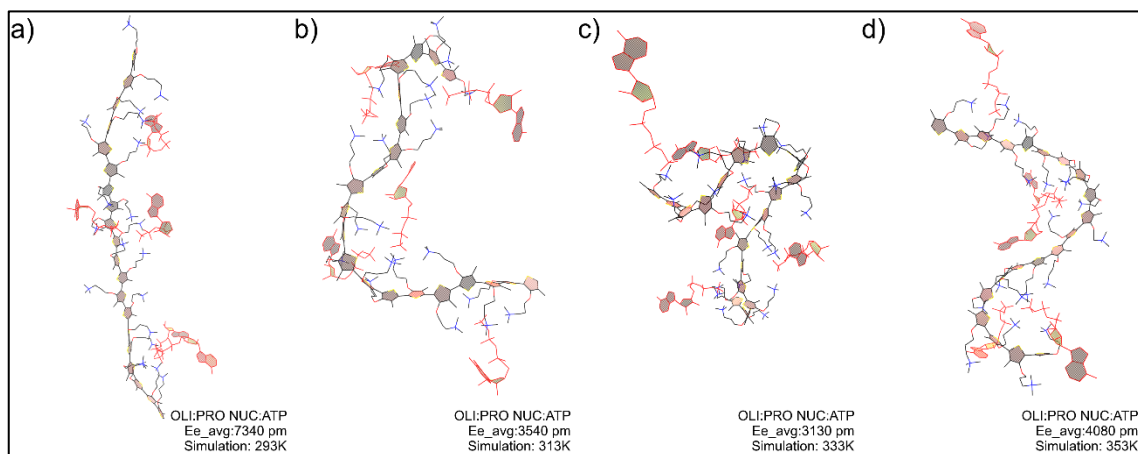Figure F. 1. Snapshots of O1 in water and different adenosine nucleotides medium at maximum R_{ee}
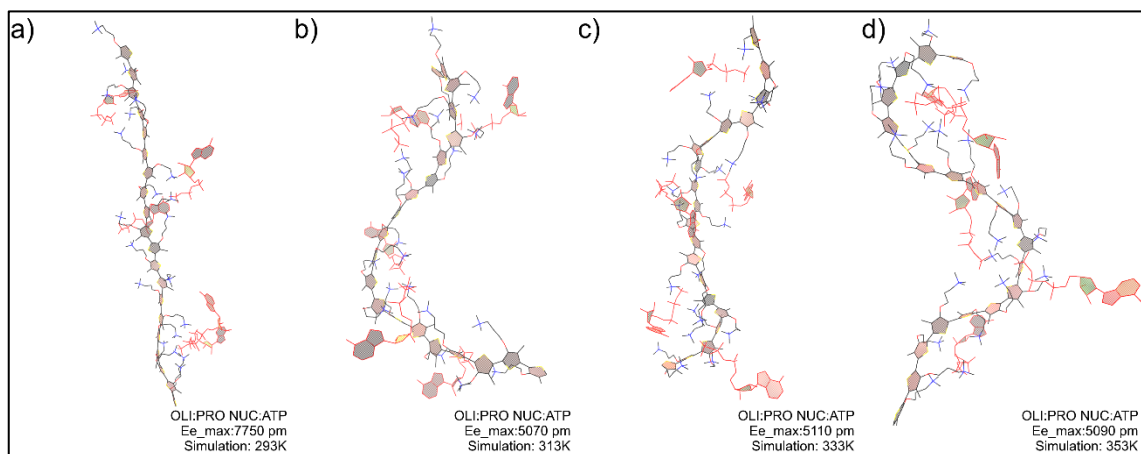
Figure F. 2. Snapshots which is recorded maximum R_{ee} of O1 in ATP medium at increasing temperature
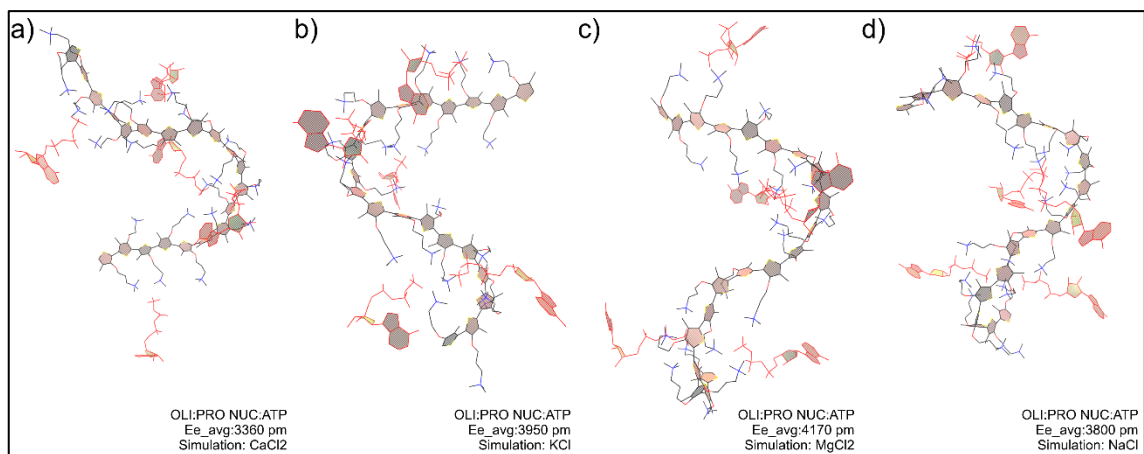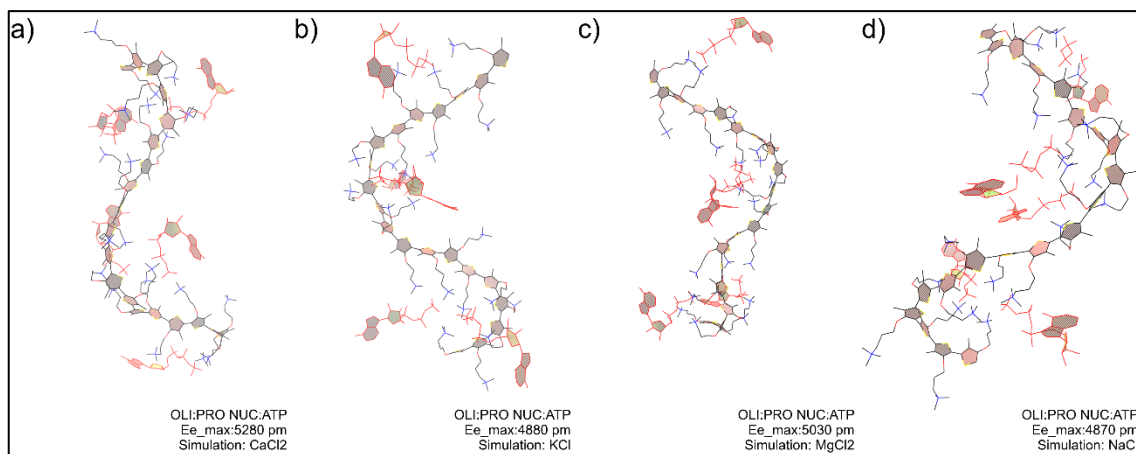
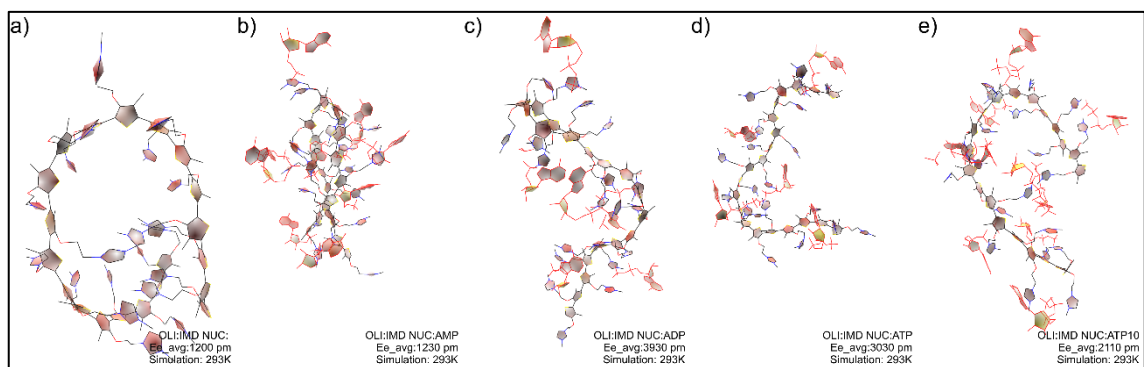Figure F. 3. Snapshots which is recorded maximum R_{ee} of O1 in ATP medium at presence of different salts
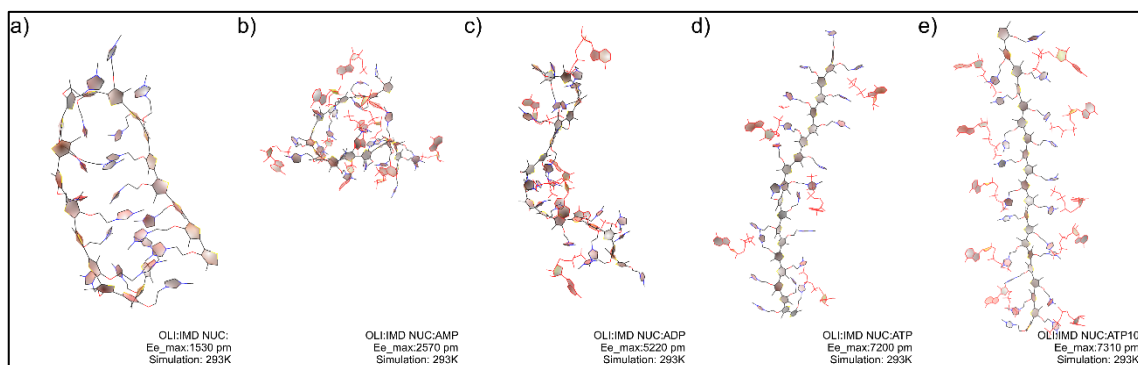
Figure F. 4. Snapshots of O2 in water and different adenosine nucleotides medium at maximum R_{ee}
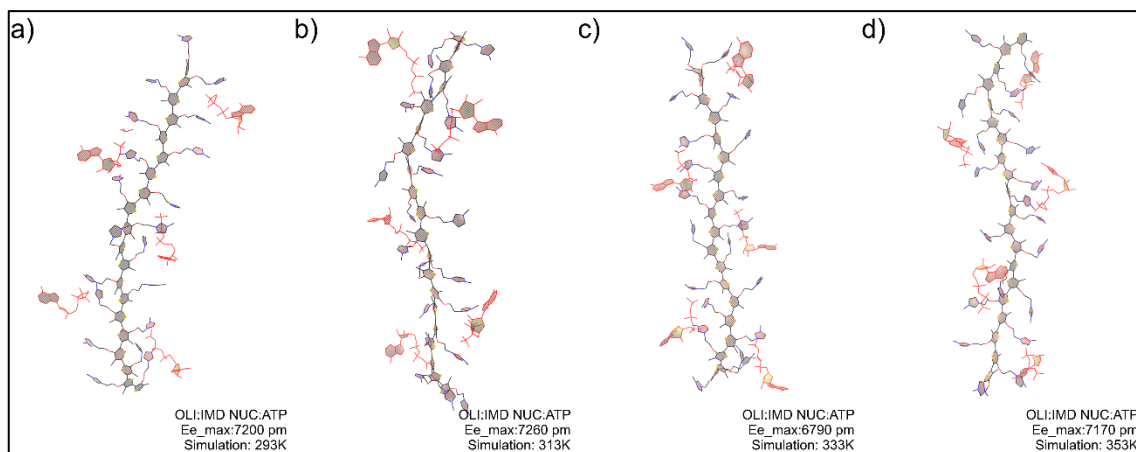
Figure F. 5. Snapshots which is recorded maximum R_{ee} of O2 in ATP medium at increasing temperature
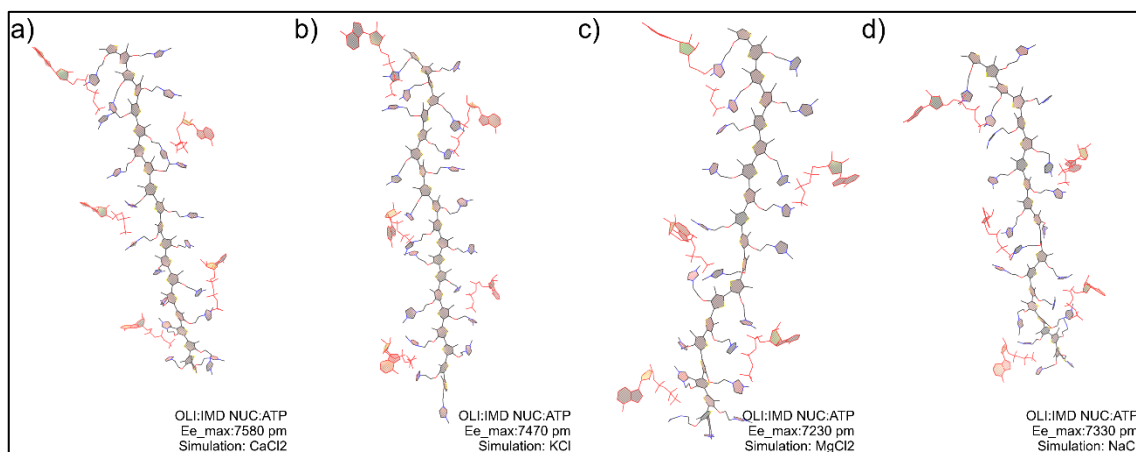
Figure F. 6. Snapshots which is recorded maximum R_{ee} of O3 in ATP medium at presence of different salts
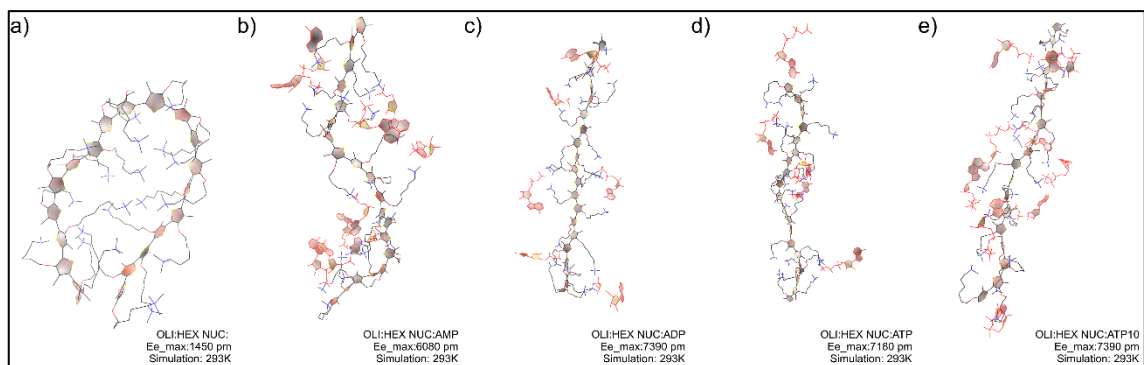
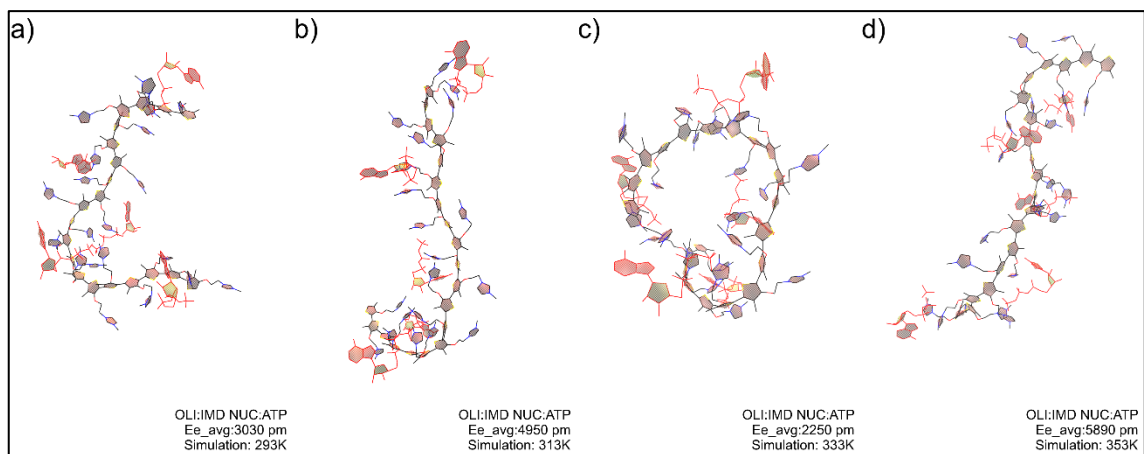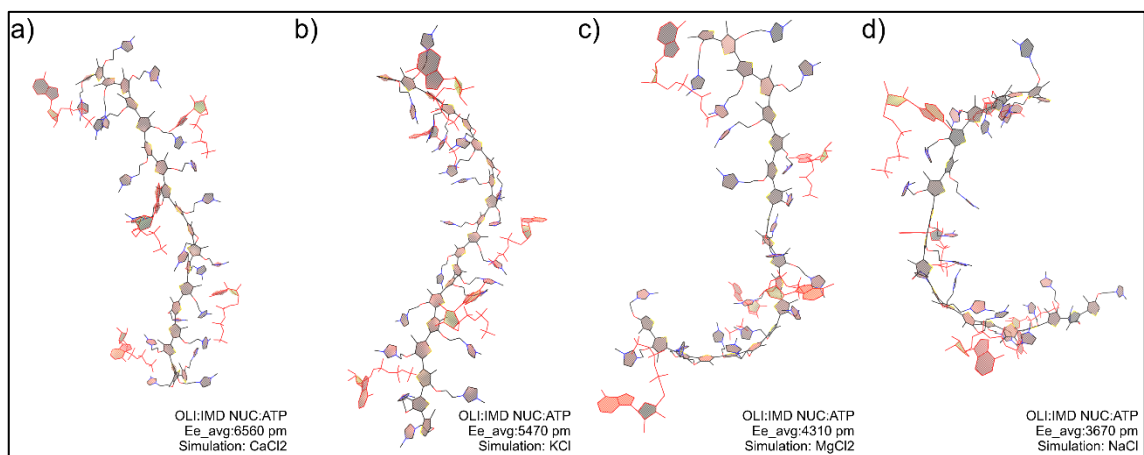Figure F. 7. Snapshots of O3 in water and different adenosine nucleotides medium at maximum R_{ee}
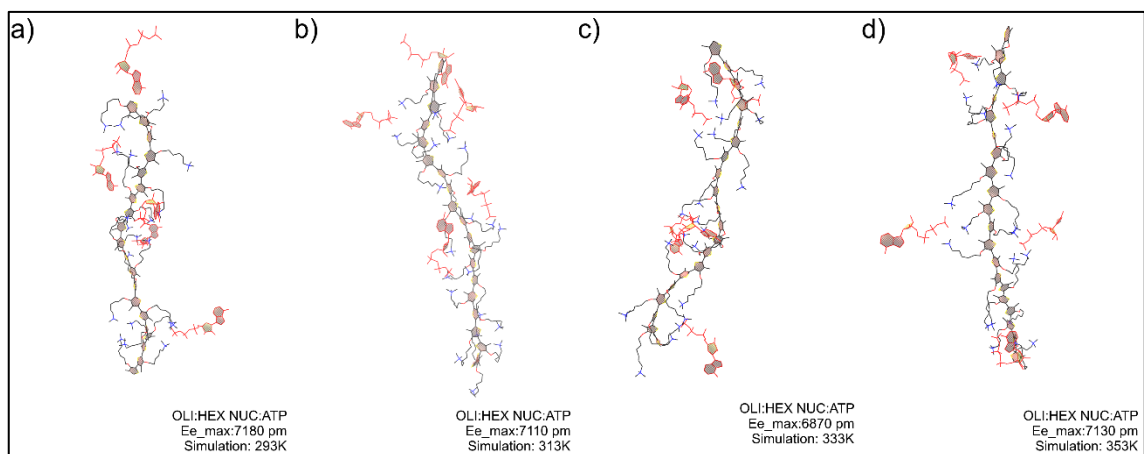
Figure F. 8. Snapshots which is recorded maximum R_{ee} of O3 in ATP medium at increasing temperature

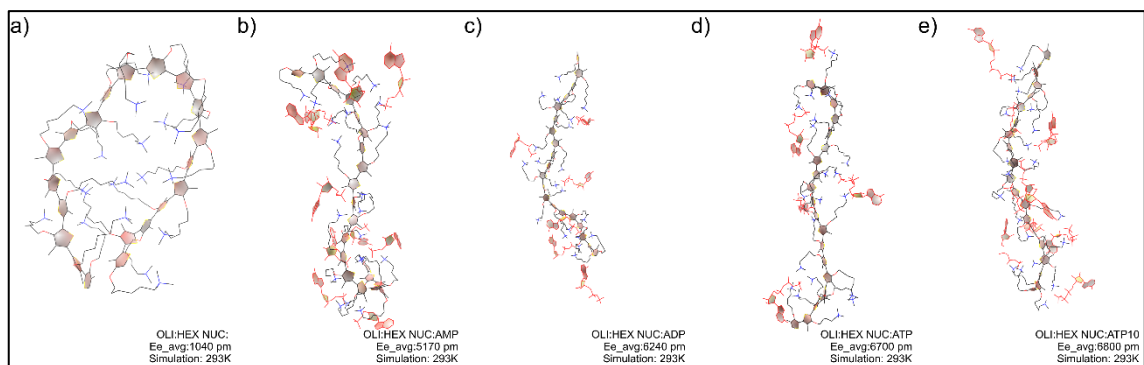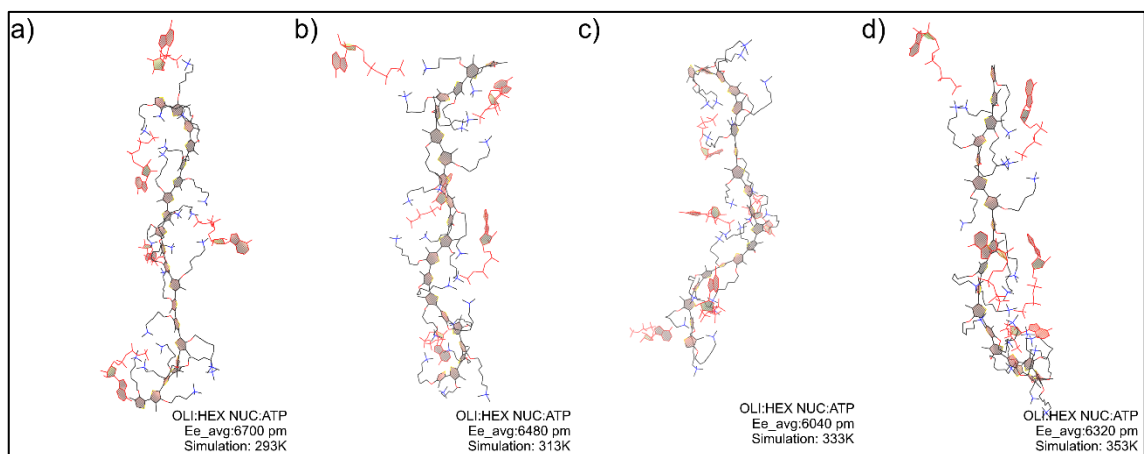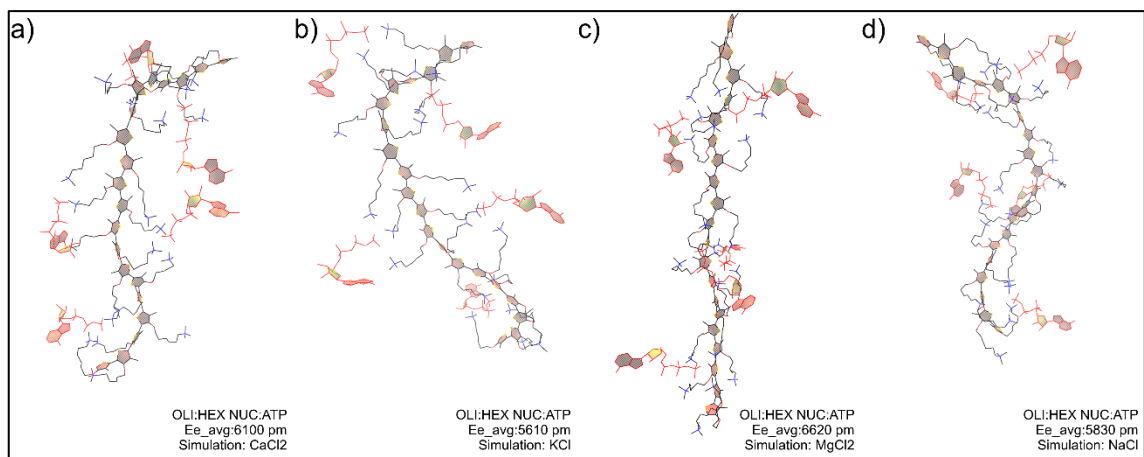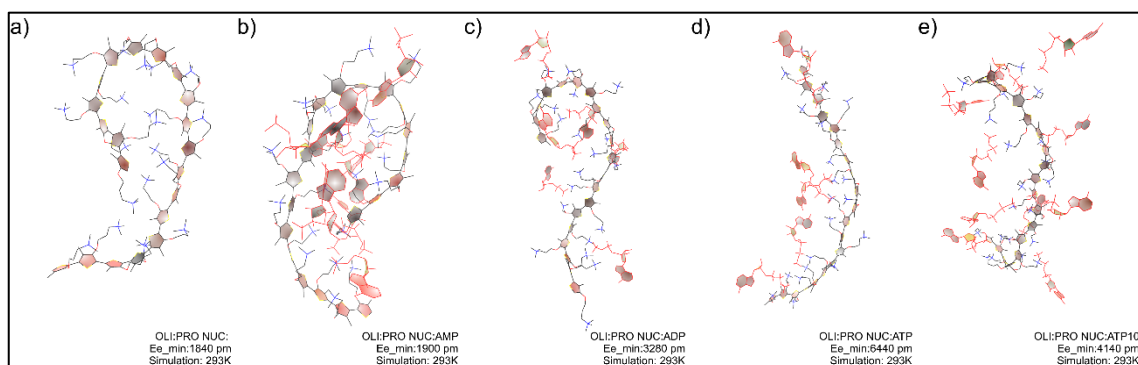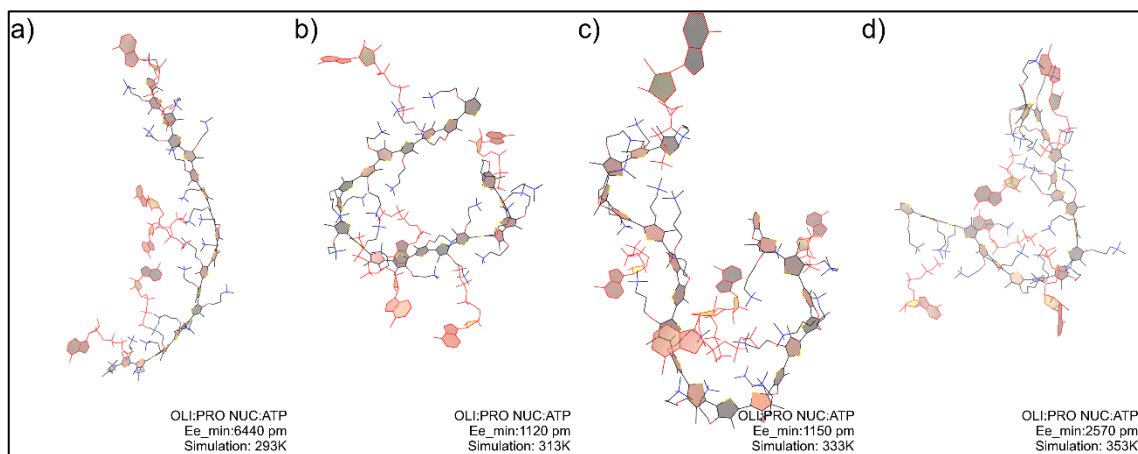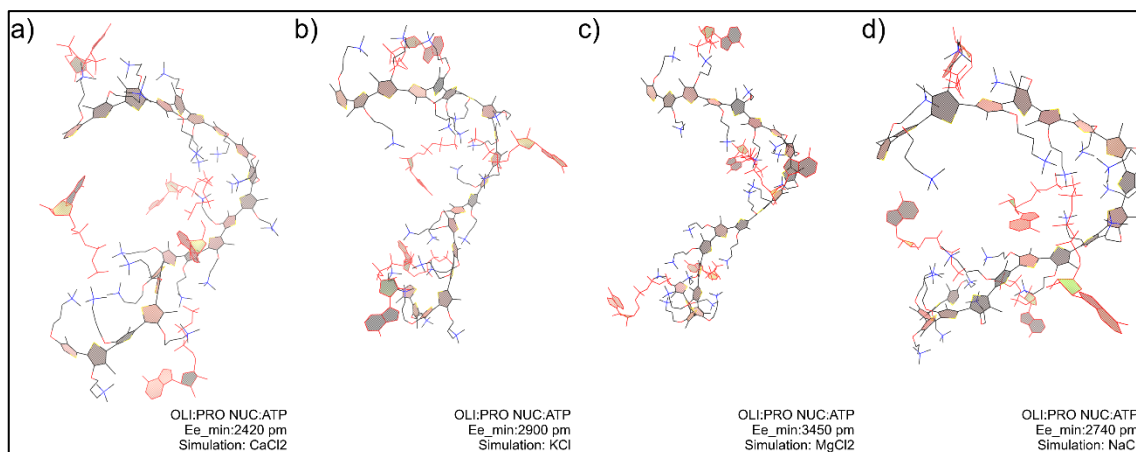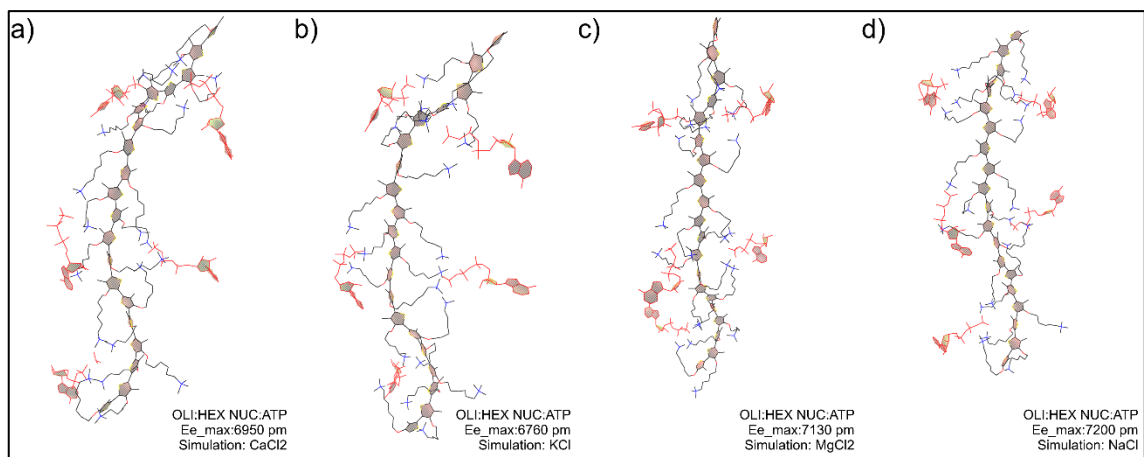Figure F. 9. Snapshots which is recorded maximum R_{ee} of O3 in ATP medium at presence of different salts

APPENDIX G

MISSING PARAMETERS OF OLIGOMER CREATED BY

FFTK

Table G. 1. Poly - N, N, N-trimethyl-3-(4-methylthiophen-3-yl) oxy) propan-1-aminium

BONDS

ATOM TYPE	K_b (kcal x Å^2 /mole)	b0 (Å)
CG2R51 OG301	398.520	1.3770

ANGLES

ATOM TYPE	K_θ (kcal x rad^2 /mole)	θ_0 (degree)
CG2R57 CG2R51 OG301	82.275	122.17
CG2R51 OG301 CG321	65.00	108.00

DIHEDRALS

ATOM TYPE	K_χ (kcal/mole)	n (multiplicity)	Δ (degree)
OG301 CG2R51 CG2R51 CG2R57	2.0840	2	180.00
OG301 CG2R51 CG2R51 CG331	2.0100	2	180.00
CG331 CG2R51 CG2R57 SG2R50	1.3060	2	180.00
OG301 CG2R51 CG2R57 SG2R50	0.7800	2	180.00
CG2R57 CG2R51 OG301 CG321	0.4320	2	180.00
CG2R57 CG2R51 OG301 CG321	0.1400	4	180.00
OG301 CG321 CG321 CG324	1.0810	1	0.00
OG301 CG321 CG321 CG324	1.5870	2	0.00
CG2R51 CG2R57 CG2R57 CG2R51	2.9690	2	0.00
CG2R51 CG2R57 CG2R57 CG2R51	0.0040	4	180.00
SG2R50 CG2R57 CG2R57 SG2R50	1.1850	2	180.00
SG2R50 CG2R57 CG2R57 SG2R50	2.3220	4	0.00
CG2R51 CG2R57 CG2R57 SG2R50	0.6380	2	180.00
CG2R51 CG2R57 CG2R57 SG2R50	0.6670	4	180.00

APPENDIX H

MISSING PARAMETERS OF OLIGOMER CREATED BY

CHARMM

Table H. 1. Poly- N, N, N-trimethyl-3-(4-methylthiophen-3-yl) oxy) propan-1-aminium and Poly- N, N, N-trimethyl-3-(4-methylthiophen-3-yl) oxy) hexane -1-aminium

BONDS

ATOM TYPE	K_b (kcal x Å^2 /mole)	b0 (Å)
CG2R51 OG301	300.00	1.3820

ANGLES

ATOM TYPE	K_θ (kcal x rad^2 /mole)	θ_0 (degree)
CG2R57 CG2R51 OG301	120.00	123.20
CG2R51 OG301 CG321	65.00	108.00

DIHEDRALS

ATOM TYPE	K_χ (kcal/mole)	n (multiplicity)	Δ (degree)
OG301 CG2R51 CG2R51 CG2R57	4.3000	2	180.00
OG301 CG2R51 CG2R51 CG331	6.3600	2	180.00
CG331 CG2R51 CG2R57 SG2R50	2.2100	2	180.00
OG301 CG2R51 CG2R57 SG2R50	7.0000	2	180.00
CG2R57 CG2R51 OG301 CG321	1.6200	2	180.00
CG2R57 CG2R51 OG301 CG321	0.1900	4	180.00
CG321 CG321 OG301 CG2R51	0.2400	1	0.00
CG321 CG321 OG301 CG2R51	0.2900	2	0.00
CG321 CG321 OG301 CG2R51	0.0200	3	0.00
CG331 CG2R51 CG2R51 OG301	6.3600	2	180.00
CG324 CG321 CG321 OG301	2.1691	1	0.00
CG324 CG321 CG321 OG301	0.9924	2	0.00
CG324 CG321 CG321 OG301	0.0802	3	180.00
CG324 CG321 CG321 OG301	0.1765	4	180.00
CG324 CG321 CG321 OG301	0.3634	5	180.00
CG324 CG321 CG321 OG301	0.0731	6	0.00
CG321 CG321 CG324 NG3P0	2.4785	1	180.00
CG321 CG321 CG324 NG3P0	0.3318	2	0.00
CG321 CG321 CG324 NG3P0	0.2520	3	180.00
CG321 CG321 CG324 NG3P0	0.2355	4	180.00
CG321 CG321 CG324 NG3P0	0.4598	5	180.00
CG321 CG321 CG324 NG3P0	0.2834	6	180.00
CG2R51 CG2R57 CG2R57 CG2R51	0.7396	2	180.00
SG2R50 CG2R57 CG2R57 SG2R50	0.4350	1	0.00
SG2R50 CG2R57 CG2R57 SG2R50	0.8979	2	180.00
SG2R50 CG2R57 CG2R57 SG2R50	0.1171	3	0.00
SG2R50 CG2R57 CG2R57 SG2R50	0.0906	4	0.00
CG2R51 CG2R57 CG2R57 SG2R50	0.3937	1	180.00
CG2R51 CG2R57 CG2R57 SG2R50	1.0053	2	180.00
CG2R51 CG2R57 CG2R57 SG2R50	0.0353	3	180.00

CG2R51 CG2R57 CG2R57 SG2R50	0.1095	4	180.00

NBFIX

ATOM TYPE	E_{min} (kcal/mole)	R_{min} (Å)
NG3P0 OG2P1	-1.50000	2.875
CG334 OG2P1	-2.00000	2.750
CG324 OG2P1	-2.00000	2.750
HGP5 OG2P1	-0.09000	2.540
PG2 NG3P0	-2.50000	4.417
PG2 CG334	-3.00000	3.914
NG3P0 OG2P1	-0.154919	3.710
CG2R51 CG334	-0.07505	4.2208
CG2R51 CG324	-0.07505	4.2208
CG2R51 NG3P0	-0.1000	4.4600
CG2R57 CG334	-0.07505	4.2208
CG2R57 CG324	-0.07505	4.2208
CG2R57 NG3P0	-0.1000	4.4600
SG2R50 CG334	-0.7241	4.1800
SG2R50 CG324	-0.7241	4.1800
SG2R50 NG3P	-0.6000	4.4200
NG3P0 CLA	-0.00050	3.5000
CG334 CLA	-2.00000	3.3200

Table H.2 Parametrization of Poly-(3-(2-((4-methylthiophen-3-yl) oxy) ethyl)-1-methyl-4H-1λ4-imidazol-3-ium)

DIHEDRALS

ATOM TYPE	K_χ (kcal/mole)	n (multiplicity)	Δ (degree)
OG301 CG321 CG324 NG2R52	1.0858	1	0.00
CG321 CG324 NG2R52 CG2R51	0.0732	3	180.00
CG321 CG324 NG2R52 CG2R53	0.2943	3	180.00

NBFIX

ATOM TYPE	E_{min} (kcal/mole)	R_{min} (Å)
NG2R52 OG2P1	-20.00000	2.1000
CG2R53 OG2P1	-10.00000	2.5500
CG2R51 CLA	-3.75000	3.1000
CG2R53 CLA	-3.75000	3.1000
CG2R53 NG2R62	-0.20132	3.8397

APPENDIX I

MOLVIB RESULTS OF CHARMM PARAMETRIZATION

Table I.2. Symbolic PED (Potential Energy Distribution) matrix [%] by MOLVIB package of CHARMM

No	Gaussian 09							CHARMM				
	Freq	Type	Int	Type	Int	Type	Int	Freq	Type	Int	Type	Int
1	31.1	tC1-C6	63					31.2	tC1-C6	79		
2	79.3	tNC1	52					92.4	tNC1	42	tC6-C5	26
3	160.3	tC6-C5	60					175.8	tC6-C5	40	tNC1	31
4	191.4	sciNC1	63					219.8	sciNC1	53	rNC3	32
5	224.5	tCH3(C2N)	72					271.2	tCH3(C2N)	98		
6	264.1	tCH3(C2N)	40	sciNC1	27			286.7	tC5-OH1	66		
7	279.2	tCH3(C2N)	77					289.2	tC5-OH1	30	sciNC1	25
8	296.3	tCH3(C2N)	69					299.5	tCH3(C2N)	81		
9	310	tC5-OH1	80					303.9	tCH3(C2N)	98		
10	351.9	rNC3'	49	dNC3a'	25			381.5	rNC3'	42	dNC3a	30
11	363	dNC3a'	26	dNC3a	25			382.2	dNC3a'	35		
12	422.5	dNC3	29	sciNC1	26			437	sciNC1	27		
13	438	dNC3a'	30					454.9	rNC3'	36		
14	461.2	sciNC1	33					485.6	sciNC1	50		
15	523.1	dNC3	36	sciNC1	36			529.3	dNC3	47	sciNC1	32
16	734.3	sNC3	65					787	rCH2	83		
17	757.1	rCH2	73					794.7	sNC3	66		
18	874.1							861.6	rCH2	64		
19	914.5	C6-C5	26					924.3	rCH2	45		
20	923.1	N-C1	25					957.9	N-C1	27		
21	947	sNC3a'	41					977.7				

Table I.3 (Cont.)

22	960.6	sNC3a	32	rCH3	25	993.1	rCH3	40		
23	1032.9	rCH3	56			1022.7	rCH2	34		
24	1034.9					1044.5	rCH3	68		
25	1061.4	C5-OH1	48			1050.3	wCH2	35	C6-C5	29
26	1066.9	rCH3'	35			1069.3	rCH3'	49		
27	1102.7	rCH3'	41			1078.8	rCH3'	50	rCH3	36
28	1121.7	rCH2	34			1086.5	C1-C6	36		
29	1161.9					1160.5	tCH2	84		
30	1193.8	tCH2	47			1178.9	tCH2	81		
31	1225	rCH3	27			1238.9				
32	1235.4	tCH2	31			1255.2	sNC3a	29		
33	1253.7	rCH3'	45			1273.3	wCH2	40	dC5OH1HO	36
34	1284.6	tCH2	53			1294.2	dC5OH1HO	30		
35	1306.9	wCH2	68			1319	wCH2	35		
36	1321.2	tCH2	69			1374.7	sciCH2	35	wCH2	35
37	1368.5	wCH2	77			1403.3	tCH2	65		
38	1402.5	dCH3	44	wCH2	42	1421.7	dCH3a'	69		
39	1404.6	dCH3	96			1429.7	dCH3a'	43	dCH3a	37
40	1405.8	dCH3	59	wCH2	30	1436.1	dCH3a	87		
41	1439.8	dCH3	54			1444.1	dCH3a'	81		
42	1442.8	dCH3a'	66			1455.8	dCH3a	52		
43	1448	dCH3a	36			1456.5	dCH3a	46	dCH3a'	29

Table G.4 (Cont.)

	Freq	Int.							Freq	Int.			
44	1451.9	dCH3a	83						1463	sciCH2	88		
45	1461.1	sciCH2	64						1475.8	sciCH2	92		
46	1465.6	dCH3a'	46	sciCH2	33				1483.6	dCH3	97		
47	1475.9	dCH3a	42	dCH3a'	41				1487.5	dCH3	94		
48	1479.8	dCH3a	33	sciCH2	30	dCH3a'	25		1512.7	dCH3	90		
49	1489.8	dCH3a	35	dCH3a'	32				1529.1	sciCH2	59		
50	1500.8	sciCH2	101						1564.7	wCH2	82		
51	2902.3	sCH2	91						2814.8	sCH2	99		
52	2951.7	sCH2	82						2847.1	sCH2a	96		
53	2957.7	sCH2	59	sCH3	25				2864.4	sCH2	95		
54	2960.7	sCH3	69						2888.3	sCH2a	99		
55	2963.4	sCH3	95						2897.5	sCH2a	99		
56	2963.8	sCH2a	44	sCH2	44				2918.1	sCH3a	80		
57	2968.7	sCH3	93						2919.5	sCH3a'	80		
58	3013.7	sCH2a	96						2921.2	sCH3a'	67	sCH3a	33
59	3036.3	sCH2a	94						2923.7	sCH3a	78		
60	3065.1	sCH3a'	98						2924.1	sCH3a	65	sCH3a'	34
61	3067.6	sCH3a	54	sCH3a'	46				2927.2	sCH3a'	77		
62	3071	sCH3a'	78						2979.2	sCH2	100		
63	3072.3	sCH3a	89						3042.7	sCH3	100		
64	3081.6	sCH3a	97						3043.2	sCH3	100		
65	3088.7	sCH3a'	63	sCH3a	36				3053.4	sCH3	100		
66	3560.3	OH1-HO1	100						3683.9	OH1-HO1	100		

Freq:Frequancy;Int.:Intensity;s:Streching;d:deformation;w:wagging,r:rocking;sci:scissoring;t:tortion;a:antisymetrical

APPENDIX J

WATER INTERACTION RESULTS OF CHARMM

PARAMETRIZATION

Table J. 1. Water Interaction Results of CHARMM Parametrization

| Int	QM Dist (Å)	QM Int Ene (kcal/mol)	QM Scaled Int Ene (kcal/mol)	MM Ene (kcal/mol)	Ene Diff (kcal/mol)	MM Dist. (Å)	Dist Diff (Å)
H21 - OHH	2.26	-8.205484	-9.52	-9.77	-0.25	2.12	-0.14
H22 - OHH	2.29	-8.244828	-9.56	-9.45	0.12	2.14	-0.15
H23 - OHH	2.3	-8.01692	-9.3	-9.68	-0.38	2.14	-0.16
H31 - OHH	2.26	-7.571144	-8.78	-8.44	0.34	2.13	-0.13
H32 - OHH	2.42	-7.776148	-9.02	-7.35	1.67	2.37	-0.05
H33 - OHH	2.3	-8.120332	-9.42	-9.08	0.34	2.16	-0.14
H41 - OHH	2.39	-7.810096	-9.06	-8.63	0.43	2.21	-0.18
H42 - OHH	2.3	-8.099938	-9.4	-9.25	0.15	2.15	-0.15
H43 - OHH	2.3	-8.165637	-9.47	-9.2	0.27	2.15	-0.15
H11 - OHH	2.36	-7.807774	-9.06	-10.06	-1.01	2.1	-0.26
H12 - OHH	2.62	-4.658916	-5.4	-4.81	0.59	2.54	-0.08
H61 - OHH	2.71	-5.898668	-6.84	-4.96	1.89	2.79	0.08
H62 - OHH	2.49	-6.265944	-7.27	-5.54	1.73	2.67	0.18
H51 - OHH	2.56	-4.743692	-5.5	-4.68	0.82	2.65	0.09
H52 - OHH	2.46	-4.873019	-5.65	-4.04	1.62	2.63	0.17
OH1 - HOH	2.47	0.072434	0.08	-0.82	-0.9	2.06	-0.41
HO1 - HOH	1.91	-9.971457	-11.57	-10.75	0.82	1.79	-0.12

*Ene: Energy, Dist: Distance, Diff:Difference
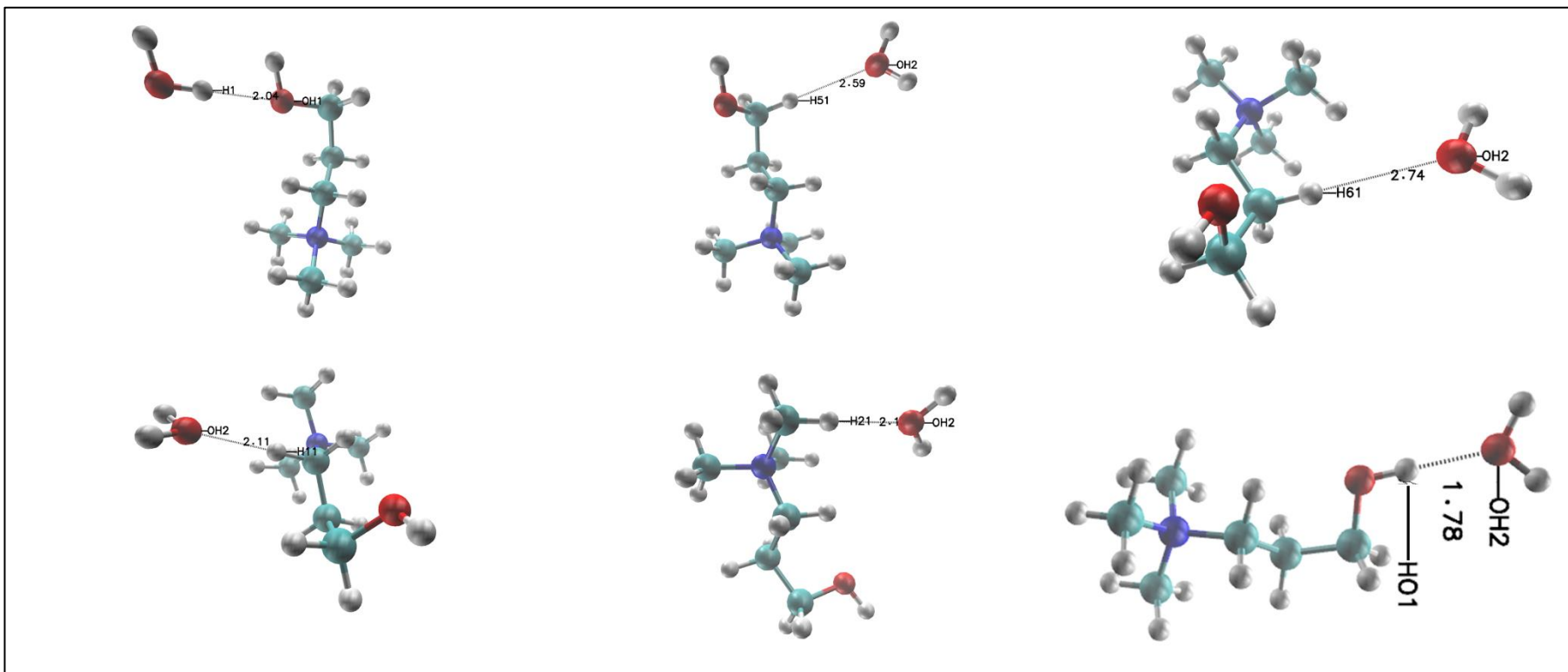
Figure J. 1. Some Water Interactions Examples

CURRICULUM VITAE

Personal Information

Name: Erman KIBRIS

Birthplace: İzmir

Birth Date: 16 February 1987

Education

2016 - 2022	PhD - Computational Chemistry, İzmir Institute of Technology, Chemistry Department.
2013 - 2016	MS, - Organic Chemistry, İzmir Institute of Technology, Chemistry Department.
2006 - 2013	BS, İzmir Institute of Technology, Chemistry Department.

Experience

2014 -	Research Assistant, İzmir Institute of Technology, Chemistry Department

Thesis

Synthesis of allyl alcohols by palladium-catalyzed 1,3-substitution reactions of alkenyl epoxides with organoborons (Ref No. 10021844, 2016)

Molecular Modeling of Polyelectrolytes - Nucleotides Nucleic Acids Interaction (Ref No. 10148473, 2022)

Projects

Rhodium Catalyzed Reactions of Alkenyl Oxirane with Organoborons : In The 4- Aril Or 4- Alkenil Substituted Allyl Alcohols Synthesis, Regio, and Selective a Method (114Z228)

Molecular Dynamics Simulations of Cationic Polythiophenes and Phosphate-Based Biological Compounds(119Z100)

Publications

Kıbrıs, E., Barbak, N.N. & Irmak, N.E. CHARMM force field generation for a cationic thiophene oligomer with ffTK. J Mol Model 27, 34 (2021). https://doi.org/10.1007/s00894-020-04610-2